NAVAL POSTGRADUATE SCHOOL

MONTEREY, CALIFORNIA

THESIS

PERFORMANCE ANALYSIS OF *IEEE 802.11g* RECEIVERS WITH ERASURE DECODING TO MITIGATE THE EFFECTS OF PULSE-NOISE INTERFERENCE

by

Georgios Zouros

December 2006

Thesis Advisor:	R. Clark Robertson
Thesis Co-Advisor:	Richard Harkins

Approved for public release; distribution is unlimited

THIS PAGE INTENTIONALLY LEFT BLANK

REPORT DOCUMENTATION PAGE		Form Approved OMB No. 0704-0188

1. AGENCY USE ONLY *(Leave blank)*	2. REPORT DATE December 2006	3. REPORT TYPE AND DATES COVERED Master's Thesis

4. TITLE AND SUBTITLE: Performance Analysis of *IEEE 802.11g* Receivers With Erasure Decoding to Mitigate the Effects of Pulse-Noise Interference.	5. FUNDING NUMBERS
6. AUTHOR Georgios Zouros	
7. PERFORMING ORGANIZATION NAME(S) AND ADDRESS(ES) Naval Postgraduate School Monterey, CA 93943-5000	8. PERFORMING ORGANIZATION REPORT NUMBER
9. SPONSORING /MONITORING AGENCY NAME(S) AND ADDRESS(ES) N/A	10. SPONSORING/MONITORING AGENCY REPORT NUMBER

11. SUPPLEMENTARY NOTES The views expressed in this thesis are those of the author and do not reflect the official policy or position of the Department of Defense or the U.S. Government.

12a. DISTRIBUTION / AVAILABILITY STATEMENT Approved for public release; distribution is unlimited	12b. DISTRIBUTION CODE A

13. ABSTRACT (maximum 200 words)

The performance of *IEEE 802.11g* wireless local area network (WLAN) standard receivers when the signal is transmitted over a frequency-selective, slowly fading Nakagami channel in a pulse-noise interference environment when errors-and-erasures Viterbi decoding is used is examined. The different combinations of modulation (both binary and non-binary) and convolutional code rate specified by the WLAN standard are examined. The performance obtained with errors-and-erasures decoding (EED) is compared with the performance obtained with errors-only hard decision Viterbi decoding (HDD) as well as that obtained with soft decision Viterbi decoding (SDD) for binary modulation, while for non-binary modulation, EED performance is compared with HDD performance. It was found that EED can significantly improve performance under some conditions when pulse-noise interference is present.

14. SUBJECT TERMS *IEEE 802.11g* WLAN Standard, Nakagami Fading Channel, Hard Decision Decoding, Errors and Erasures Decoding, Soft Decision Decoding, Pulse-Noise Interference.	15. NUMBER OF PAGES 125
	16. PRICE CODE

17. SECURITY CLASSIFICATION OF REPORT	18. SECURITY CLASSIFICATION OF THIS PAGE	19. SECURITY CLASSIFICATION OF ABSTRACT	20. LIMITATION OF ABSTRACT
Unclassified	Unclassified	Unclassified	UL

NSN 7540-01-280-5500

Standard Form 298 (Rev. 2-89)
Prescribed by ANSI Std. 239-18

THIS PAGE INTENTIONALLY LEFT BLANK

Approved for public release; distribution is unlimited

PERFORMANCE ANALYSIS OF IEEE 802.11G RECEIVERS WITH ERASURE DECODING TO MITIGATE THE EFFECTS OF PULSE-NOISE INTERFERENCE

Georgios Zouros
Lieutenant, Hellenic Navy
Bachelor of Science, Hellenic Naval Academy, 1994

Submitted in partial fulfillment of the
requirements for the degree of

MASTER OF SCIENCE IN ELECTRICAL ENGINEERING
and
MASTER OF SCIENCE IN APPLIED PHYSICS

from the

NAVAL POSTGRADUATE SCHOOL
December 2006

Author: Georgios Zouros

Approved by: R. Clark Robertson
Thesis Advisor

Richard Harkins
Co-Advisor

Jeffrey B. Knorr
Chairman, Department of Electrical and Computer Engineering

James Luscombe
Chairman, Department of Physics

THIS PAGE INTENTIONALLY LEFT BLANK

ABSTRACT

The performance of *IEEE 802.11g* wireless local area network (WLAN) standard receivers when the signal is transmitted over a frequency-selective, slowly fading Nakagami channel in a pulse-noise interference environment when errors-and-erasures Viterbi decoding is used is examined. The different combinations of modulation (both binary and non-binary) and convolutional code rate specified by the WLAN standard are examined. The performance obtained with errors-and-erasures decoding (EED) is compared with the performance obtained with errors-only hard decision Viterbi decoding (HDD) as well as that obtained with soft decision Viterbi decoding (SDD) for binary modulation, while for non-binary modulation, EED performance is compared with HDD performance. It was found that EED can significantly improve performance under some conditions when pulse-noise interference is present.

THIS PAGE INTENTIONALLY LEFT BLANK

TABLE OF CONTENTS

LIST OF FIGURES

THIS PAGE INTENTIONALLY LEFT BLANK

LIST OF TABLES

THIS PAGE INTENTIONALLY LEFT BLANK

ACKNOWLEDGMENTS

This thesis would not have been possible without the initial ideas, the clear explanation and the constant advice of Professor R. Clark Robertson.

I also want to express my sincere appreciation to Professor Richard Harkins for serving as my co-advisor.

Finally, I want to thank my wife Maria, and my children Andrea and Stratos, for their loving support and the many sacrifices they made not only during this research but throughout my whole academic experience at the Naval Postgraduate School.

THIS PAGE INTENTIONALLY LEFT BLANK

EXECUTIVE SUMMARY

The performance of *IEEE 802.11g* wireless local area network (WLAN) standard receivers when the signal is transmitted over a frequency-selective, slowly fading Nakagami channel in a pulse-noise interference environment when errors-and-erasures Viterbi decoding is used is examined. The different combinations of modulation (both binary and non-binary) and convolutional code rate specified by the WLAN standard are examined. The performance obtained with errors-and-erasures decoding (EED) is compared with the performance obtained with errors-only hard decision Viterbi decoding (HDD) as well as that obtained with soft decision Viterbi decoding (SDD) for binary modulation, while for non-binary modulation, EED performance is compared with HDD performance. Since the *IEEE 802.11g* standard is used for military applications and the presence of a pulse-noise interferer is possible, this thesis gives useful information and conclusions about the performance of a system that operates in a pulse-noise interference environment.

There are several probability distributions that have been considered as models for the statistical characteristics of the fading channel. In this thesis the fading channel is modeled as a Nakagami channel since it includes the Rayleigh fading channel as a special case but also allows for the examination of the effect of fading channels either more or less severe than Rayleigh as well as channels that approach the case of no fading. It has been shown that the Nakagami-*m* distribution is the best fit for data signals received over urban radio multipath channels [1].

Prior to the analysis, all the background information and concepts utilized by the *IEEE 802.11g* WLAN standard are discussed, and a brief overview of fundamental topics that will be used for the examination is provided.

After that, the concept of errors-and-erasures decoding is introduced, and the upper bound on the probability of information bit error is developed as a function of the probability of channel bit error, channel bit erasure, and correct channel bit detection.

Next, the performance of BPSK/QPSK signals with the convolutional code rates specified by the WLAN standard in the presence of a pulse-noise interferer in addition to additive Gaussian noise is investigated. The performance is analyzed both for no fading and when the channel is modeled as a Nakagami fading channel. The performance is examined for hard decision decoding, errors-and-erasure decoding, and soft decision decoding with linear combining. The findings indicate that errors-and-erasures decoding effectively minimizes the effect of pulse-noise interference and outperforms soft decision decoding with linear combining given an advantage in E_b/N_0, where the required advantage is relatively small for channels with no fading, increases as *m* decreases for Nakagami fading channels, and exceeds 10 dB when channel fading is severe.

Finally, the case of *M*QAM modulation with all binary convolutional coding as specified by the standard is considered as well as the effect of PNI. For this case, EED performance is compared only with HDD performance for a non-fading channel as well as for a Nakagami fading channel. The findings show that EED effectively minimizes the effect of pulse-noise interference and outperforms HDD whether the channel experiences fading or not, and it was found that performance is determined by the combination of modulation and code rate, especially when channel fading is a factor.

I. INTRODUCTION

When the underlying information bits are convolutionally encoded prior to transmission over the channel, soft decision decoding (SDD) receivers that are optimized for the additive white Gaussian noise (AWGN) channel perform poorly when narrowband noise such as pulse-noise interference (PNI) is present in addition to AWGN. A number of different receiver structures to either eliminate or minimize the performance degradation that results from PNI have been considered, but for SDD decoders, practical implementation may be problematic. For example, one technique that has been considered to minimize the degradation due to PNI is noise-normalized combining, where the decision variable for each channel bit is normalized by the noise power received during the corresponding channel bit interval prior to decoding [2], [3], [4]. This technique works very well to effectively eliminate performance degradation due to PNI, but the receiver must be able to make an accurate, real-time estimate of the noise power received during each channel bit. Consequently, while the noise-normalized receiver theoretically works very well, asymptotically approaching the performance of the SDD receiver optimized for the AWGN channel for a very large average energy per information bit-to-pulse-noise interference energy ratio (E_b / N_I), in practice implementation may not be practical.

It has been shown that hard decision Viterbi decoding (HDD), while asymptotically inferior to SDD when $E_b / N_I >> 1$ (the principle source of performance degradation is AWGN), is effective in minimizing performance degradation due to PNI, and HDD does not suffer from implementation problems like the noise-normalized, SDD receiver does.

A decoding procedure commonly used with block codes to improve performance, particularly when narrowband noise that affects some channel bits and not others is present in addition to AWGN, is errors-and-erasures decoding (EED) as opposed to errors-only decoding [5], [6]. EED can be thought of as an intermediate step between HDD and SDD. Presumably, EED decoding has not been applied to convolutional codes due to the ease with which SDD can be implemented, and, when only AWGN is present,

SDD significantly outperforms EED. It seems clear, however, that when PNI is present, EED will yield all of the benefits of errors-only HDD with respect to minimizing the effects of PNI while simultaneously improving performance over what can be obtained with errors-only HDD. The advantage of EED as compared to SDD designed to minimize the performance degradation due to PNI is that implementation of an EED decoder is relatively straightforward and is not significantly more difficult than errors-only HDD.

There are several probability distributions that can be considered in the attempt to model the statistical characteristics of the fading channel. If the process is zero-mean, then the envelope of the channel response at any time instant has a Rayleigh probability distribution. An alternative statistical model is the Nakagami-*m* distribution which is a flexible model for the fading channel since it includes the Rayleigh fading channel as a special case but also allows for the examination of the effect of fading channels either more or less severe than Rayleigh as well as channels that approach the case of no fading. It has been shown that the Nakagami-*m* distribution is the best fit for data signals received in urban radio multipath channels [1].

A. OBJECTIVE

WLANs are increasingly important in meeting the needs of next generation broadband wireless communications systems for both commercial and military applications. Specifically, the WLANs that are used for military applications must operate in a hostile interference environment. The analysis of the effects of both fading and interference are essential to the design of a robust communication system.

In this thesis, the performance of an *IEEE 802.11g* WLAN standard compliant signal when transmitted over a frequency-selective, slowly fading, Nakagami channel with PNI in addition to AWGN is examined for all possible combinations of modulation type (both binary and non-binary) and convolutional code rates specified by the WLAN standard.

The underlying information bits are assumed to be convolutionally encoded prior to transmission over the channel. The performance obtained with EED is compared for channels with fading and no fading with the performance obtained with errors-only HDD as well as that obtained with SDD for binary modulation, while for non-binary modulation, EED performance is compared with HDD performance.

B. THESIS OUTLINE

After this introduction, the remainder of this thesis is organized into five additional chapters. Chapter II discusses all the background information and concepts utilized by the *IEEE 802.11g* WLAN standard and provides a brief overview of fundamental topics that are used in the following chapters. In Chapter III the fundamentals concepts of errors-and-erasures decoding are analyzed. In Chapter IV the performance of a system that utilizes a binary phase-shift keyed (BPSK) waveform transmitted over a frequency-selective, slowly fading Nakagami channel with PNI in addition to AWGN is examined. The performance obtained with EED is compared with the performance obtained with errors-only HDD as well as SDD with linear combining. The analysis continues with the non-binary modulations specified in the *IEEE 802.11g* standard (16QAM and 64QAM) in Chapter V, where the performance obtained with EED is compared with the performance obtained with errors-only HDD. Finally, Chapter VI reviews and summarizes the thesis results from Chapters IV and V.

THIS PAGE INTENTIONALLY LEFT BLANK

II. BACKGROUND

A. PERFORMANCE OF BPSK/QPSK AND *M*QAM IN AWGN

When AWGN is present with power spectral density $N_0/2$, then it can been shown that the probability for bit error for coherently demodulated binary phase-shift keying (BPSK) and quadriphase-shift keying (QPSK) are the same (the symbol error probabilities are not equal) and exact [7] and given by

$$p = Q\left(\sqrt{\frac{2E_b}{N_0}}\right) \tag{2.1}$$

where E_b is the average energy per bit, which is equal to $\alpha_C^2 T_b$, where α_C^2 is the average received signal power, T_b is the bit duration, and $Q(\bullet)$ is the Q-function.

If we define γ_b as the average energy per bit-to-AWGN power spectral density ratio

$$\gamma_b = \frac{E_b}{N_0} = \frac{\alpha_C^2 T_b}{N_0} \tag{2.2}$$

then (2.1) can be rewritten as

$$p = Q\left(\sqrt{\gamma_b}\right) \tag{2.3}$$

For *M*-ary quadrature amplitude modulation (*M*QAM) where $M = 2^q$ and q is even (a square constellation and Gray coding is assumed), the bit error probability is tightly-bounded by [1]

$$p \le \frac{4}{q}\left(1 - \frac{1}{\sqrt{M}}\right) Q\left(\sqrt{\frac{3qE_b}{(M-1)N_0}}\right) \tag{2.4}$$

or

$$p \le \frac{4}{q}\left(1 - \frac{1}{\sqrt{M}}\right) Q\left(\sqrt{\frac{3q\gamma_b}{M-1}}\right) \tag{2.5}$$

B. PERFORMANCE IN AWGN WITH PULSE-NOISE INTERFERENCE

When a channel is affected by pulse-noise interference, then the noise signal $n(t)$ that arrives at the receiver cannot be assumed to be uniform. The noise power (the variance of the Gaussian random variable) at the integrator output is

$$\sigma_{X_k}^2 = \begin{cases} \sigma_0^2 & \text{with probability } 1-\rho \\ \sigma_0^2 + \sigma_I^2 & \text{with probability } \rho \end{cases} \tag{2.6}$$

where $\sigma_o^2 = N_0 / T_b$ and $\sigma_I^2 = N_I / \rho T_b$ are the noise powers at the integrator output due to AWGN and pulse-noise interference, respectively, and ρ is the probability that the k^{th} received channel bit experiences narrowband Gaussian noise in addition to AWGN (which corresponds to the fraction of time that a pulse-noise interferer is on). The one-sided power spectral density of the pulse-noise interference is N_I / ρ, which implies that the average interference power is the same for all values of ρ. It is clear that for $\rho = 1$, the pulse noise interference is always on and we have barrage noise interference.

Consequently, the conditional probability of channel bit error given that noise interference is present ($p(pulse\,noise\,on)$) is obtained from the conditional probability of channel bit error given that AWGN is present ($p(pulse\,noise\,off)$)by replacing N_0 with $N_0 + N_I / \rho$.

The total probability of channel bit error when pulse-noise interference is present is obtained from

$$p_b = P_r(pulse\,noise\,on)\,p(pulse\,noise\,on) + P_r(pulse\,noise\,off)\,p(pulse\,noise\,off) \tag{2.7}$$

Since ρ is the probability that a channel bit will experience pulse-noise interference, equation (2.7) can be rewritten as

$$p_b = \rho\ p(pulse\,noise\,on) + (1-\rho)\ p(pulse\,noise\,off) \tag{2.8}$$

C. SLOW, FLAT, FADING CHANNELS

When the channel is modeled as a slow, flat, fading channel, the received signal amplitude α_C is modeled as a random variable. In this thesis, the channel is modeled as a

Nakagami fading channel. As a result, α_C is a Nakagami-*m* random variable with probability density function [1]

$$f_{A_C}(\alpha_C) = \frac{2}{\Gamma(m)} \left(\frac{m}{\overline{\alpha_C^2}} \right)^m \alpha_C^{2m-1} \, e^{-m\alpha_C^2 / \overline{\alpha_C^2}} \, u(\alpha_C) \tag{2.9}$$

where $\Gamma(\bullet)$ is the Gamma function and $u(\bullet)$ is the unit step function. The fading figure is given by

$$m = \frac{\overline{\alpha_C^2}^2}{E\left[\left(\alpha_C^2 - \overline{\alpha_C^2} \right)^2 \right]} \tag{2.10}$$

where $m \geq 1/2$. For $m < 1$ system performance is poorer than for Rayleigh fading, and for $m > 1$, system performance is superior to that obtained for Rayleigh fading. The last condition $(m > 1)$ usually implies that a line-of-sight (LOS) exists between the two communication points. When $m = 1$ we have Rayleigh fading, while when $m \to \infty$, there is no fading.

Since from (2.2) γ_b is a function of α_C, then γ_b is a random variable, and from (2.9) we get the probability density function

$$f_{\Gamma_b}(\gamma_b) = \frac{1}{\Gamma(m)} \left(\frac{m}{\overline{\gamma}_b} \right)^m \gamma_b^{m-1} e^{-m\gamma_b / \overline{\gamma}_b} \, u(\gamma_b) \tag{2.11}$$

where $\overline{\gamma_b} = \overline{\alpha_C^2} T_b / N_0$.

Hence, when we have a fading channel, all the expressions for the probability of channel bit error, which are functions of a random variable γ_b, are conditional probabilities. In order to find the unconditional probability of channel bit error or, in other words, to obtain the average probability of bit error, we must calculate the expected value of $p(\gamma_b)$:

$$p = \int_0^\infty p(\gamma_b) \; f_{\Gamma_b}(\gamma_b) \, d\gamma_b \tag{2.12}$$

D. FORWARD ERROR CORRECTION CODING

In a system that utilizes forward error correction (FEC) coding, *n* coded bits are transmitted in the time it otherwise takes to transmit *k* information bits (data bits), where *n>k.* Therefore, if $r = k/n$ is the code rate with $r < 1$, T_b, R_b, E_b are the duration, the rate and the average energy per uncoded bit, respectively, and $T_{b_C}, R_{b_C}, E_{b_C}$ are the duration, the rate and the average energy per coded bit, respectively, then

$$T_{b_C} = rT_b \tag{2.13}$$

$$R_{b_C} = \frac{R_b}{r} \tag{2.14}$$

$$E_{b_C} = rE_b \tag{2.15}$$

When FEC with a convolutional code is employed, there is not an expression that exactly computes the probability of bit error. For Viterbi decoding of a rate $r = k/n$ convolutional code, the probability of bit error is upper bounded by [8]

$$P_b < \frac{1}{k} \sum_{d=d_{free}}^{\infty} B_d \; P_d \tag{2.16}$$

where d_{free} is the free distance of the convolutional code, B_d is the total number of information bit ones on all weight *d* paths, and P_d is the probability of selecting a weight *d* output sequence as the transmitted code sequence. The quantities B_d and d_{free} are parameters of the convolutional code chosen, and P_d is determined by the type of modulation, channel, and decoding used (HDD, EED, SDD).

1. Hard Decision Decoding (HDD)

In HDD the output of a binary symmetric channel is used as the decoder input. Each coded bit is demodulated prior to decoding and a decision is made as to whether the received signal represents a transmitted bit zero or one. For HDD the probability of selecting a weight *d* output sequence as the transmitted code sequence is [8]

$$P_d = \begin{cases} \displaystyle\sum_{i=(d+1)/2}^{d} \binom{d}{i} p^i (1-p)^{d-i} & \text{for } d \text{ odd} \\ \\ \displaystyle\frac{1}{2}\binom{d}{d/2}\left[p(1-p)\right]^{d/2} + \sum_{i=1+d/2}^{d} \binom{d}{i} p^i (1-p)^{d-i} & \text{for } d \text{ even} \end{cases} \tag{2.17}$$

where p is the probability of channel bit error.

Equation (2.17) is used in (2.16) to obtain the upper bound on the probability of information bit error for HDD. The performance of HDD was examined in [9] and is examined here in order to compare it with the performance obtained with EED.

2. Soft Decision Decoding (SDD)

For a receiver with SDD, there is a quantization circuit, and rather than simply assign a zero or a one to each received signal, four or more regions are established. Hence, we can have a "strong zero" or a "weak zero." The *IEEE 802.11g* standard utilizes eight levels. A special case is when we have only two quantization levels, which is simply HDD.

There are several types of receivers which use SDD. Many of them were examined in [10] and [11]. In this thesis we will use the linear combining receiver in order to compare its performance with the performances obtained with HDD and EED. Although its performance, as analyzed in [10], is not very good, especially when E_b / N_I is small, compared with the other receivers, it is a very practical receiver since no side information is assumed.

E. *IEEE 802.11g* STANDARD

The *IEEE 802.11g* WLAN standard has the ability to transfer data at various data rates over a restricted bandwidth and utilizes both binary and non-binary modulation techniques. Furthermore, in order to enhance the recovery of the actual data bits, *802.11g* applies forward error correction coding using a variety of convolutional codes. In Table 1 [12] are shown the various data rates with the corresponding modulation techniques and coding rates as specified by the *IEEE 802.11g* WLAN standard.

Table 1. Rate dependent parameters (From Ref. [12]).

Data rate (Mbits/s)	Modulation	Coding rate (R)	Coded bits per subcarrier (N_{BPSC})	Coded bits per OFDM symbol (N_{CBPS})	Data bits per OFDM symbol (N_{DBPS})
6	BPSK	1/2	1	48	24
9	BPSK	3/4	1	48	36
12	QPSK	1/2	2	96	48
18	QPSK	3/4	2	96	72
24	16-QAM	1/2	4	192	96
36	16-QAM	3/4	4	192	144
48	64-QAM	2/3	6	288	192
54	64-QAM	3/4	6	288	216

The values of B_d and d_{free} for the constraint length $\nu = 7$ convolutional codes which we use in the analysis are shown in Table 2.

Table 2. Weight structure of the convolutional codes.

Rates	d_{free}	$B_{d_{free}}$	$B_{d_{free}+1}$	$B_{d_{free}+2}$	$B_{d_{free}+3}$	$B_{d_{free}+4}$	$B_{d_{free}+5}$	$B_{d_{free}+6}$	$B_{d_{free}+7}$
r=1/2	10	36	0	211	0	1404	0	11633	0
r=2/3	6	3	81	402	1487	6793	-	-	-
r=3/4	5	42	252	1903	11995	72115	-	-	-

We use only these terms in (2.16) since it is generally accepted that the first few terms dominate performance for realistic values of P_b.

With regard to the parameters shown in Table 2, those for $r = 1/2$ are given for the code specified by the standard [13]. According to the standard, the $r = 2/3$ and $r = 3/4$ codes are obtained by puncturing the $r = 1/2$ code, and, unfortunately, only the free distance and $B_{d_{free}}$ are available for these codes. Therefore, the remaining B_d s for the $r = 2/3$ and $r = 3/4$ codes shown in Table 2 are taken from the parameters for the

optimum $r = 2/3$ and $r = 3/4$ codes [14]. Since the leading term in (2.16) dominates P_b, this should not result in any significant error. Essentially, we are slightly underestimating an upper bound.

In this chapter, we addressed all the background information and concepts that are necessary to examine the performance of the *IEEE 802.11g* receiver in a Nakagami fading channel with PNI in addition to AWGN. First we illustrated the performance of BPSK/QPSK and *M*QAM in AWGN, and then we examined how the probability of channel bit error changes when a pulse-noise interferer is present in addition to AWGN and the channel is modeled as a Nakagami fading channel. At the end, we showed the probability of information bit error for a system utilizing FEC for the various data rates and corresponding modulation techniques and code rates as specified by the *IEEE 802.11g* WLAN standard. In the next chapter, the fundamentals concepts of errors-and-erasures decoding are analyzed.

THIS PAGE INTENTIONALLY LEFT BLANK

III. ERRORS-AND-ERASURES DECODING (EED)

An alternative decoding procedure to errors-only HDD is errors-and-erasures decoding (EED), which is the simplest form of SDD. When EED is implemented, the receiver replaces the symbols that are received ambiguously or unreliably with an erasure (*e*). Hence, the number of possible outputs is the number of symbols plus the erasure symbol. For example, in binary erasure decoding, the output of the demodulator is not binary but ternary. The three possible outputs corresponding to bit *1*, *0*, and *e* for the binary symmetric channel are shown in Figure 1.

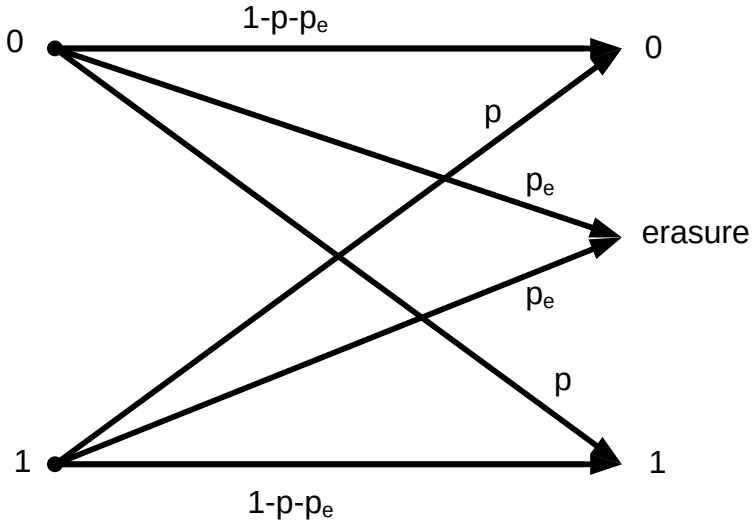

Figure 1. Binary symmetric erasure channel.

Suppose that a received code sequence has a single erased bit. Now all valid code sequences are separated by a Hamming distance of at least $d_{free}-1$. In general, given i erasures in a received code sequence, all valid code sequences are separated by a Hamming distance of at least $d_{free}-i$. Hence, the effective free distance between valid code sequences is

$$d_{free_{eff}} = d_{free} - i \tag{3.1}$$

Therefore, the number of errors j in the non-erased bits of the code sequence that can be corrected is given by

$$d_{free_{eff}} = d_{free} - i \geq 2j + 1 \tag{3.2}$$

or

$$j = \frac{1}{2}\left\lfloor d_{free} - i - 1 \right\rfloor \tag{3.3}$$

where $\lfloor x \rfloor$ implies the integer portion of x. Thus, a code with free distance d_{free} can correct any pattern of j errors and i erasures as long as

$$2j + i < d_{free} \tag{3.4}$$

Hence, twice as many erasures as errors can be corrected. Intuitively, this makes sense because we have more information about the erasures. The locations of the erasures are known, but the locations of the errors are not.

For block codes, there are three steps in simultaneous error-and-erasure correction. First, the i erased bits (positions) are replaced with zeros. This generates $i_0 \leq i$ additional errors. The resulting code sequence which contains $j + i_0$ errors is decoded normally. Next, the i erased bits (positions) are replaced with ones. This generates $i_1 = i - i_0 \leq i$ additional errors, and the resulting code sequence which contains $j + i_1 = j + i - i_0$ errors is decoded normally. Of the two decoded code sequences, at least one is correct and the code sequence with the best metric (the smallest number of errors corrected outside the e erased positions) is selected as the decoded code sequence. For convolutional codes, the Viterbi algorithm with HDD can easily be modified to perform EED. Essentially, any erased bit is given a bit metric of 1/2 when compared to either a bit one or a bit zero for the path metric being computed, and the survivor paths are chosen in the same manner as for HDD.

For EED, the probability that there are a total of i erasures and j errors in a sequence of d bits is given by

$$\Pr(i, j) = \binom{d}{i}\binom{d-i}{j} p_e^i p^j p_c^{d-i-j} \tag{3.5}$$

where p is the probability of channel bit error, p_e is the probability of channel bit erasure, the probability of correct channel bit detection p_c is

$$p_c = 1 - p_e - p \tag{3.6}$$

and each channel bit is assumed to be received independently.

We define P_{C_d} as the probability of not selecting a weight d output sequence as the transmitted code sequence instead of the correct code sequence. Since a weight d sequence will not be incorrectly chosen as long as

$$i + 2j < d \tag{3.7}$$

then from (3.5) we get

$$P_{C_d} = \sum_{i=0}^{d-1} \binom{d}{i} p_e^i \Omega_{d-i} \tag{3.8}$$

where

$$\Omega_k = \begin{cases} \displaystyle\sum_{j=0}^{(k-1)/2} \binom{k}{j} p^j p_c^{k-j} & \text{for } k \text{ odd} \\ \displaystyle\frac{1}{2}\binom{k}{k/2}(pp_c)^{k/2} + \sum_{j=0}^{(k/2)-1} \binom{k}{j} p^j p_c^{k-j} & \text{for } k \text{ even} \end{cases} \tag{3.9}$$

Now the probability of selecting a weight d output sequence instead of the correct output sequence is given by

$$P_d = 1 - P_{C_d} \tag{3.10}$$

Equations (3.8) and (3.9) are used to compute (3.10), which in turn is used in (2.16) to obtain an upper bound on the probability of information bit error.

We have seen in this chapter how errors-and-erasures decoding works with convolutional codes and how we obtain an upper bound on the probability of information bit error when the system utilizes errors-and erasures decoding. In the next chapter, the

performance of a system that utilizes a BPSK/QPSK waveform transmitted over a Nakagami fading channel with PNI in addition to AWGN is examined for HDD, EED, and SDD with linear combining for code rates 1/2 and 3/4. At the end of the chapter, we compare the performances of all these decoding procedures and code rates.

IV. BPSK/QPSK SIGNALS

A. HARD DECISION DECODING (HDD)

1. Performance in AWGN with PNI (No Fading)

The model of a BPSK receiver which utilizes HDD is shown in Figure2.

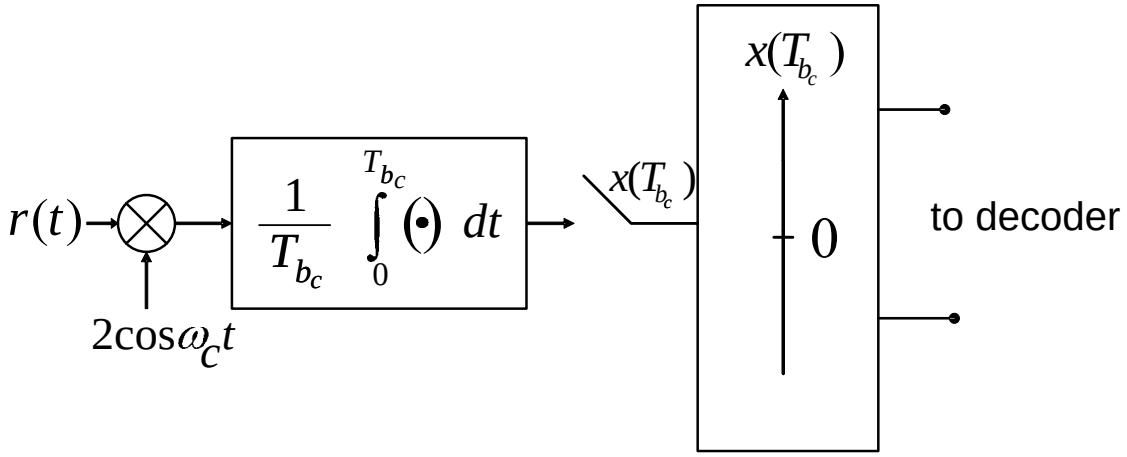

Figure 2. BPSK receiver with hard decision decoding.

In order to calculate the performance of a coded BPSK/QPSK signal in AWGN with PNI, we must find the channel transition probability. When a BPSK/QPSK system utilizes FEC, this probability is obtained from (2.1) and (2.15) as

$$p = Q\left(\sqrt{\frac{2rE_b}{N_0}}\right) \tag{4.1}$$

Now we can find the probability of channel bit error with PNI by combining (4.1) and (2.8) to get

$$p = \rho\, Q\left(\sqrt{\frac{2rE_b}{N_0 + N_I/\rho}}\right) + (1-\rho)\, Q\left(\sqrt{\frac{2rE_b}{N_0}}\right) \tag{4.2}$$

or, in terms of γ_b and $\gamma_I = E_b/N_I$,

$$p = \rho\, Q\left(\sqrt{\frac{2r\gamma_b}{1+\gamma_b/(\gamma_I\rho)}}\right) + (1-\rho)\, Q\left(\sqrt{2r\gamma_b}\right) \tag{4.3}$$

If we assume that $E_b/N_I >> 1$ and $N_I/\rho >> N_0$, which are generally true since in a jamming environment we use the maximum possible transmitter power and thermal noise is negligible compared with interference power, then (4.2) becomes

$$p \approx \rho\, Q\left(\sqrt{\frac{2r\rho E_b}{N_I}}\right) \tag{4.4}$$

Since $\left[zQ(z)\right]_{\max} = 0.1657$ when $z = 1.44$, the value for the parameter ρ which maximizes the probability of bit error (worst case) is

$$\rho_{wc} = \frac{0.72}{r\ E_b/N_I} \tag{4.5}$$

Of course, the duty factor ρ must be less than or equal to unity. Thus, (4.5) applies only when $E_b/N_I \geq 0.72/r$.

Consequently, from (4.4) the maximum probability of bit error for ρ_{wc} is

$$p_{\max} \approx \frac{0.08285}{r\ E_b/N_I} = \frac{0.08285}{r\ \gamma_I} \tag{4.6}$$

Equations (4.3) and (4.6) are used to compute (2.17), which in turn is used in (2.16) with the values of B_d and d_{free} corresponding to the code rate shown in Table 2 to obtain an upper bound on the probability of information bit error.

a. BPSK/QPSK r=1/2

For bit rates of 6 and 12 Mbps, BPSK and QPSK are used, respectively, with the code rate of 1/2. Figure 3 is a plot of the performance obtained with HDD for various values of the factor ρ when $E_b/N_0 = 15\,\text{dB}$. It can be seen that varying ρ affects the receiver performance significantly, especially when E_b/N_I is small.

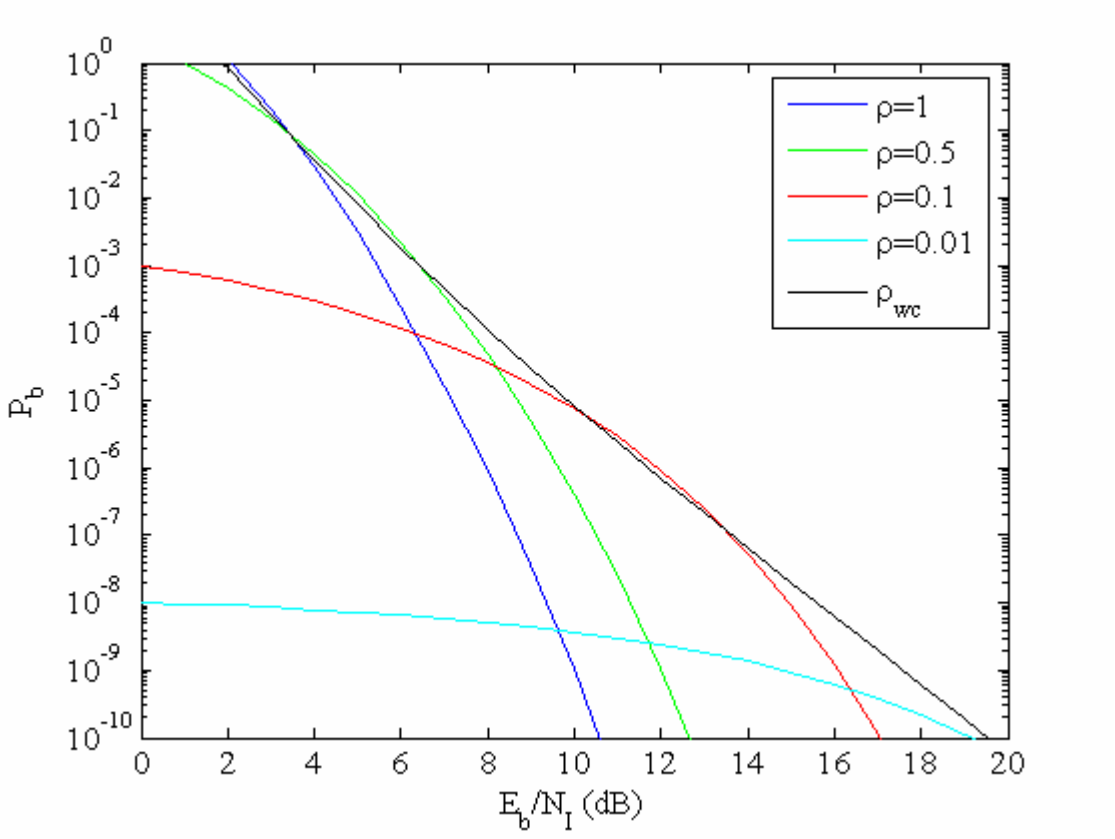

Figure 3. Performance of BPSK/QPSK in AWGN and PNI with r=1/2 convolutional source coding and HDD for a channel with no fading ($E_b/N_0 = 15\,\text{dB}$).

b. BPSK/QPSK r=3/4

For bit rates of 9 and 18 Mbps, BPSK and QPSK are used, respectively, with the code rate of 3/4. In Figure 4, in a manner analogous to Figure 3, the performance obtained with HDD for various values of the factor ρ when $E_b/N_0 = 15\,\text{dB}$ is plotted. In this case the results for the various values of ρ are analogous to the results shown in Figure 3 (r=1/2). However, the effect of the PNI on the receiver is more severe.

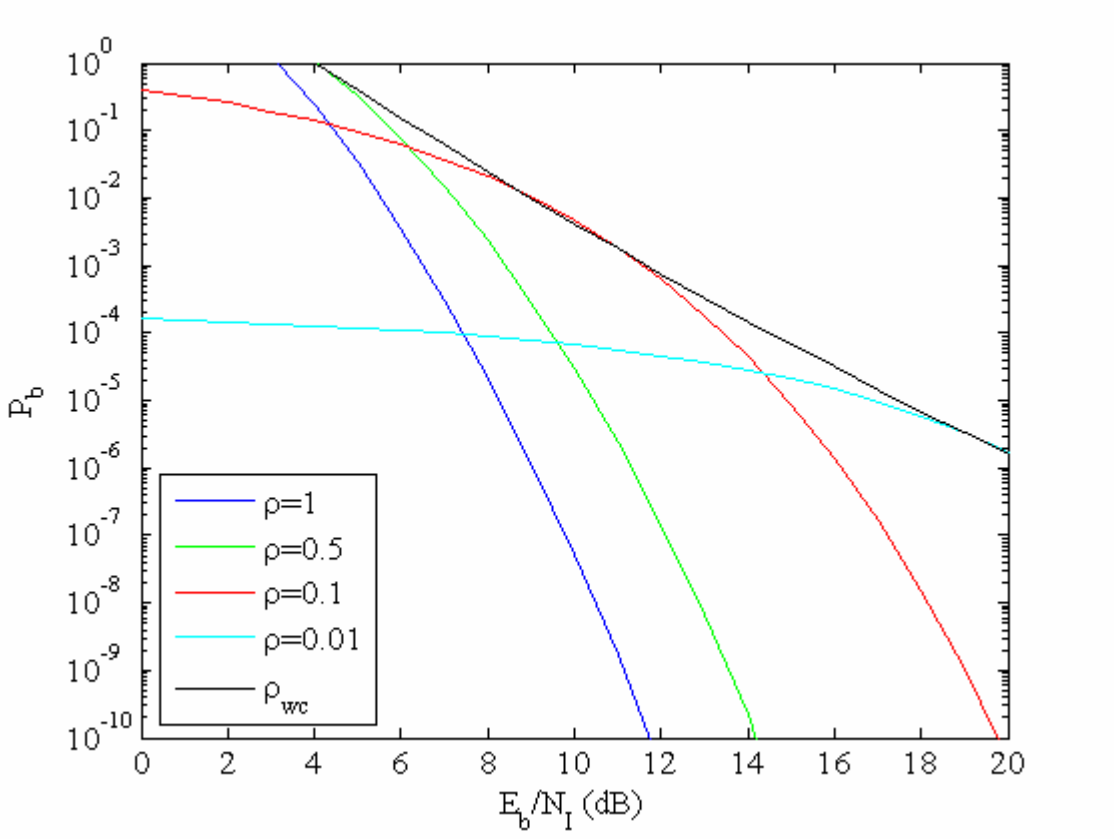

Figure 4. Performance of BPSK/QPSK in AWGN and PNI with r=3/4 convolutional source coding and HDD for a channel with no fading ($E_b/N_0 = 15\,\text{dB}$).

2. Performance in AWGN with PNI and Fading

When the channel is modeled as a Nakagami fading channel, then (4.3) is a conditional probability. The unconditional probability of channel bit error is now found by substituting (4.3) into (2.12) to obtain

$$p = \int_0^\infty \left\{ \rho Q\left(\sqrt{\frac{2r\gamma_b}{1+\overline{\gamma}_b/(\overline{\gamma}_I \rho)}} \right) + (1-\rho) Q\left(\sqrt{2r\gamma_b} \right) \right\} \frac{1}{\Gamma(m)} \left(\frac{m}{\overline{\gamma}_b} \right)^m \gamma_b^{m-1} e^{-m\gamma_b / \overline{\gamma}_b} d\gamma_b \quad (4.7)$$

We can obtain a numerical solution for this equation or we can find an analytic solution using the following identity

$$\int_0^\infty Q\left(\sqrt{2r\zeta\gamma_b}\right) f_{\Gamma_b}(\gamma_b)\,d\gamma_b = \frac{\Gamma(m+\frac{1}{2})(r\zeta\,\overline{\gamma}_b/m)^{1/2}}{2\sqrt{\pi}\Gamma(m+1)(1+r\zeta\,\overline{\gamma}_b/m)^{m+1/2}} \times {}_2F_1\left(1, m+\frac{1}{2}; m+1; \frac{1}{1+r\zeta\,\overline{\gamma}_b/m}\right) \tag{4.8}$$

where ${}_2F_1\left(1, b+\frac{1}{2}; b+1; z\right)$ is Gauss' hypergeometric function.

Equation (4.7) is used to compute (2.17), which in turn is used in (2.16) with the values of B_d and d_{free} corresponding to the code rate shown in Table 2 to obtain an upper bound on the probability of information bit error.

a. BPSK/QPSK r=1/2

In Figure 5, the performance is plotted for different fading conditions. In order to validate the results obtained using the analytical solution, the performance is obtained both analytically and numerically. For this figure, $E_b/N_0 = 15\,\text{dB}$ and $\rho = 0.5$.

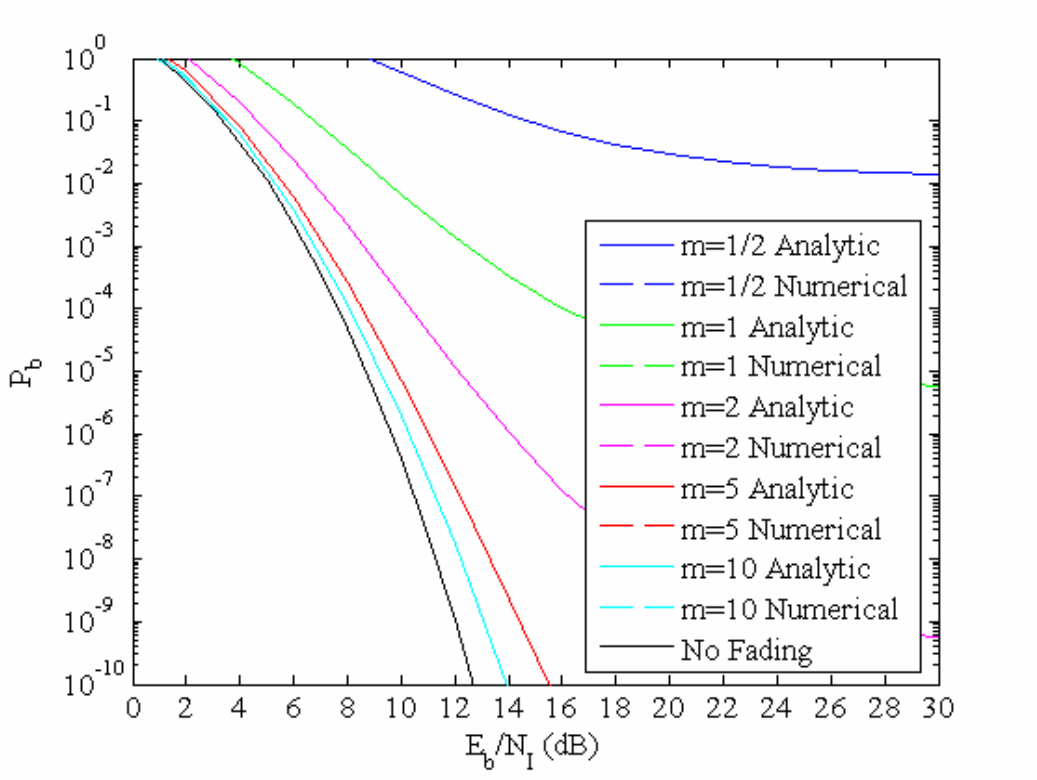

Figure 5. Performance of BPSK/QPSK in AWGN and PNI (ρ=0.5) with r=1/2 convolutional source coding and HDD for a Nakagami fading channel ($E_b/N_0 = 15\,\text{dB}$) computed both analytically and numerically.

It is clear from Figure 5 that both methods give virtually identical results for all fading conditions. Additionally, the performance observed for $m = 10$ is very close to the performance for a non-fading channel. As expected, the performance improves as m increases and approaches the non-fading condition $(m \to \infty)$.

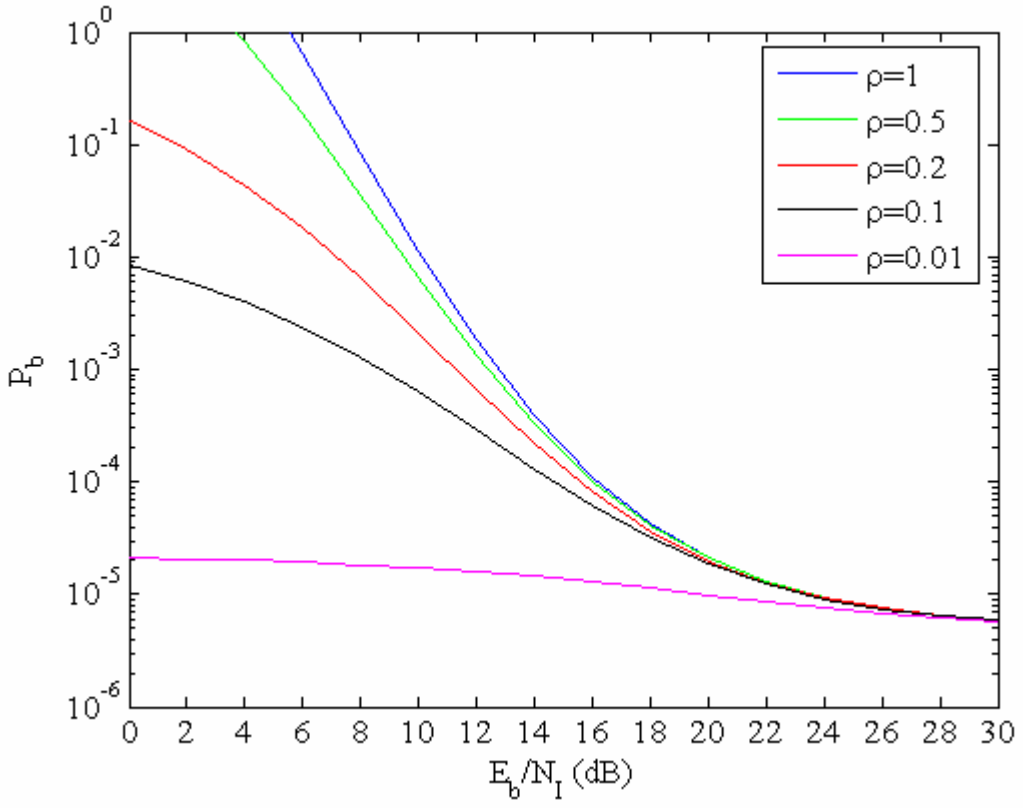

Figure 6. Performance of BPSK/QPSK in AWGN and PNI with *r*=1/2 convolutional source coding and HDD for a Nakagami fading channel (*m*=1) ($E_b/N_0 = 15\,\text{dB}$).

In Figure 6 the effect of the factor ρ on the receiver's performance is investigated. In this figure the performance is plotted for various values of ρ with $E_b/N_0 = 15\,\text{dB}$ and $m = 1$.

As can be seen, varying ρ affects the receiver performance significantly, particularly when $E_b/N_I < 12\,\text{dB}$. Moreover, it is seen that the barrage noise interference $(\rho = 1)$ is more effective than PNI. As ρ approaches zero, the performance converges to the AWGN limit. In conclusion, the bigger the value of ρ is, the poorer the performance.

b. BPSK/QPSK r=3/4

Figures 7 and 8 are analogous to Figures 5 and 6, respectively, for code rate $r = 3/4$ instead of $r = 1/2$ and with $E_b/N_0 = 24\,\text{dB}$. In this case, the receiver performance also worsens as the fading conditions worsen, and the factor ρ has the same effect on receiver performance as in the previous case for $r = 1/2$. It is obvious that in this case the effect of the channel fading is more severe, but the effect of PNI is very similar for both code rates.

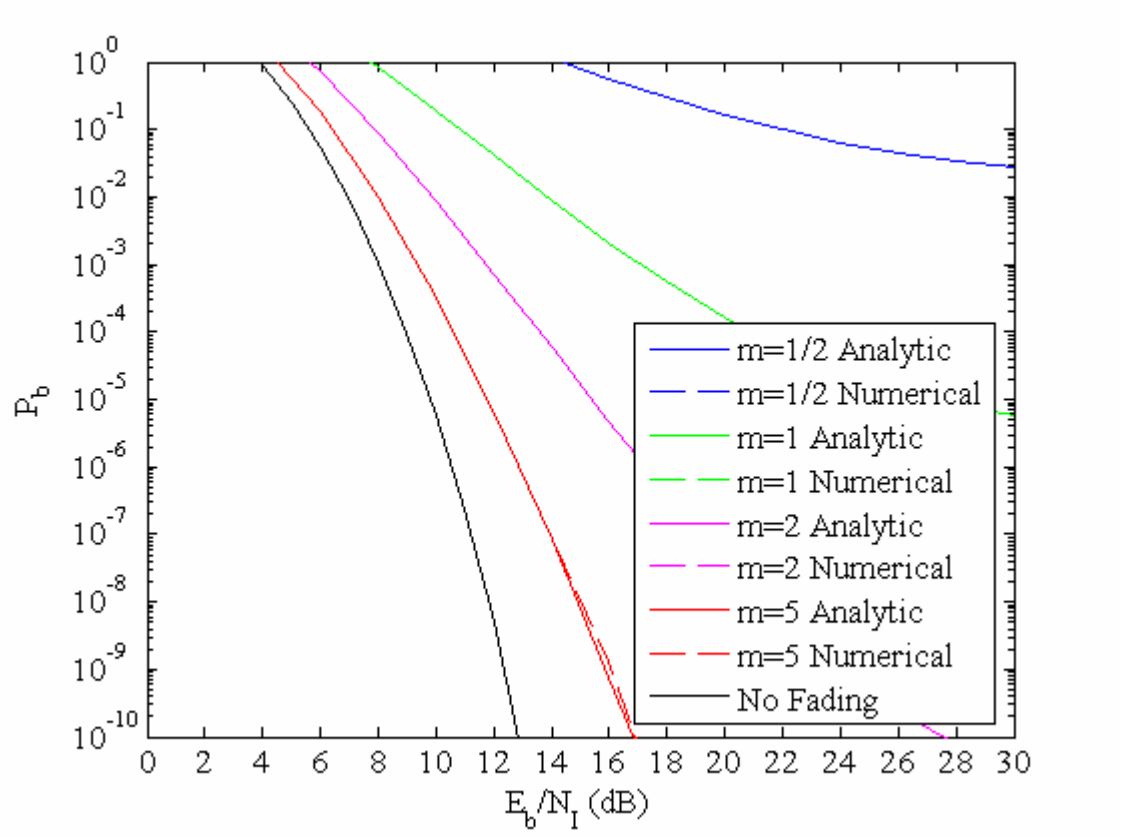

Figure 7. Performance of BPSK/QPSK in AWGN and PNI (ρ=0.5) with r=3/4 convolutional source coding and HDD for a Nakagami fading channel ($E_b/N_0 = 24\,\text{dB}$) computed both analytically and numerically.

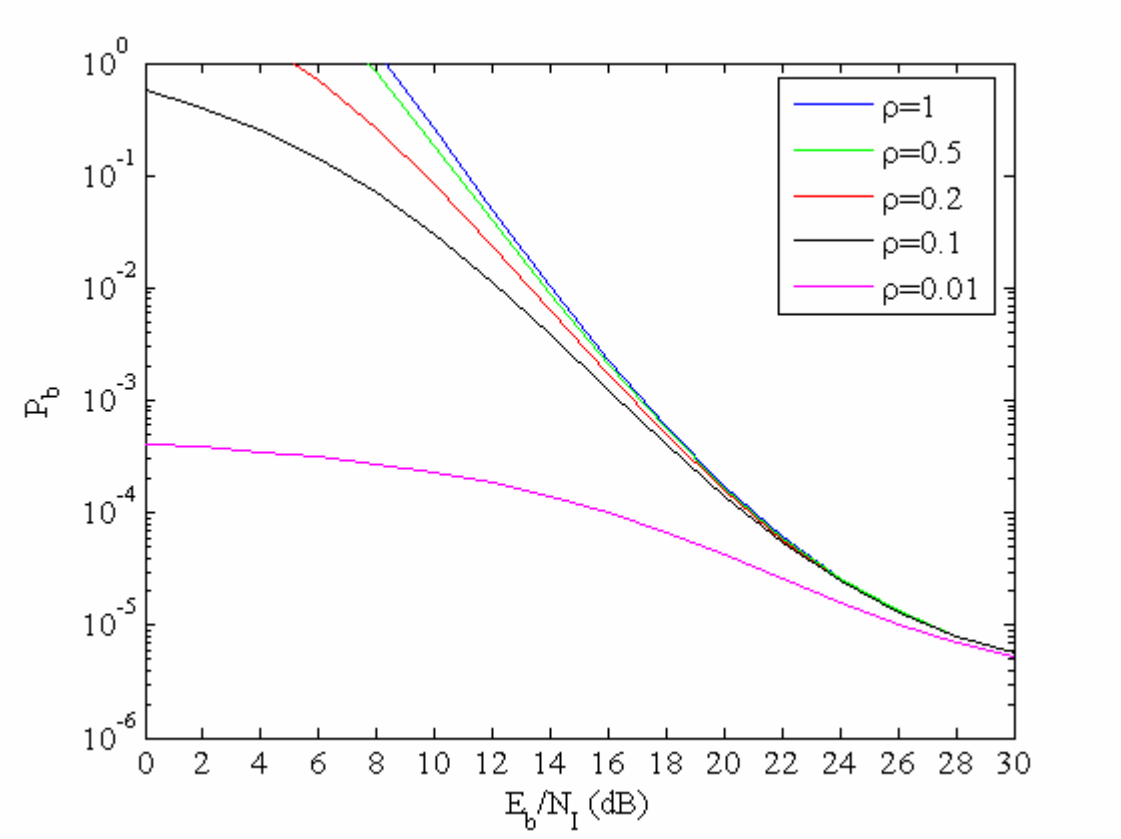

Figure 8. Performance of BPSK/QPSK in AWGN and PNI with r=3/4 convolutional source coding and HDD for a Nakagami fading channel (m=1) ($E_b/N_0 = 24\,\text{dB}$).

B. ERRORS-AND-ERASURES DECODING (EED)

For the BPSK errors-and-erasures demodulator shown in Figure 9 and for AWGN or any other symmetric noise, the probability of channel bit error is

$$p = \Pr(X > V_T \mid 0) = \Pr(X < -V_T \mid 1) \tag{4.9}$$

Clearly, p is smaller for an errors-and-erasures demodulator than for an errors-only demodulator where $V_T = 0$. The probability of channel bit erasure is

$$p_e = \Pr(V_T \geq X \geq -V_T \mid 0) = \Pr(V_T \geq X \geq -V_T \mid 1) \tag{4.10}$$

where p_e increases as V_T increases.

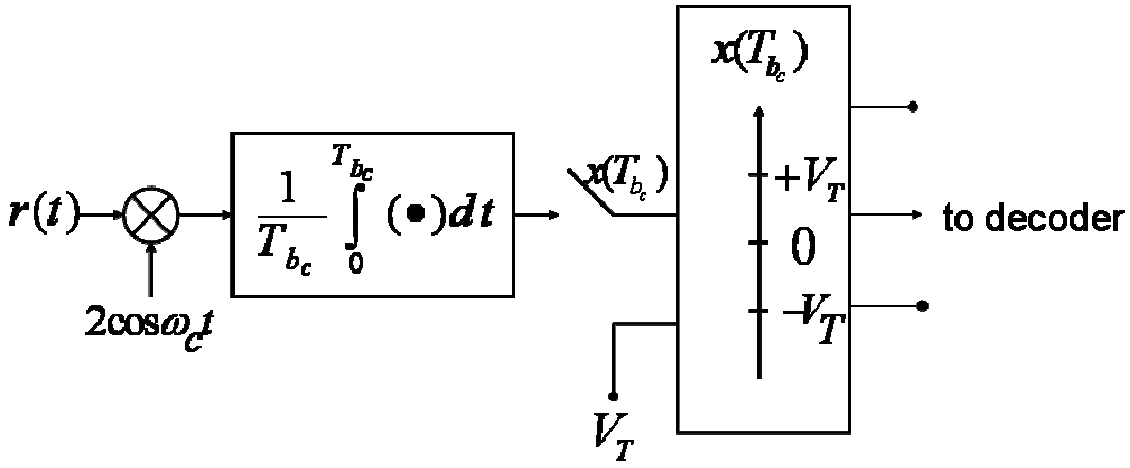

Figure 9. BPSK receiver with errors-and-erasures demodulation.

The received signal is given as

$$r(t) = \sqrt{2}\alpha_c d(t)\cos(\omega_c t) + n(t) \tag{4.11}$$

where $d(t)$ is the baseband, non-return-to-zero waveform that corresponds to the information bits with $|d(t)| = 1$, and $n(t)$ is the total noise waveform. For either AWGN or narrowband Gaussian noise, the integrator output in Figure 5 is modeled as the Gaussian random variable X with $|\bar{X}| = \sqrt{2}\alpha_c$ and $\sigma^2 = N_T / rT_b$, where N_T is the total one-sided noise power spectral density.

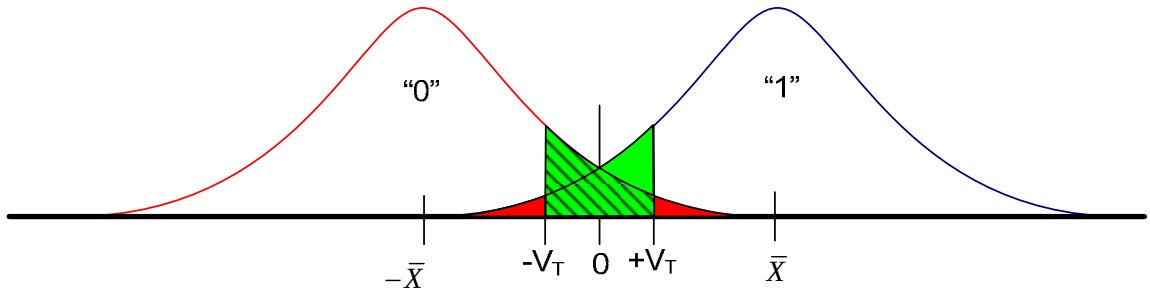

Figure 10. Gaussian probability density function for BPSK.

The probability of channel bit error with AWGN only can be found from (4.9), as illustrated in Figure 10, as

$$p = Q\left(\frac{+V_T - (-\overline{X})}{\sigma}\right) = 1 - Q\left(\frac{-V_T - \overline{X}}{\sigma}\right) \tag{4.12}$$

Similarly, the probability of channel bit erasure with AWGN only is, from (4.10),

$$p_e = Q\left(\frac{-V_T - (-\overline{X})}{\sigma}\right) - Q\left(\frac{+V_T - (-\overline{X})}{\sigma}\right) \tag{4.13}$$

or

$$p_e = 1 - Q\left(\frac{+V_T - \overline{X})}{\sigma}\right) - \left[1 - Q\left(\frac{-V_T - \overline{X})}{\sigma}\right)\right] \tag{4.14}$$

Defining $V_T = \alpha\sqrt{2}\alpha_c$ where $0 < \alpha \le 1$, we obtain from (4.12)

$$p = Q\left[(1+\alpha)\sqrt{\frac{2r\alpha_c^2 T_b}{N_0}}\right] = Q\left[(1+\alpha)\sqrt{2r\gamma_b}\right] \tag{4.15}$$

and from (4.14)

$$p_e(\alpha_c) = Q\left[(1-\alpha)\sqrt{\frac{2r\alpha_c^2 T_b}{N_0}}\right] - Q\left[(1+\alpha)\sqrt{\frac{2r\alpha_c^2 T_b}{N_0}}\right] \tag{4.16}$$

Since the second term in (4.16) is p, then (4.16) simplifies to

$$p_e = Q\left[(1-\alpha)\sqrt{2r\gamma_b}\right] - p \tag{4.17}$$

Substituting (4.15) and (4.17) into (3.6), we get the probability of correct channel bit detection

$$p_c = 1 - Q\left[(1-\alpha)\sqrt{2r\gamma_b}\right] \tag{4.18}$$

For $\alpha = 0$ we have the results for HDD since $V_T = 0$. For $\alpha = 0$, the probability of channel bit error (4.15) reduces to (4.1), and the probability of channel bit erasure (4.17) goes to zero.

1. Performance in AWGN with PNI (No Fading)

The probability of channel bit error, channel bit erasure, and correct channel bit detection with PNI can be found if we combine (4.15), (4.17), and (4.18) with (2.8) to get, respectively,

$$p = \rho\, Q\left[(1+\alpha)\sqrt{\frac{2r\gamma_b}{1+N_I/\rho N_0}}\right] + (1-\rho)\, Q\left[(1+\alpha)\sqrt{2r\gamma_b}\right] \tag{4.19}$$

$$\begin{aligned} p_e = {} & \rho\left\{Q\left[(1-\alpha)\sqrt{\frac{2r\gamma_b}{1+N_I/\rho N_0}}\right] - Q\left[(1+\alpha)\sqrt{\frac{2r\gamma_b}{1+N_I/\rho N_0}}\right]\right\} \\ & + (1-\rho)\left\{Q\left[(1-\alpha)\sqrt{2r\gamma_b}\right] - Q\left[(1+\alpha)\sqrt{2r\gamma_b}\right]\right\} \end{aligned} \tag{4.20}$$

and

$$p_c = \rho\left\{1 - Q\left[(1-\alpha)\sqrt{\frac{2r\gamma_b}{1+N_I/\rho N_0}}\right]\right\} + (1-\rho)\left\{1 - Q\left[(1-\alpha)\sqrt{2r\gamma_b}\right]\right\} \tag{4.21}$$

These equations are used to compute (3.8), (3.9), and finally, (3.10), which in turn is used in (2.16) with the values of B_d and d_{free} corresponding to the code rate shown in Table 2 to obtain an upper bound on the probability of information bit error.

a. BPSK/QPSK r=1/2

Figure 11 is a plot of the performance obtained with errors-and-erasures decoding for various values of the parameter α when $\rho = 0.5$ and $E_b/N_0 = 15\,\text{dB}$. As can be seen, performance is relatively insensitive to α for $P_b > 10^{-5}$ and is relatively insensitive for $0.5 \geq \alpha \geq 0.3$ when $P_b > 10^{-10}$; although, $\alpha = 0.5$ yields the best results overall.

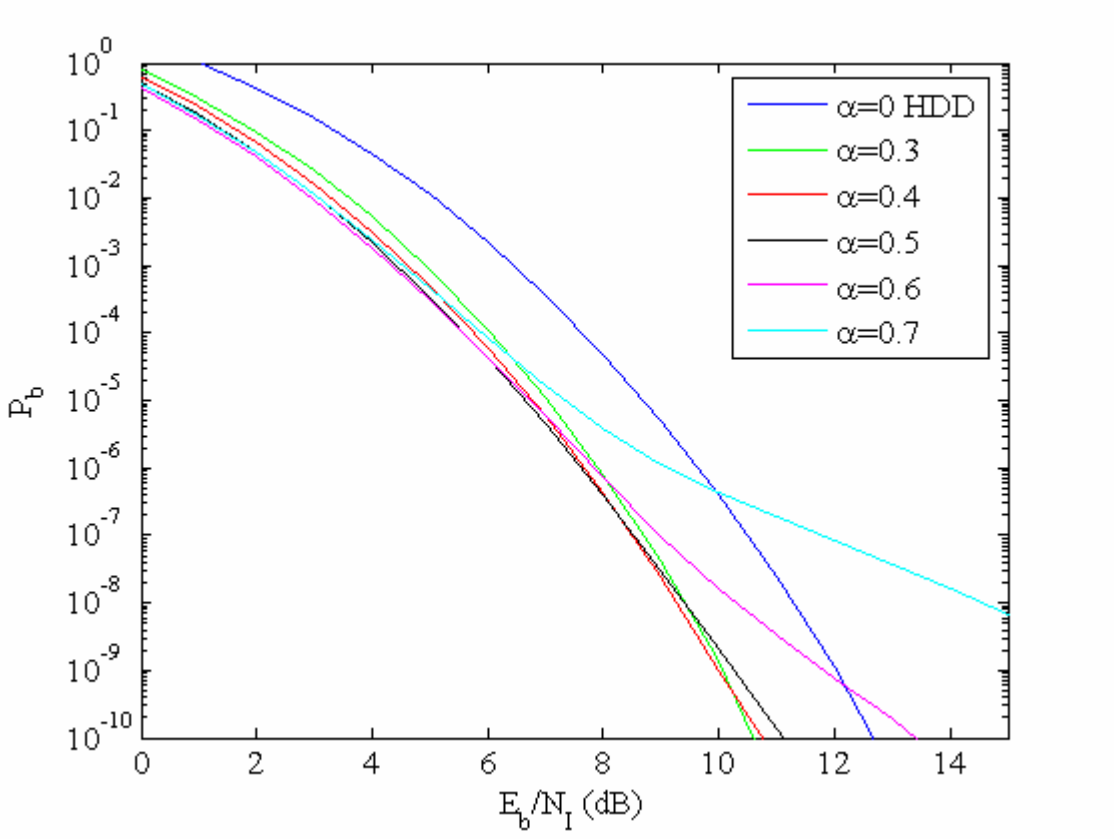

Figure 11. Performance of BPSK/QPSK in AWGN and PNI (ρ=0.5) with r=1/2 convolutional source coding and EED for a channel with no fading ($E_b/N_0 = 15\,\text{dB}$).

Figure 12 is a plot of the performance obtained with errors-and-erasures decoding for various values of the parameter ρ when $\alpha = 0.5$ and $E_b/N_0 = 7.14\,\text{dB}$. This value of E_b/N_0 was chosen since this yields $P_b = 10^{-7}$ for $E_b/N_I = 30\,\text{dB}$. As can be seen, while pulse-noise interference does somewhat degrade performance for certain values of E_b/N_I and ρ, to a large extent the effect of pulse-noise interference has been eliminated. As with HDD, as ρ approaches zero, the performance converges to the AWGN limit, and, generally, the bigger the value of ρ is, the poorer the performance. There is a small range of E_b/N_I where $\rho < 1$ results in performance poorer than for $\rho = 1$, but generally, the degradation is less than 2 dB.

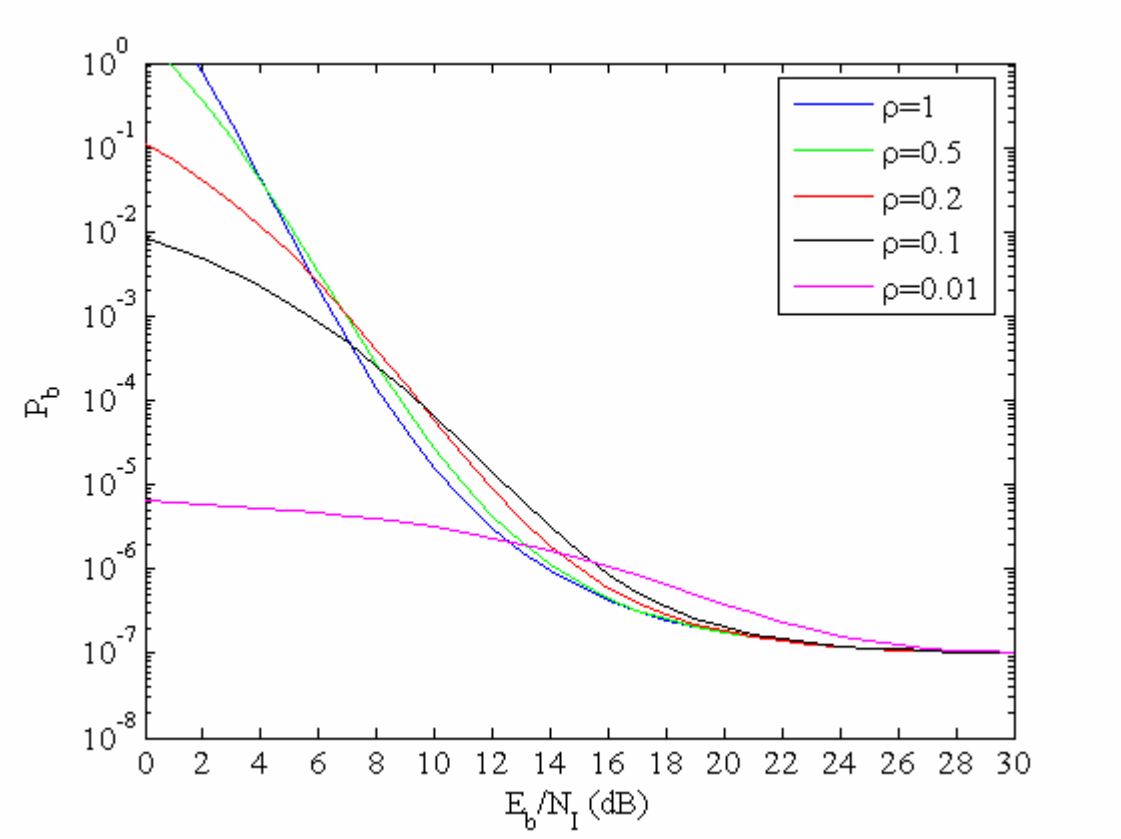

Figure 12. Performance of BPSK/QPSK in AWGN and PNI with r=1/2 convolutional source coding and EED (α=0.5) for a channel with no fading ($E_b/N_0 = 7.14\,\text{dB}$).

b. BPSK/QPSK r=3/4

Figure 13 is a plot of the performance obtained with errors-and-erasures decoding for various values of the parameter α when $\rho = 0.5$ and $E_b/N_0 = 15\,\text{dB}$. In this case, $\alpha = 0.4$ gives better results than $\alpha = 0.5$, which gave the best results for r=1/2.

Figure 14 is a plot of the performance obtained with errors-and-erasures decoding for various values of the parameter ρ when $\alpha = 0.4$ and $E_b/N_0 = 8.73\,\text{dB}$. This value of E_b/N_0 was chosen since this yields $P_b = 10^{-7}$ for $E_b/N_I = 30\,\text{dB}$. As can be seen, pulse-noise interference degrades performance much more than when r=1/2 for certain values of E_b/N_I and ρ, but the effect of pulse-noise interference is much less severe than when soft decision decoding with linear combining is used, as will be seen.

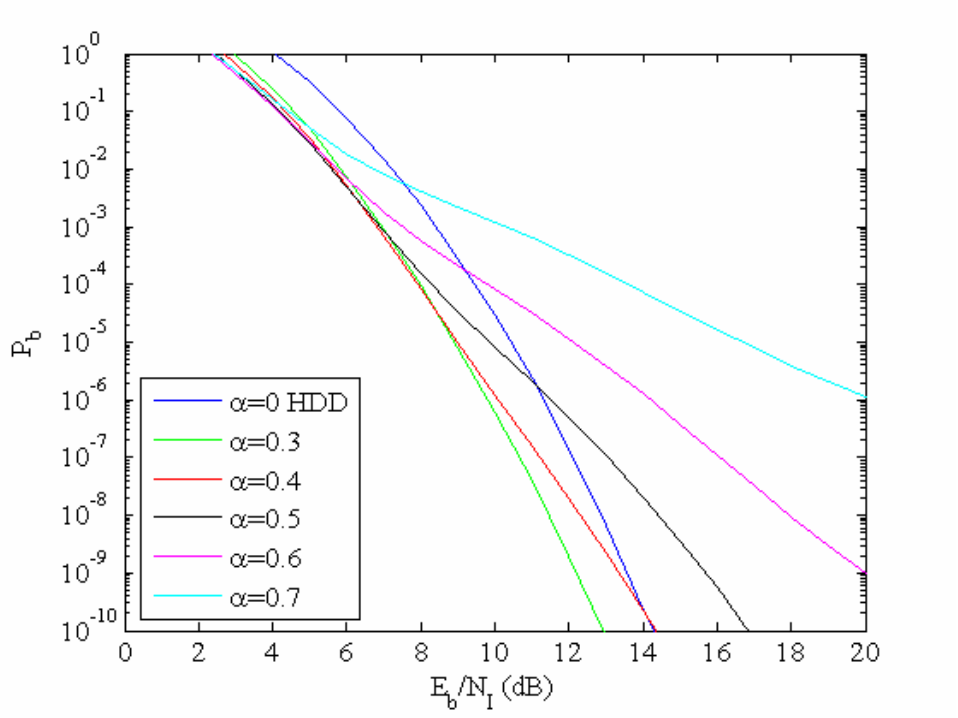

Figure 13. Performance of BPSK/QPSK in AWGN and PNI (ρ=0.5) with r=3/4 convolutional source coding and EED for a channel with no fading ($E_b/N_0 = 15\,\text{dB}$).

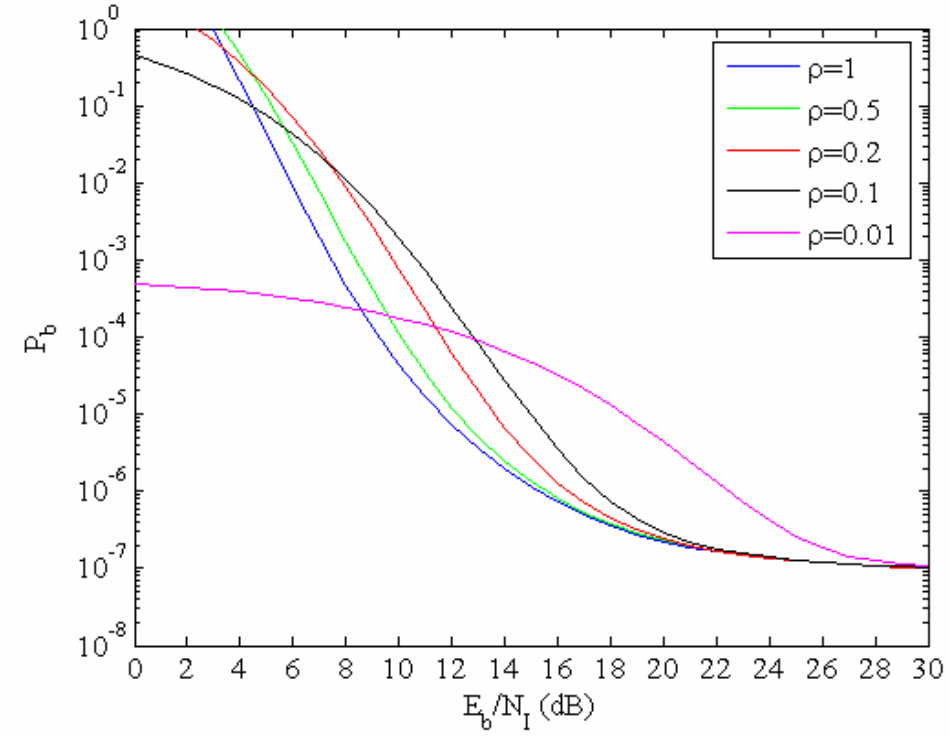

Figure 14. Performance of BPSK/QPSK in AWGN and PNI with r=3/4 convolutional source coding and EED (α=0.5) for a channel with no fading ($E_b/N_0 = 8.73\,\text{dB}$).

2. Performance in AWGN with PNI and Fading

When the channel is modeled as a Nakagami fading channel, then (4.19), (4.20), and (4.21) are conditional probabilities. The unconditional probabilities of channel bit error, channel bit erasure, and channel bit correct detection are found by substituting (4.19), (4.20), and (4.21) into (2.12), respectively. The integrations required to obtain these unconditional probabilities can be evaluated numerically or analytically using the identity (4.8).

a. BPSK/QPSK r=1/2

In Figure 15, the performance is plotted for different fading conditions. In order to validate the results obtained using the analytical solution, the performance is obtained both analytically and numerically. For this figure, $E_b/N_0 = 15\,\text{dB}$, $\rho = 0.5$, and $\alpha = 0.4$.

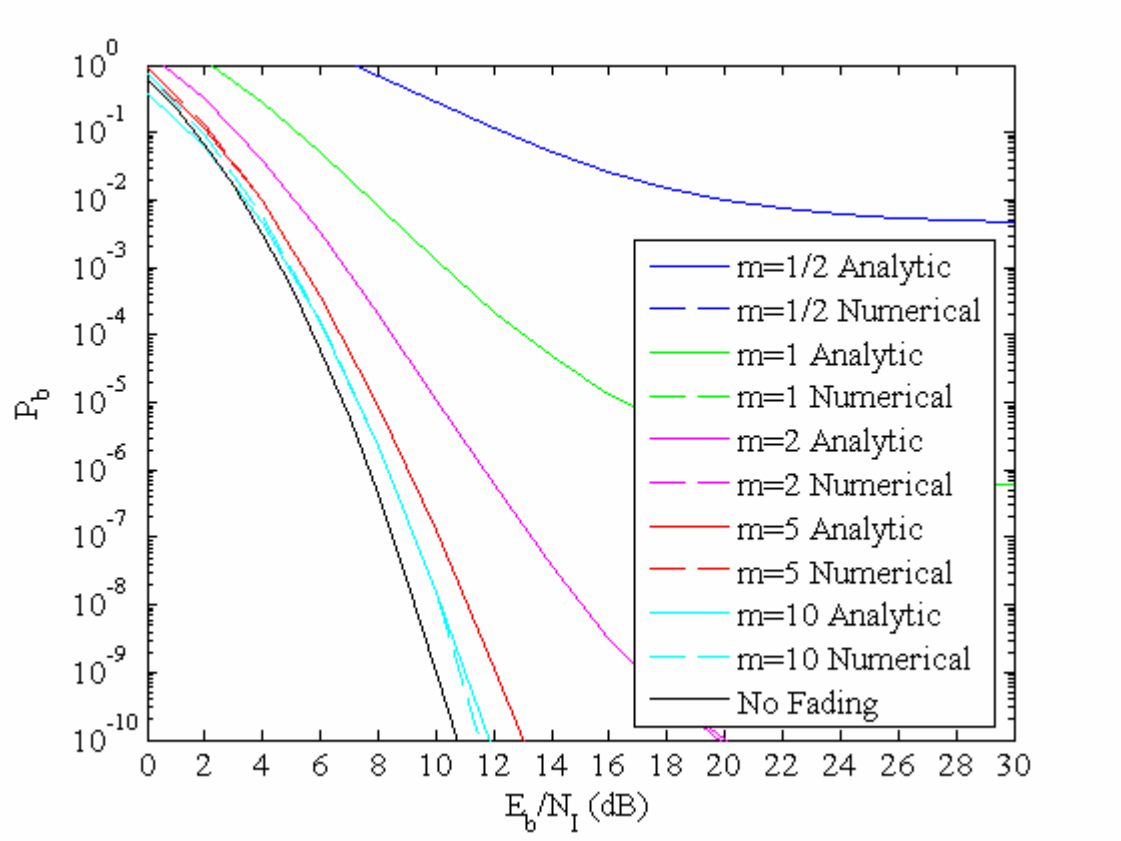

Figure 15. Performance of BPSK/QPSK in AWGN and PNI (ρ=0.5) with r=1/2 convolutional source coding and EED (α=0.4) for a Nakagami fading channel ($E_b/N_0 = 15\,\text{dB}$) computed both analytically and numerically.

It is clear that both methods give virtually identical results for all fading conditions. As can be seen, the receiver performance worsens as the fading conditions worsen and improves as m increases, approaching for m=10 the non-fading condition $(m \to \infty)$.

Figure 16 is a plot of the performance obtained with errors-and-erasures decoding for various values of the parameter α when $\rho = 0.5$, $m = 1$, and $E_b/N_0 = 15\,\text{dB}$. As can be seen, performance is relatively insensitive for $0.5 \geq \alpha \geq 0.3$; although, $\alpha = 0.4$ yields the best results overall.

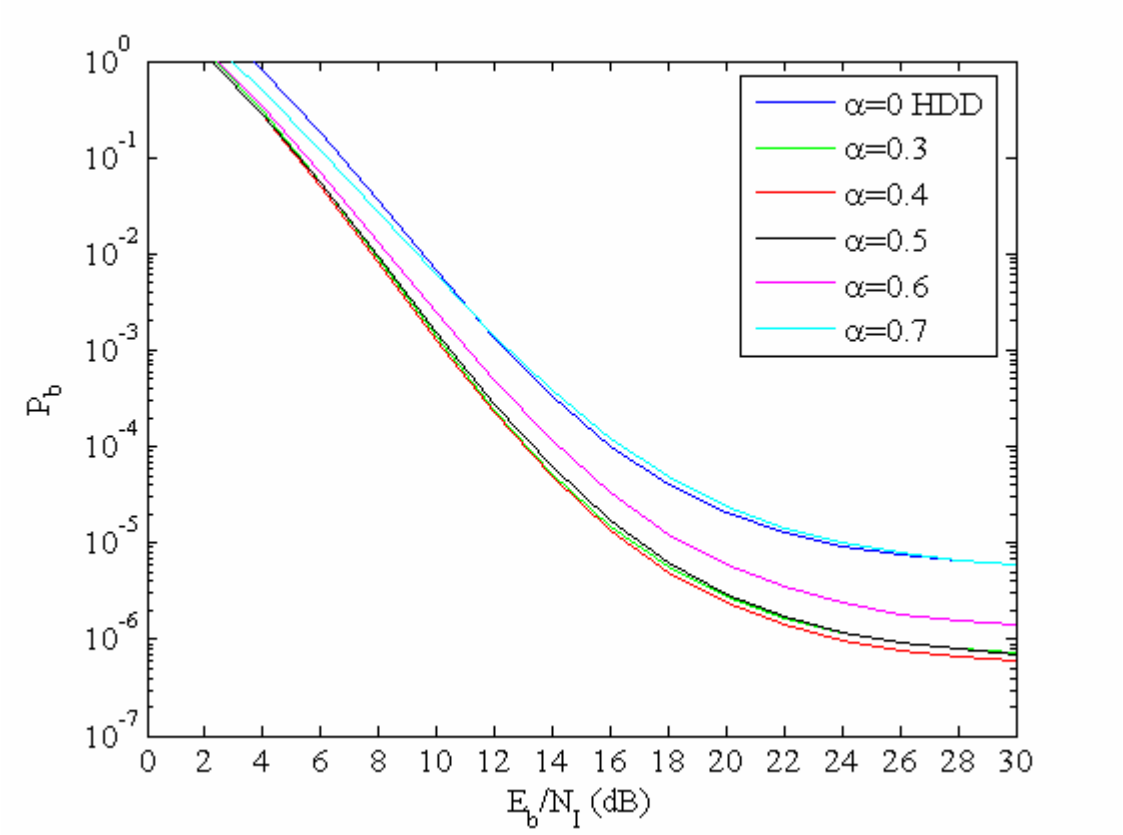

Figure 16. Performance of BPSK/QPSK in AWGN and PNI (ρ=0.5) with r=1/2 convolutional source coding and EED for a Nakagami fading channel (m=1) ($E_b/N_0 = 15\,\text{dB}$).

In Figure 17, the effect that the factor ρ has on the receiver's performance is shown. In this figure, the performance is plotted for various values of the

parameter ρ when $E_b/N_0 = 15\,\text{dB}$, $m = 1$, and $\alpha = 0.4$. As can be seen, varying ρ affects the receiver performance significantly, particularly when $E_b/N_I < 12\,\text{dB}$. Like HDD, it is clear that barrage noise interference $(\rho = 1)$ is more effective than PNI. As ρ approaches zero, the performance converges to the AWGN limit.

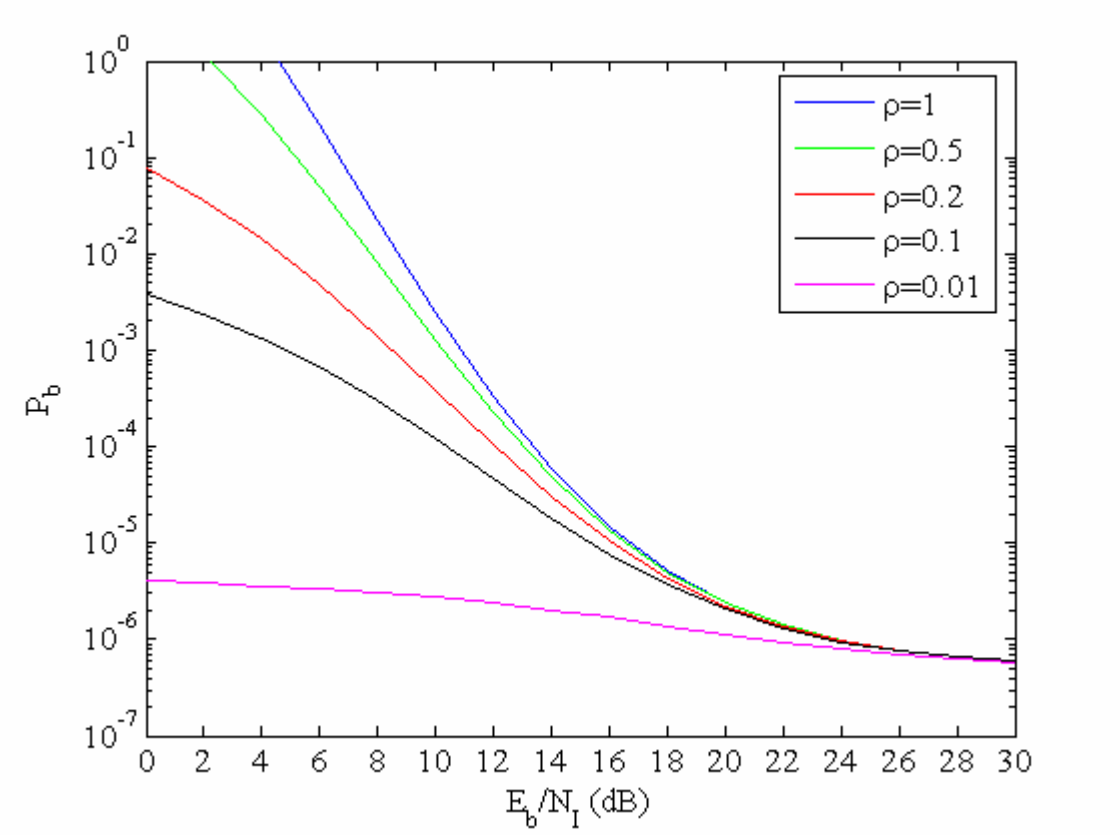

Figure 17. Performance of BPSK/QPSK in AWGN and PNI with r=1/2 convolutional source coding and EED (α=0.4) for a Nakagami fading channel (m=1) ($E_b/N_0 = 15\,\text{dB}$).

b. BPSK/QPSK r=3/4

In Figure 18, the performance is plotted for different fading conditions. In order to validate the results obtained using the analytical solution the performance is obtained both analytically and numerically. For this figure, $E_b/N_0 = 24\,\text{dB}$, $\rho = 1/2$, and $\alpha = 0.4$.

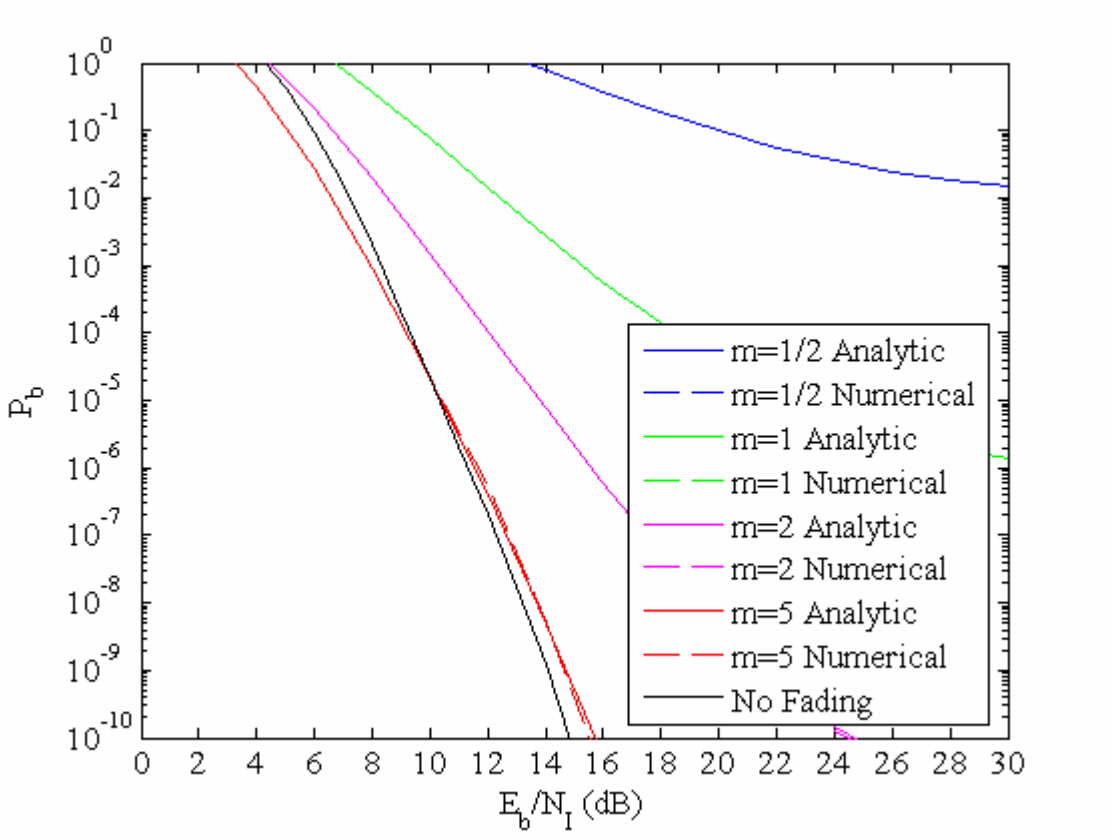

Figure 18. Performance of BPSK/QPSK in AWGN and PNI (ρ=0.5) with r=3/4 convolutional source coding and EED (α=0.4) for a Nakagami fading channel ($E_b/N_0 = 24\,\text{dB}$) computed both analytically and numerically.

Again, both methods give virtually identical results for all fading conditions. It is obvious that in this case the effect of the channel fading is more severe than for r=1/2.

Figure 19 is a plot of the performance obtained with errors-and-erasures decoding for various values of the parameter α when $\rho = 0.5$, $m = 1$, and $E_b/N_0 = 24\,\text{dB}$. In this case, performance is relatively insensitive for $0.6 \geq \alpha \geq 0.3$; although, $\alpha = 0.4$ yields the best results overall.

In Figure 20 the performance is plotted for various values of the parameter ρ when $E_b/N_0 = 24\,\text{dB}$, $m = 1$, and $\alpha = 0.4$. Like Figure 17, the bigger the value of ρ is, the poorer the performance, especially when $E_b/N_I < 12\,\text{dB}$.

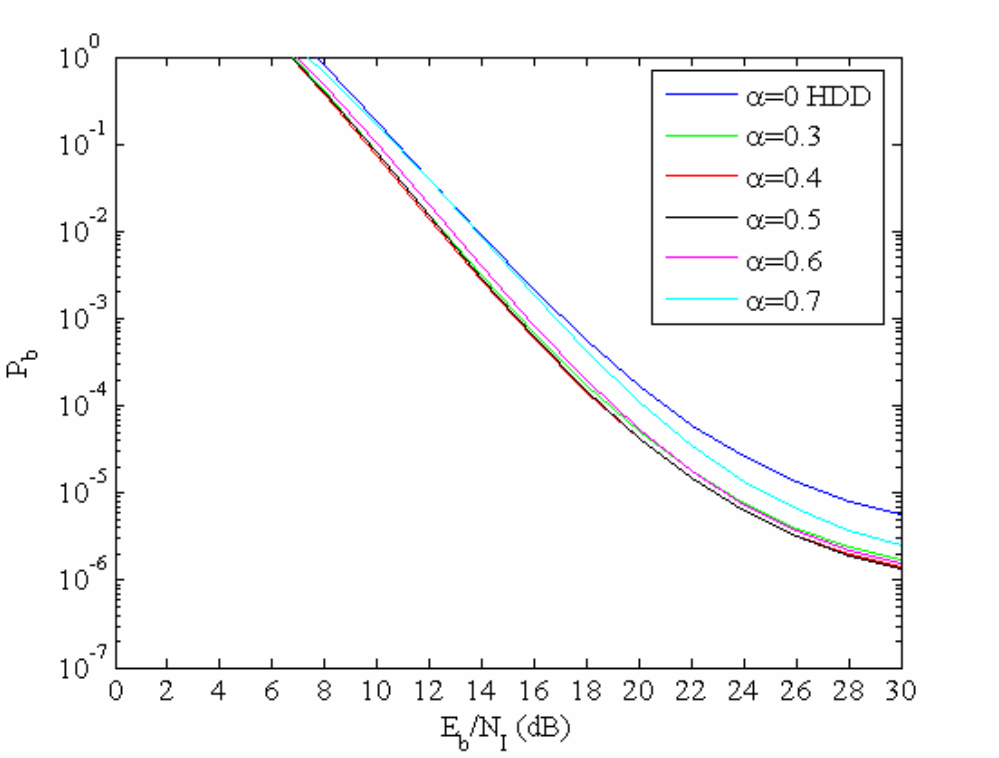

Figure 19. Performance of BPSK/QPSK in AWGN and PNI (ρ=0.5) with r=3/4 convolutional source coding and EED for a Nakagami fading channel (m=1) ($E_b/N_0 = 24\,\text{dB}$).

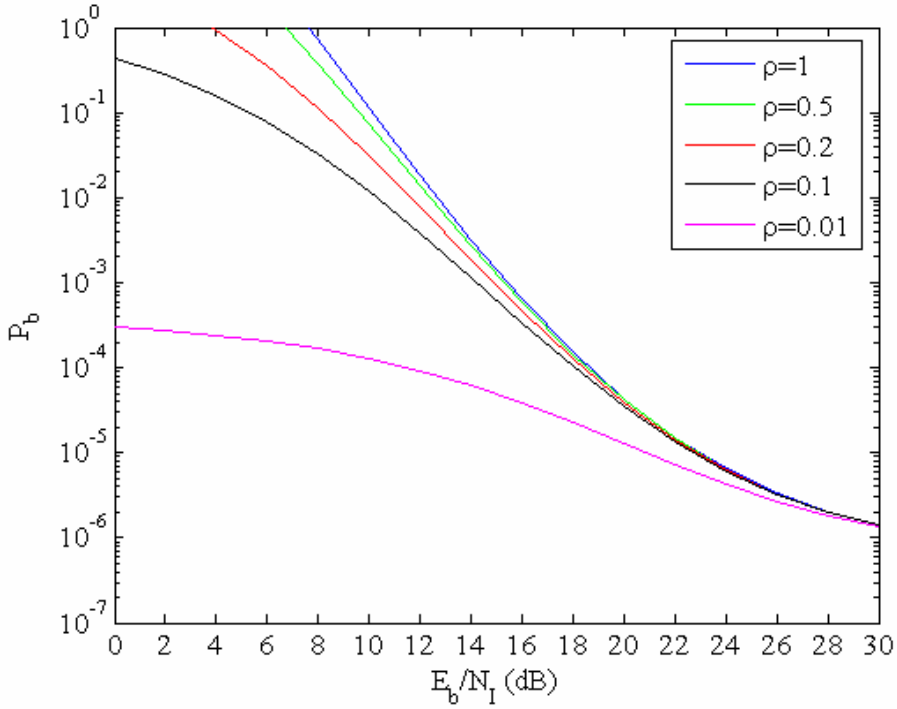

Figure 20. Performance of BPSK/QPSK in AWGN and PNI with r=3/4 convolutional source coding and EED (α=0.4) for a Nakagami fading channel (m=1) ($E_b/N_0 = 24\,\text{dB}$).

C. SOFT DECISION DECODING (SDD)

In this section we examine the performance of SDD with liner combining. The performance of this receiver was examined comprehensively in Chapters IV and III in [10] and [11], respectively. Here we will not discuss the theory of this receiver, but we report some numerical results in order to compare the performance obtained with EED to that which can be obtained with HDD and SDD with linear combining.

1. Performance in AWGN with PNI (No Fading)

a. BPSK/QPSK r=1/2

Figure 21 is a plot of the performance obtained with SDD with linear combining for various values of the parameter ρ when $E_b/N_0 = 5.36\,\text{dB}$. This value of E_b/N_0 was chosen since this yields $P_b = 10^{-7}$ for $E_b/N_I = 30\,\text{dB}$. As can be seen, unlike HDD and EED, PNI is significantly more effective than barrage noise interference ($\rho = 1$).

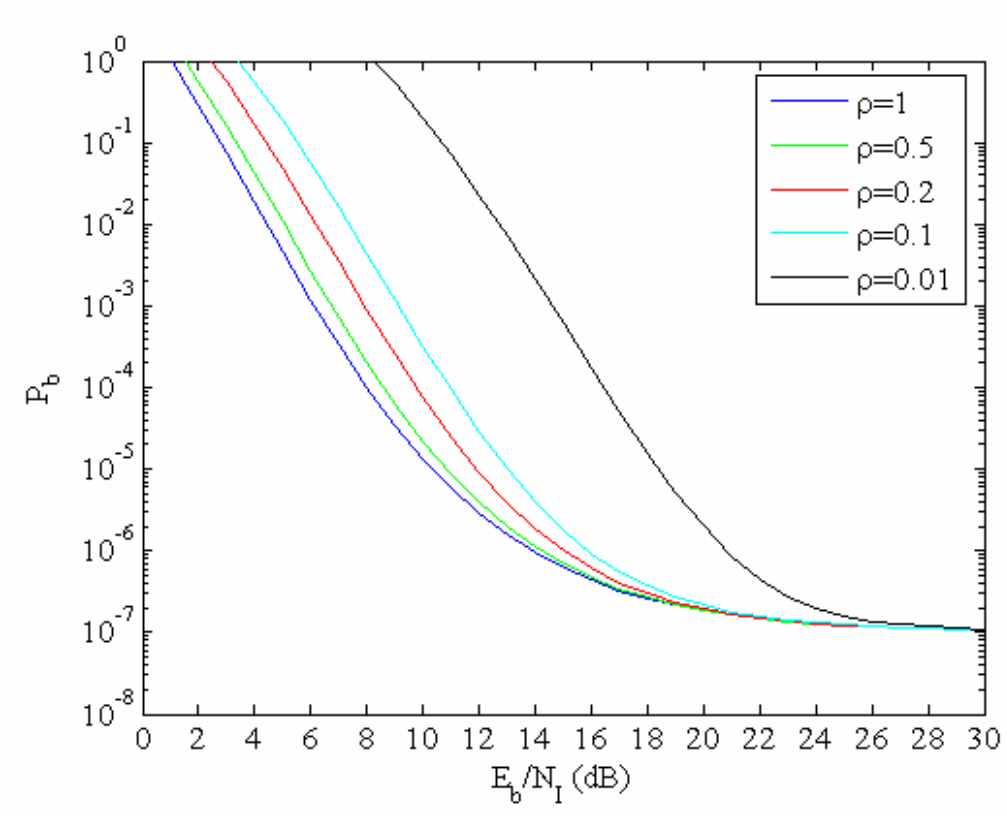

Figure 21. Performance of BPSK/QPSK in AWGN and PNI with *r*=1/2 convolutional source coding and SDD with linear combining for a channel with no fading ($E_b/N_0 = 5.36\,\text{dB}$).

b. BPSK/QPSK r=3/4

In Figure 22, which is analogous to Figure 21, the performance is plotted for various values of the parameter ρ when $E_b/N_0 = 6.4\,\text{dB}$ which yields $P_b = 10^{-7}$ for $E_b/N_I = 30\,\text{dB}$. As was the case with the previous plot, performance worsens for decreasing ρ.

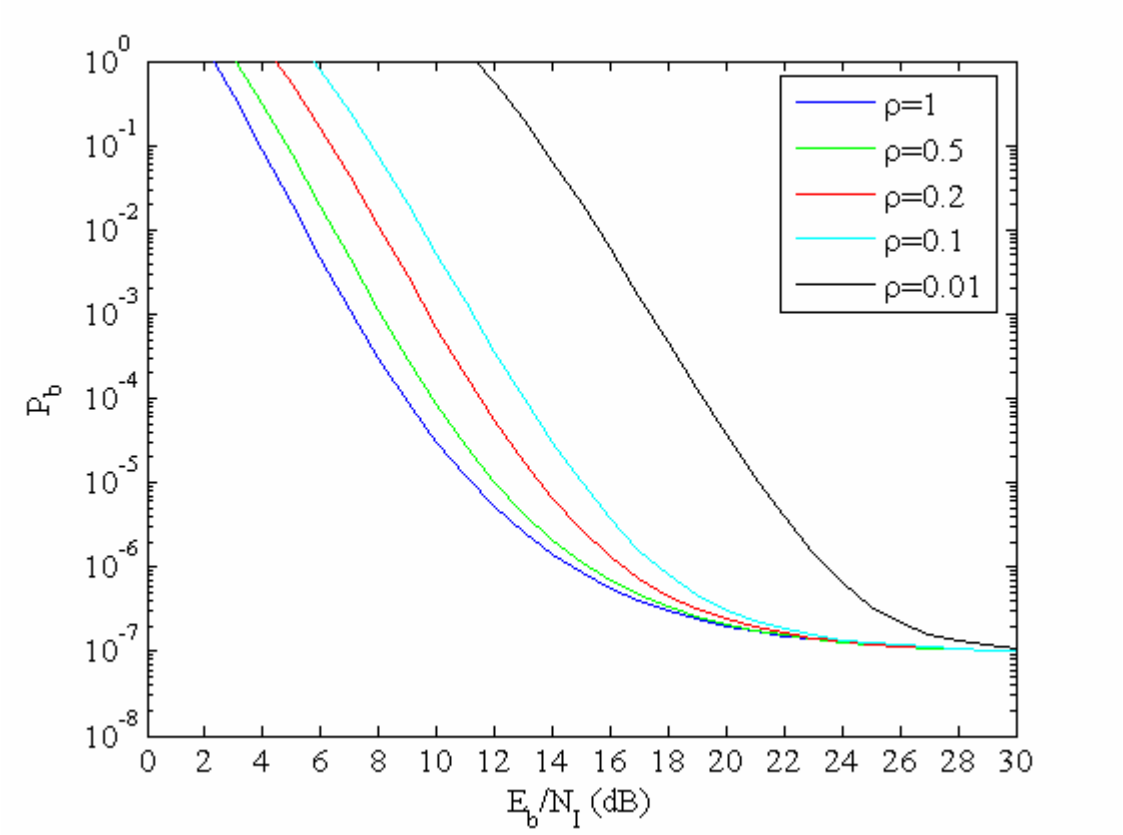

Figure 22. Performance of BPSK/QPSK in AWGN and PNI with *r*=3/4 convolutional source coding and SDD with linear combining for a channel with no fading ($E_b/N_0 = 6.4\,\text{dB}$).

2. Performance in AWGN with PNI and Fading

a. BPSK/QPSK r=1/2

In Figure 23, the performance of a receiver with SDD and linear combining is plotted for different fading conditions and various values of the parameter ρ for $E_b/N_0 = 15\,\text{dB}$. As might be expected, there is performance degradation for more severe fading conditions.

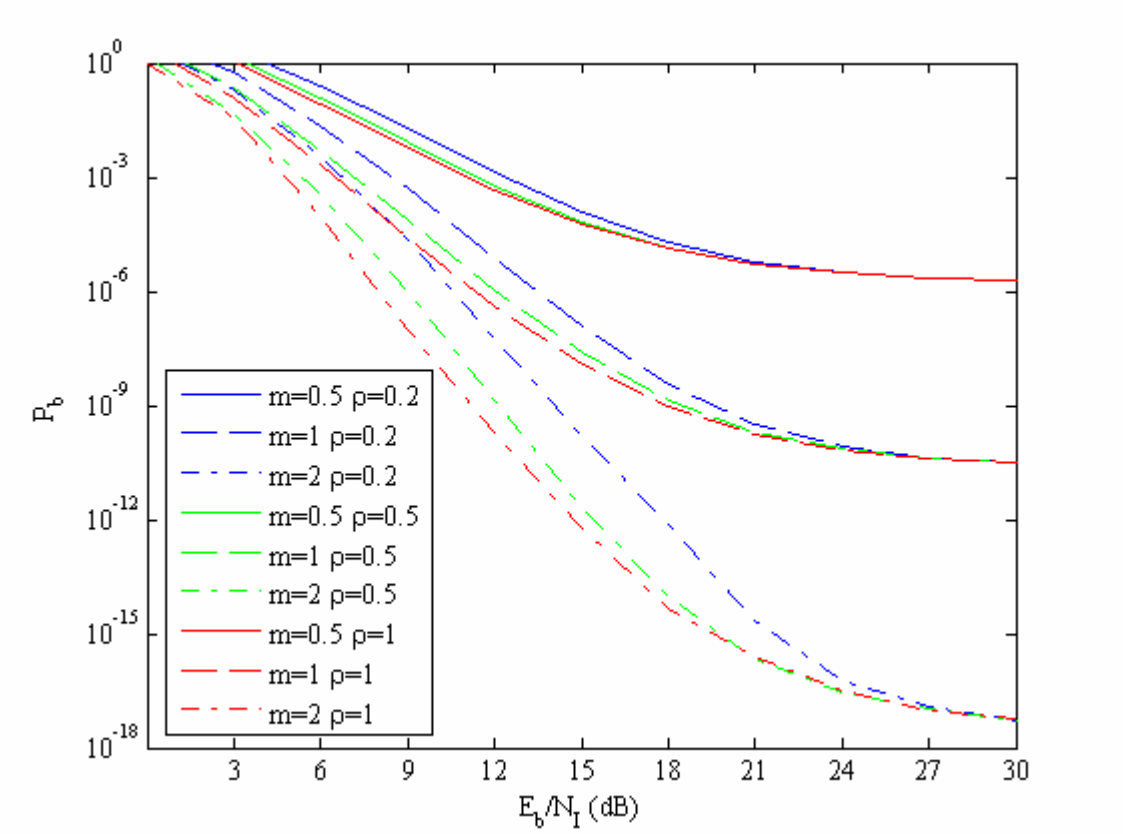

Figure 23. Performance of BPSK/QPSK in AWGN and PNI with r=1/2 convolutional source coding and SDD with linear combining for a Nakagami fading channel ($E_b/N_0 = 15\text{dB}$) (After Ref. [11]).

b. BPSK/QPSK r=3/4

In Figure 24, the performance of a receiver with SDD and linear combining is plotted for different fading conditions and for m=1 for various values of the parameter ρ, with $E_b/N_0 = 15\text{dB}$. As was the case in the previous plot, the receiver performance becomes poorer as the fading conditions worsen.

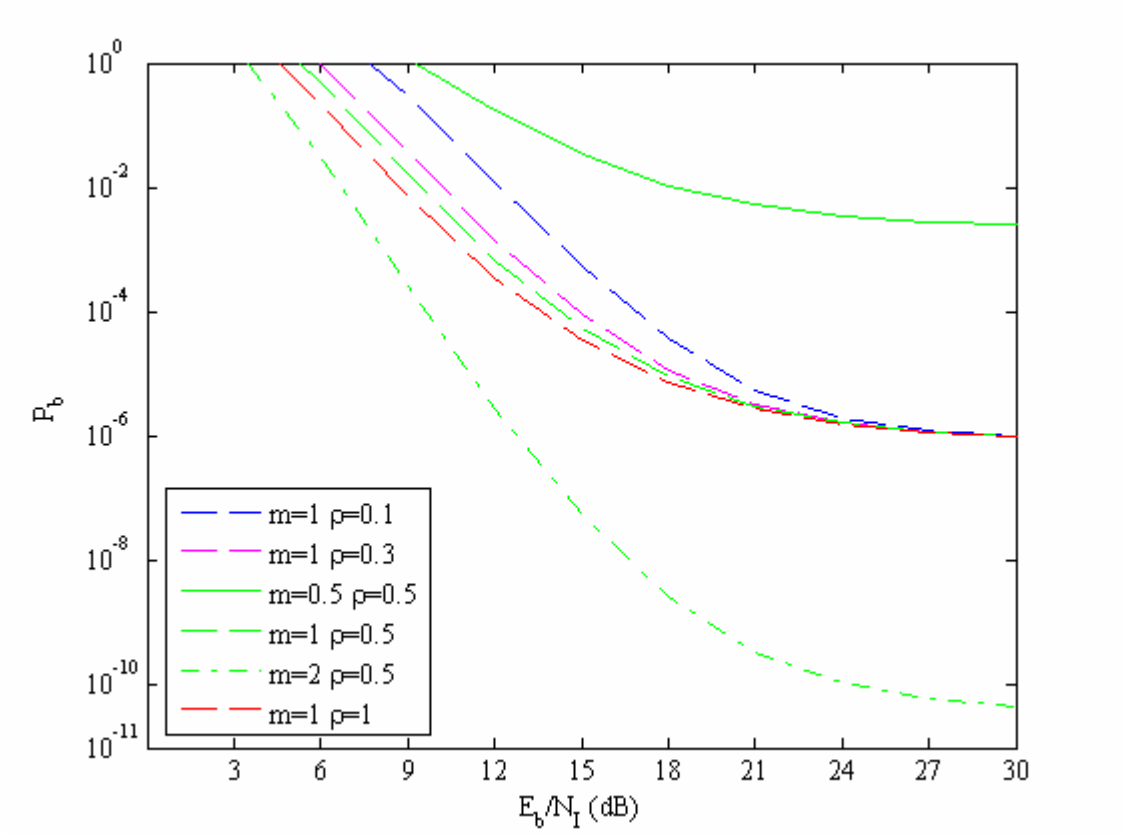

Figure 24. Performance of BPSK/QPSK in AWGN and PNI with *r*=3/4 convolutional source coding and SDD with linear combining for a Nakagami fading channel ($E_b/N_0 = 15\,\text{dB}$).

D. COMPARISONS OF THE PERFORMANCE WITH HDD, EED AND SDD.

1. Comparisons in AWGN with PNI (No Fading)

a. BPSK/QPSK r=1/2

Figures 25 through 27 are a comparison of the performance obtained with errors-and-erasures decoding (EED), hard decision decoding, and soft decision decoding with linear combining. For hard decision decoding, $E_b/N_0 = 7.14\,\text{dB}$. For soft decision decoding with linear combining, $E_b/N_0 = 5.36\,\text{dB}$, which yields $P_b = 10^{-7}$ for $E_b/N_I = 30\,\text{dB}$. The performance of errors-and-erasures decoding is plotted for both $E_b/N_0 = 5.36\,\text{dB}$, which allows comparisons with soft decision decoding with linear combining on an equal energy basis, and $E_b/N_0 = 7.14\,\text{dB}$, which allows comparisons

with soft decision decoding with linear combining where both systems have the same error floor for $E_b/N_I = 30\,\text{dB}$.

In Figure 25, ρ = 1, corresponding to continuous noise interference. In this case, given the extra 1.8 dB in E_b/N_0, the performances obtained for errors-and-erasures decoding and soft decision decoding with linear combining are virtually indistinguishable from one another, while the performance obtained with hard decision decoding is clearly inferior relative to that obtained for errors-and-erasures decoding and soft decision decoding with linear combining. When errors-and-erasures decoding and soft decision decoding with linear combining are compared for the same E_b/N_0, soft decision decoding with linear combining is clearly superior for all E_b/N_I; although, errors-and-erasures decoding with $E_b/N_0 = 5.36\,\text{dB}$ is superior to hard decision decoding with $E_b/N_0 = 7.14\,\text{dB}$ for $E_b/N_I < 10\,\text{dB}$.

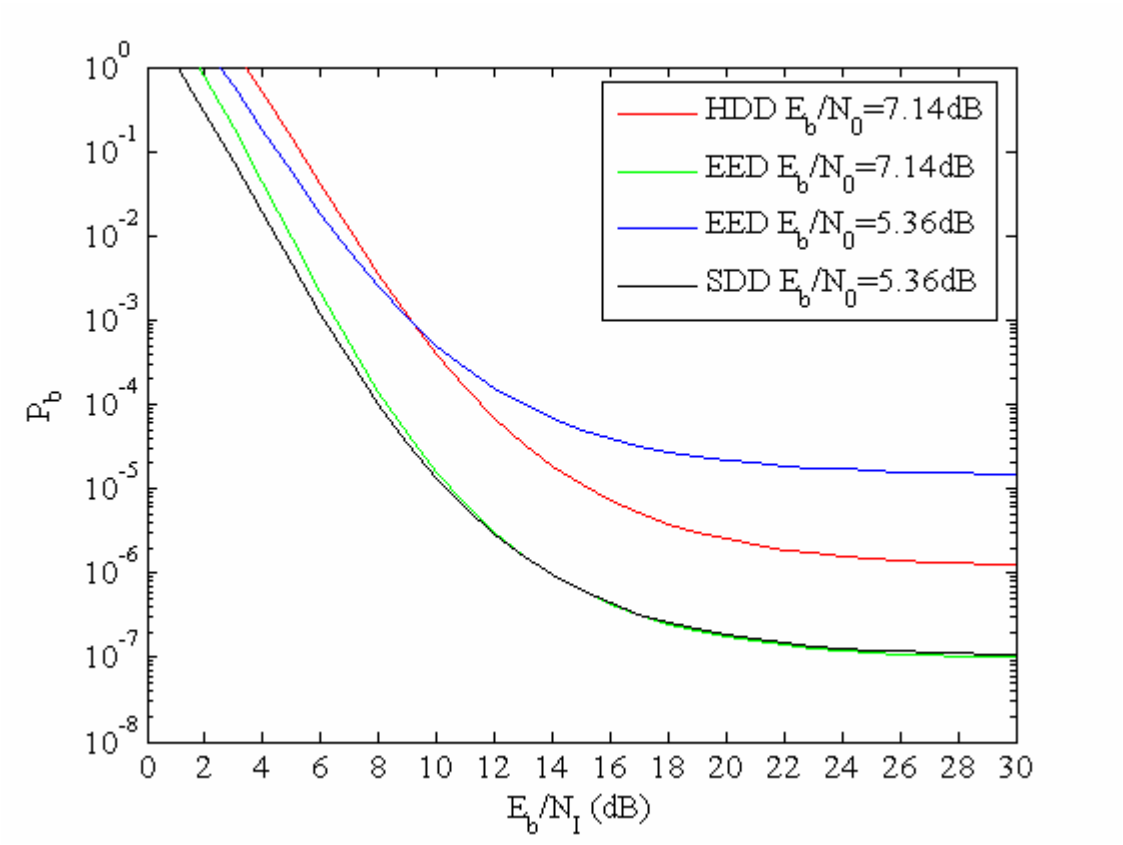

Figure 25. Performance for EED, HDD, and SDD with linear combining for a channel with no fading, α=0.5, and ρ = 1 (r=1/2).

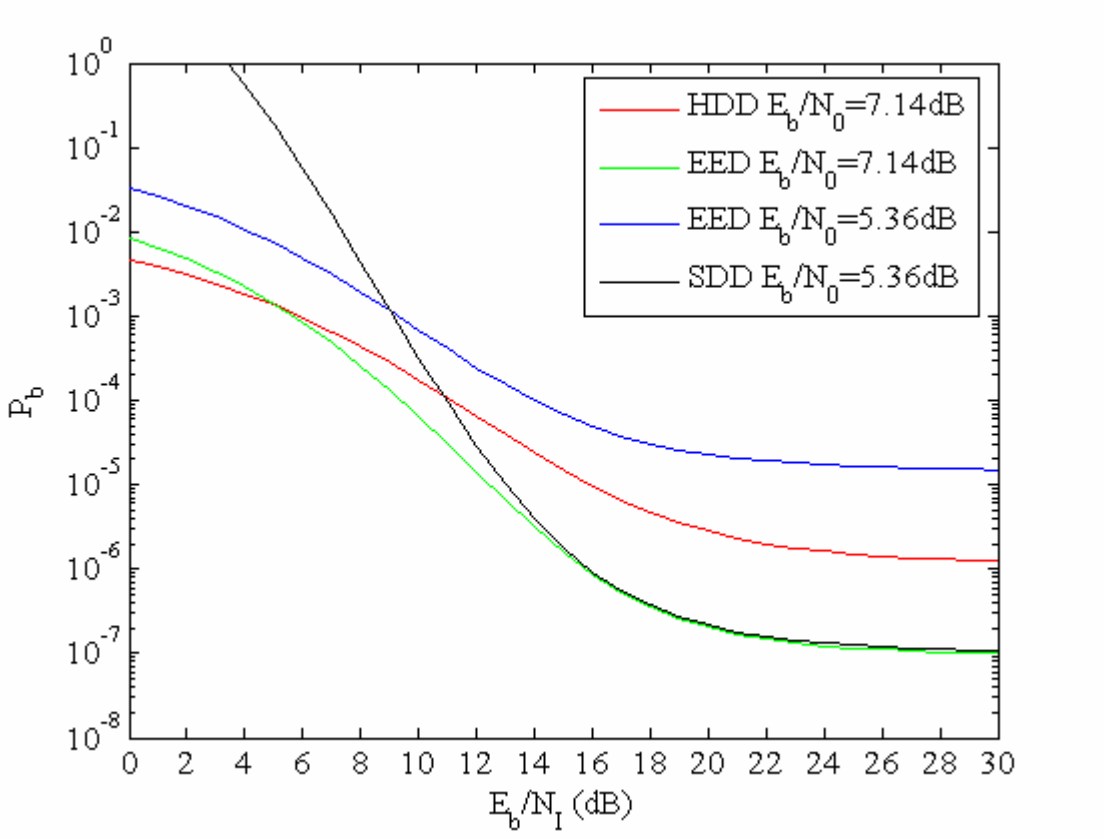

Figure 26. Performance for EED, HDD, and SDD with linear combining for a channel with no fading, α = 0.5, and ρ = 0.1 (r=1/2).

In Figure 26, ρ = 0.1. While hard decision decoding outperforms soft decision decoding with linear combining for $E_b/N_I < 11$dB (roughly $E_b/N_I < 10\log\rho^{-1}$ dB), errors-and-erasures decoding with a 1.8 dB advantage in E_b/N_0 either outperforms or is as good as soft decision decoding with linear combining for all E_b/N_I. For $E_b/N_I < 10\log\rho^{-1}$ dB, errors-and-erasures decoding has a distinct advantage over soft decision decoding with linear combining. When errors-and-erasures decoding and soft decision decoding with linear combining are compared for the same E_b/N_0, errors-and-erasures decoding has an advantage over soft decision decoding with linear combining only when $E_b/N_I < 10\log\rho^{-1}$ dB, and the error floor for errors-and-erasures decoding is two orders of magnitude higher than the error floor for soft decision decoding with linear combining.

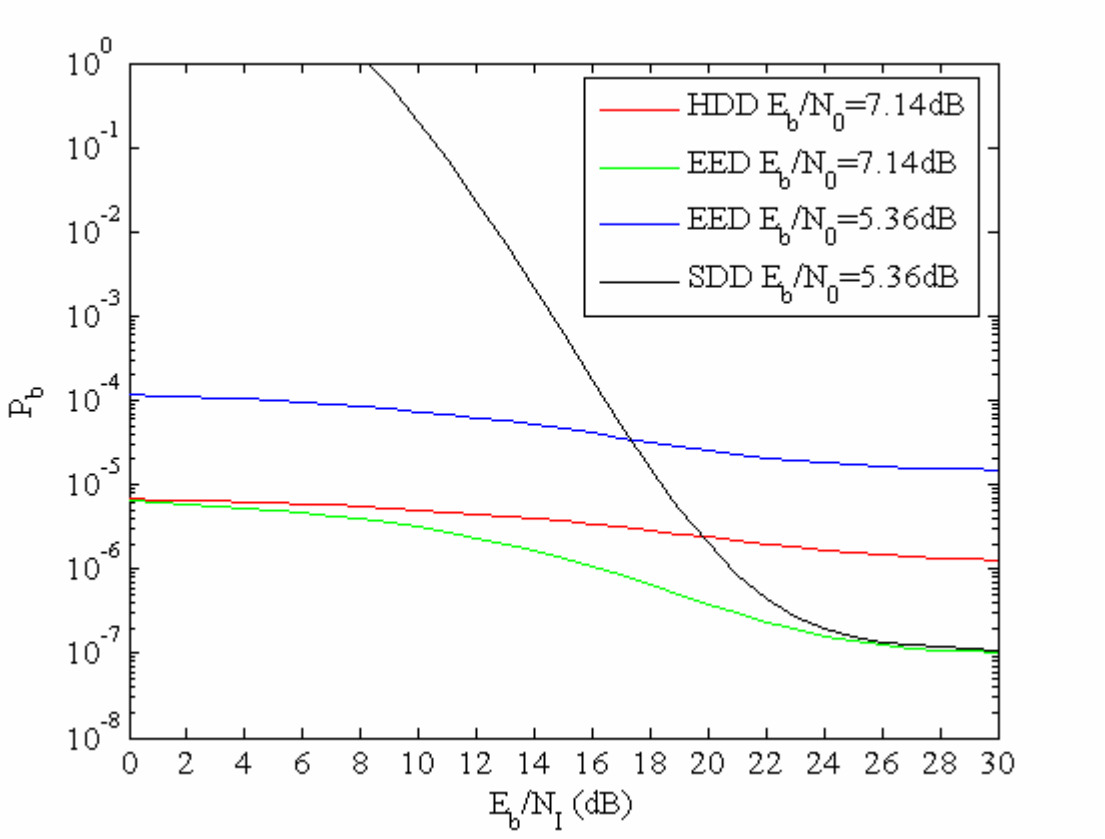

Figure 27. Performance for EED, HDD, and SDD with linear combining for a channel with no fading, α = 0.5, and ρ = 0.01 (r=1/2).

In Figure 27, ρ = 0.01, and, as with ρ = 0.1, hard decision decoding outperforms soft decision decoding with linear combining for $E_b/N_I < 20\,\text{dB}$ (again, roughly $E_b/N_I < 10\log\rho^{-1}\,\text{dB}$), and errors-and-erasures decoding with a 1.8 dB advantage in E_b/N_0 either outperforms or is as good as soft decision decoding with linear combining for all E_b/N_I. In this case, for $E_b/N_I < 10\log\rho^{-1}\,\text{dB}$, errors-and-erasures decoding has a significant advantage over soft decision decoding with linear combining.

b. BPSK/QPSK r=3/4

Figures 28 through 30, which are analogous to Figures 25 through 27, respectively, are a comparison of the performance obtained with errors-and-erasures decoding (EED), hard decision decoding, and soft decision decoding with linear combining for the code rate of 3/4. For hard decision decoding, $E_b/N_0 = 8.73\,\text{dB}$. For

soft decision decoding with linear combining, $E_b/N_0 = 6.4\,\text{dB}$, which yields $P_b = 10^{-7}$ for $E_b/N_I = 30\,\text{dB}$. The performance for errors-and-erasures decoding is plotted for both $E_b/N_0 = 6.4\,\text{dB}$, which allows comparisons with soft decision decoding with linear combining on an equal energy basis, and $E_b/N_0 = 8.73\,\text{dB}$, which allows comparisons with soft decision decoding with linear combining where both systems have the same error floor for $E_b/N_I = 30\,\text{dB}$. As might be expected, for this code rate, the effect of the PNI on the receiver is more severe than what can be obtained with a code rate of 1/2.

In Figure 28, ρ = 1, corresponding to continuous noise interference.

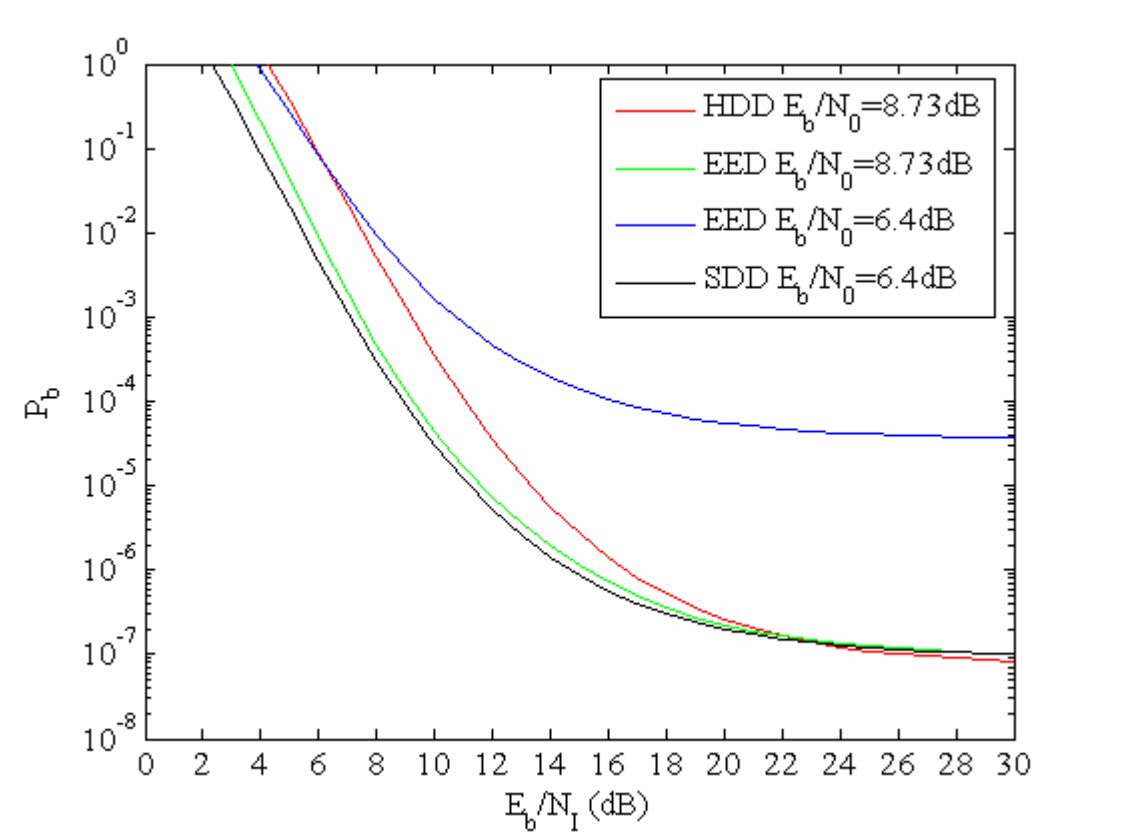

Figure 28. Performance for EED, HDD, and SDD with linear combining for a channel with no fading, α = 0.5, and ρ = 1 (r=3/4).

In this case, given the extra 2.33 dB in E_b/N_0 (0.5 dB more than the r=1/2 case), the performances obtained for errors-and-erasures decoding and soft decision decoding with linear combining are very close to each other, while the performance

obtained with hard decision decoding is clearly inferior relative to that obtained for errors-and-erasures decoding and soft decision decoding with linear combining for $E_b/N_I < 20\,\text{dB}$. The difference between Figure 28 and Figure 25 is that for $E_b/N_I > 20\,\text{dB}$, HDD, EED, and SDD with linear combining have the same performance as they converge to the AWGN limit. When errors-and-erasures decoding and soft decision decoding with linear combining are compared for the same E_b/N_0, soft decision decoding with linear combining is clearly superior for all E_b/N_I.

In Figure 29, ρ = 0.1. While hard decision decoding outperforms soft decision decoding with linear combining for $E_b/N_I < 9.5\,\text{dB}$ (roughly $E_b/N_I < 10\log\rho^{-1}\,\text{dB}$), errors-and-erasures decoding with a 2.33 dB advantage in E_b/N_0 either outperforms or is as good as soft decision decoding with linear combining for all E_b/N_I. For $E_b/N_I < 10\log\rho^{-1}\,\text{dB}$, errors-and-erasures decoding has a distinct advantage over soft decision decoding with linear combining. Again, for $E_b/N_I > 24\,\text{dB}$, all the decoding techniques have the same performance as they converge to the AWGN limit. When errors-and-erasures decoding and soft decision decoding with linear combining are compared for the same E_b/N_0, errors-and-erasures decoding has an advantage over soft decision decoding with linear combining only when $E_b/N_I < 10\log\rho^{-1}\,\text{dB}$.

In Figure 30, ρ = 0.01. In this case, hard decision decoding and errors-and-erasures decoding with a 2.33 dB advantage in E_b/N_0 either outperforms or is as good as soft decision decoding with linear combining for all E_b/N_I. Especially for $E_b/N_I < 10\log\rho^{-1}\,\text{dB}$, HDD and EED have a significant advantage over soft decision decoding with linear combining. A significant observation is that for $E_b/N_I < 18\,\text{dB}$, HDD outperforms EED.

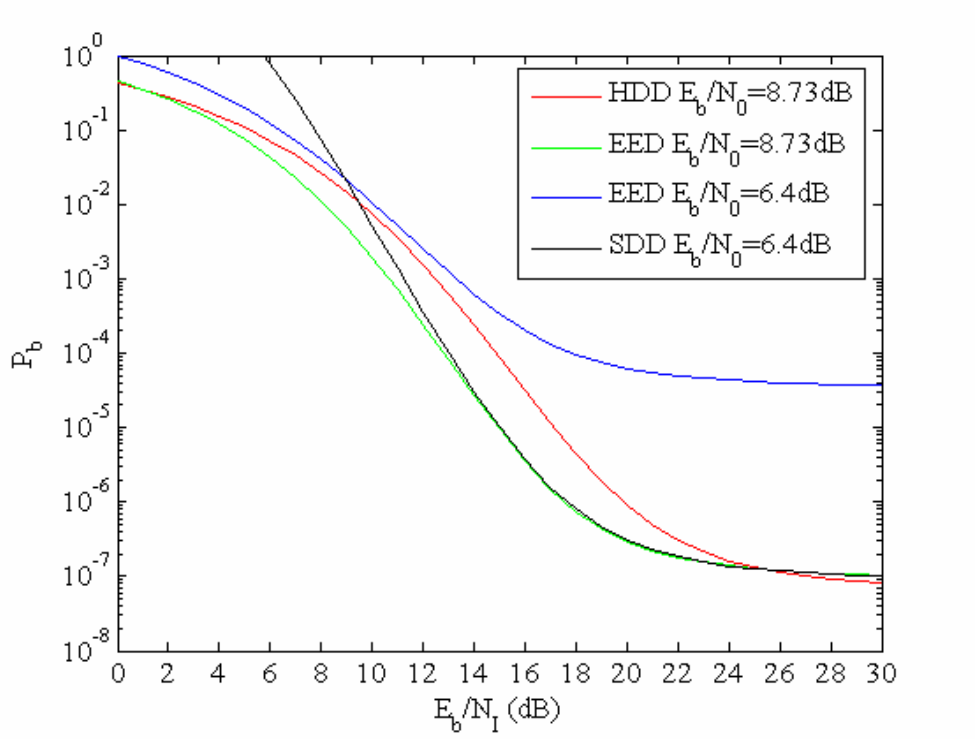

Figure 29. Performance for EED, HDD, and SDD with linear combining for a channel with no fading, α = 0.5, and ρ = 0.1 (r=3/4).

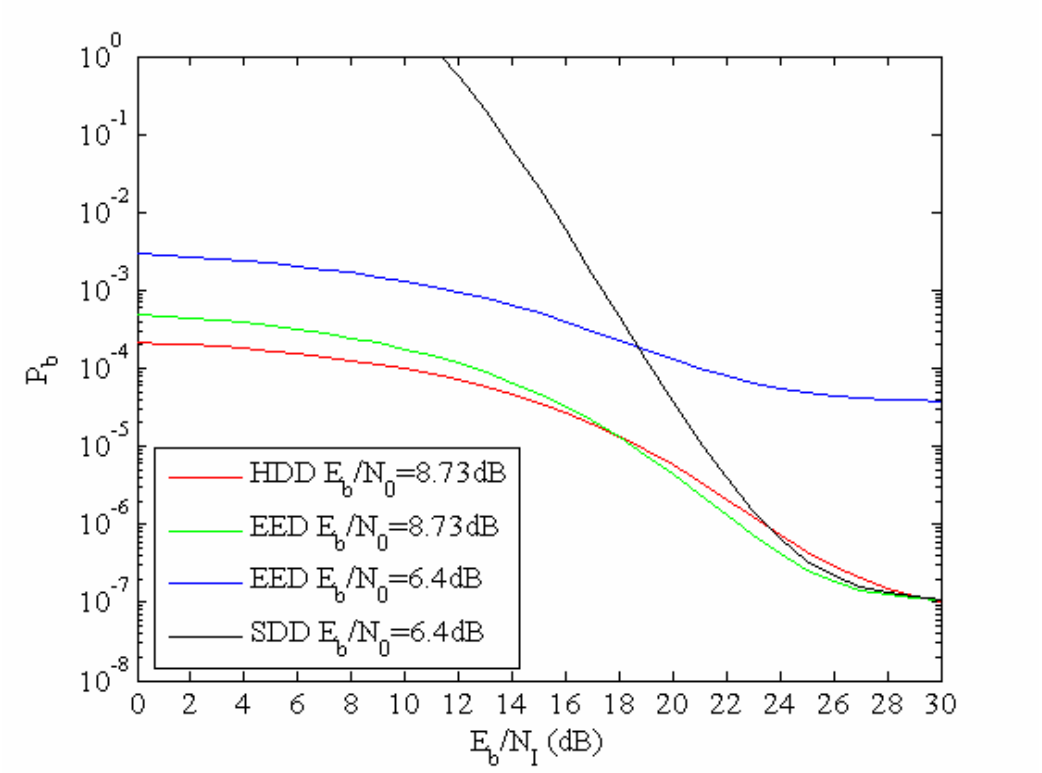

Figure 30. Performance for EED, HDD, and SDD with linear combining for a channel with no fading, α = 0.5, and ρ = 0.01 (r=3/4).

2. Comparisons in AWGN with PNI and Fading

a. BPSK/QPSK r=1/2

The effect of channel fading can be seen in Figures 31, 32, and 33, where m = 0.5, m = 1, and m = 2, respectively. In each of these three figures, $E_b/N_0 = 15\,\text{dB}$ for soft decision decoding with linear combining and $E_b/N_0 = 26\,\text{dB}$, $E_b/N_0 = 23\,\text{dB}$, and $E_b/N_0 = 18\,\text{dB}$ for errors-and-erasures decoding and hard decision decoding when m=0.5, m = 1, and m = 2, respectively. In each of these cases, we see that errors-and-erasures decoding outperforms soft decision decoding with linear combining for E_b/N_I less than about 10 dB.

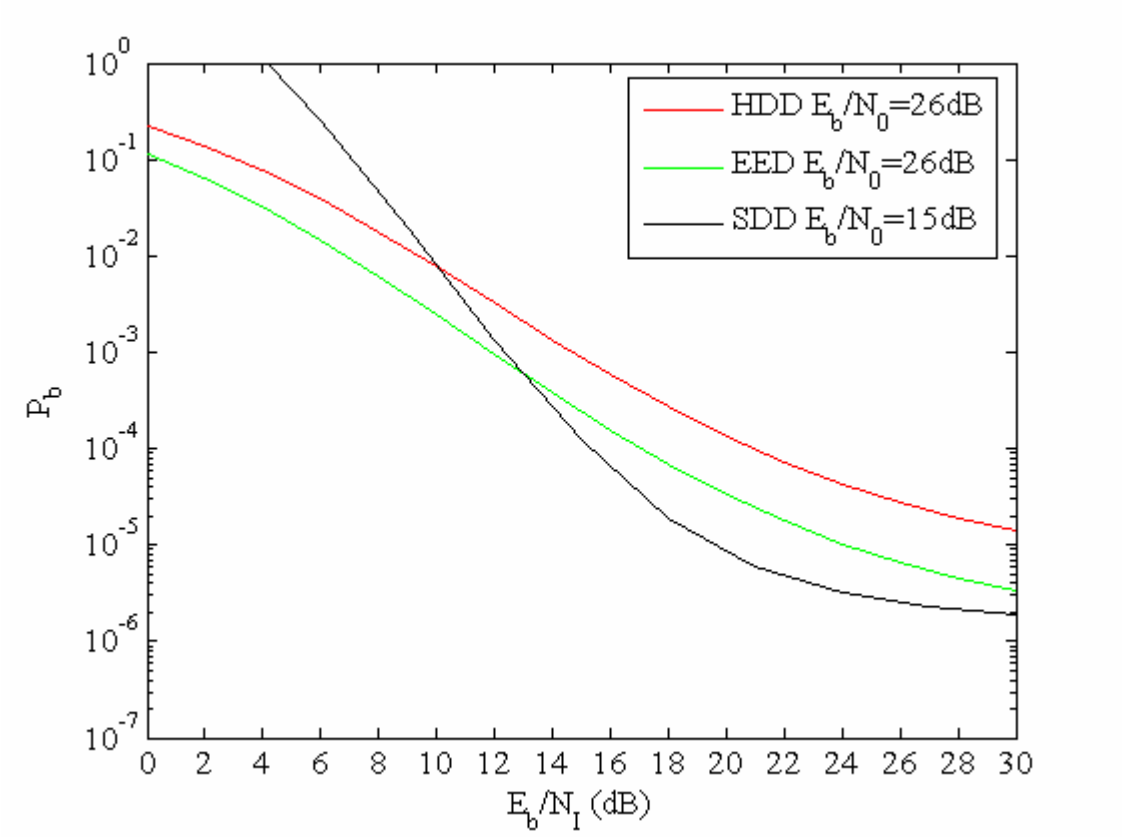

Figure 31. Performance for EED, HDD, and SDD with linear combining for a Nakagami fading channel with m=0.5, α = 0.4, and ρ = 0.2 (r=1/2).

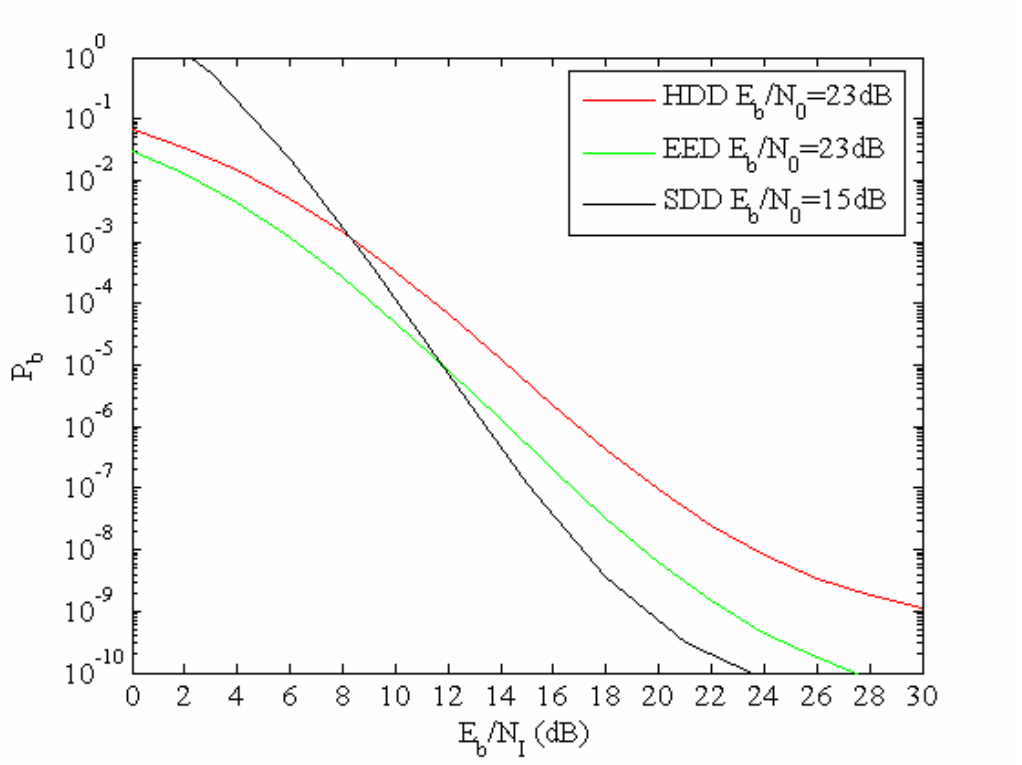

Figure 32. Performance for EED, HDD, and SDD with linear combining for a Nakagami fading channel with m=1, α = 0.4, and ρ = 0.2 (r=1/2).

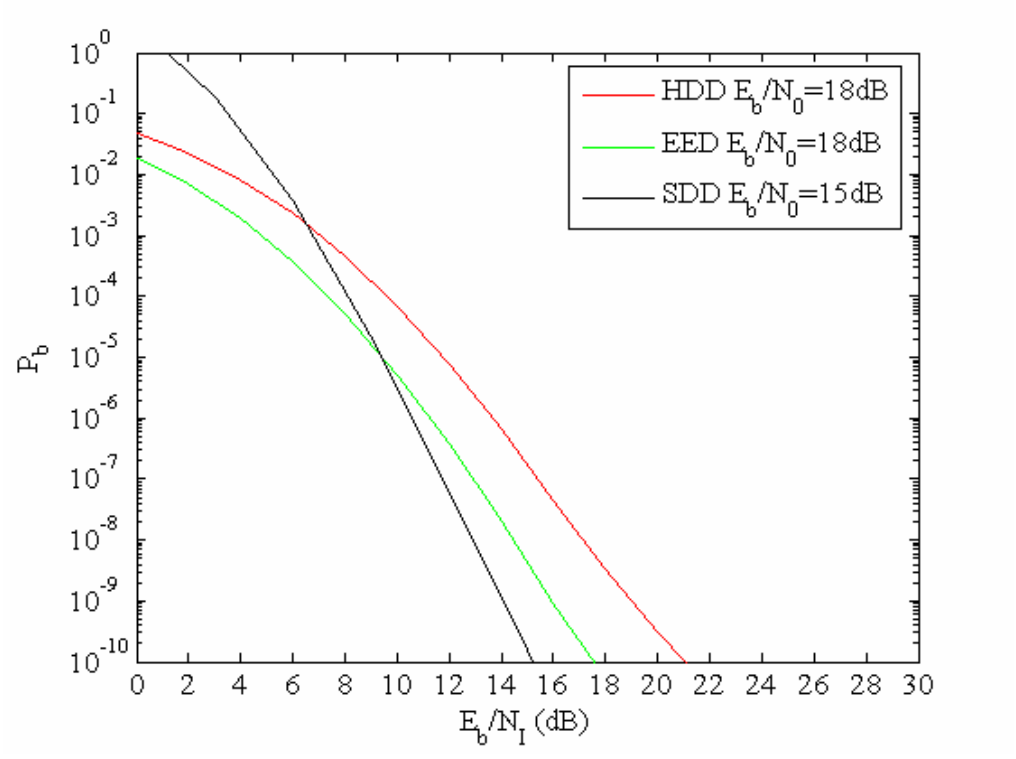

Figure 33. Performance for EED, HDD, and SDD with linear combining for a Nakagami fading channel with m=2, α = 0.4, and ρ = 0.2 (r=1/2).

b. BPSK/QPSK r=3/4

For this code rate the effect of channel fading can be seen in Figures 34, 35, and 36, where m = 0.5, m = 1, and m = 2, respectively. In each of these three figures, $E_b/N_0 = 15\,\text{dB}$ for soft decision decoding with linear combining and $E_b/N_0 = 30\,\text{dB}$, $E_b/N_0 = 25\,\text{dB}$, and $E_b/N_0 = 22\,\text{dB}$ for errors-and-erasures decoding and hard decision decoding when m=0.5, m = 1, and m = 2, respectively. In each of these cases, we see that if we give an even greater advantage in E_b/N_0 than for the code rate 1/2, soft decision decoding with linear combining always outperforms errors-and-erasures decoding and, of course, hard decision decoding for all E_b/N_I.

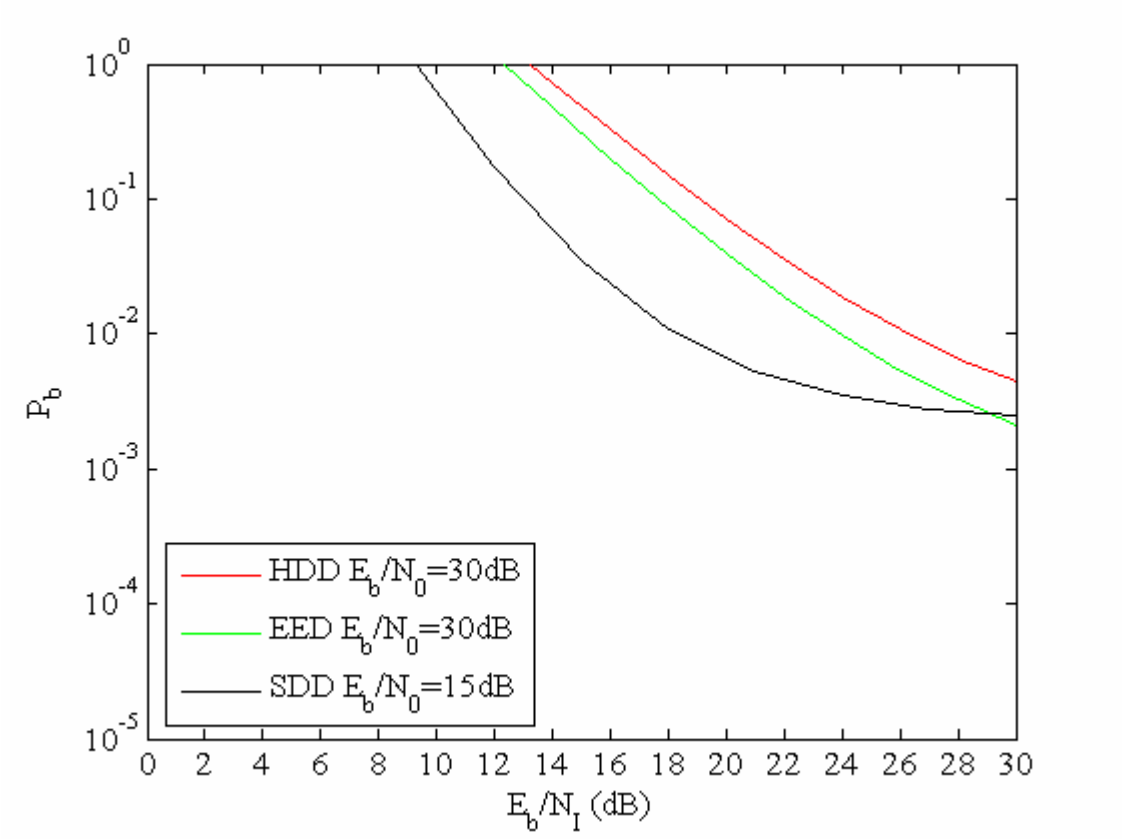

Figure 34. Performance for EED, HDD, and SDD with linear combining for a Nakagami fading channel with m=0.5, α = 0.4, and ρ = 0.5 (r=3/4).

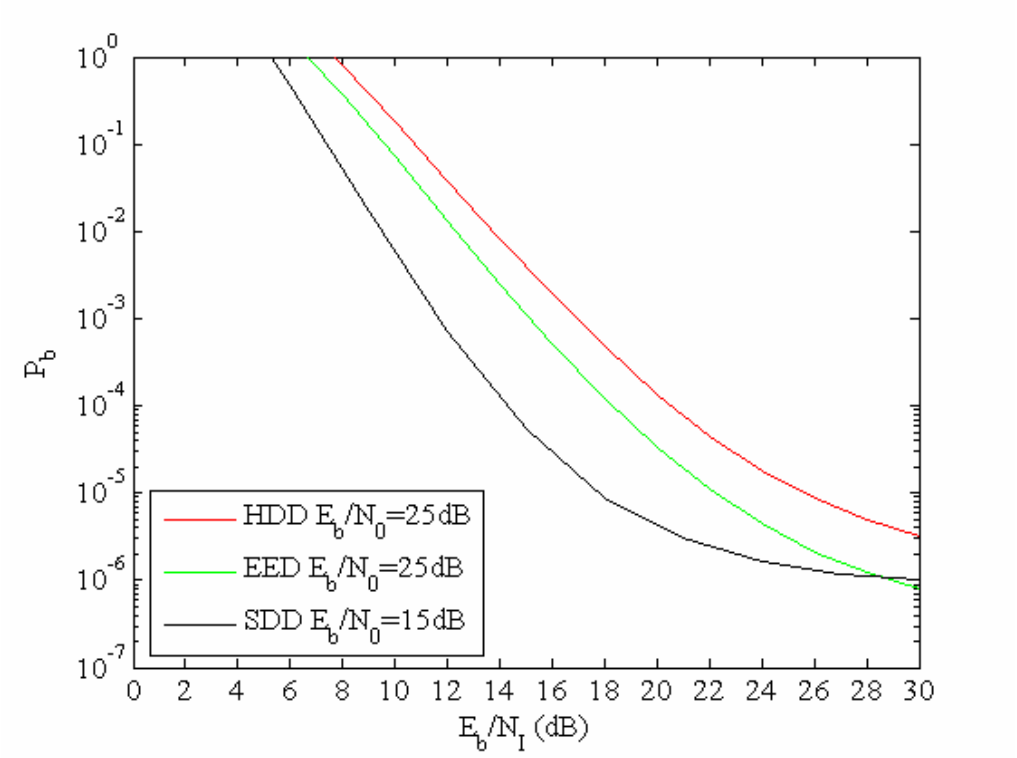

Figure 35. Performance for EED, HDD, and SDD with linear combining for a Nakagami fading channel with m=1, α = 0.4, and ρ = 0.5 (r=3/4).

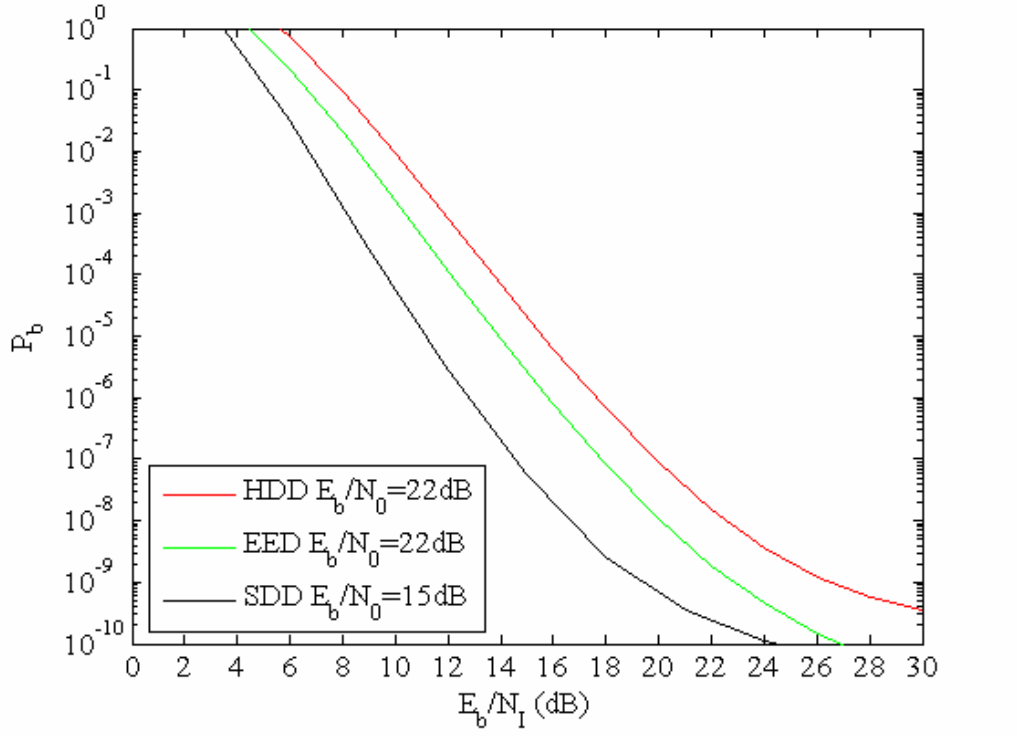

Figure 36. Performance for EED, HDD, and SDD with linear combining for a Nakagami fading channel with m=2, α = 0.4, and ρ = 0.5 (r=3/4).

E. CONCLUSIONS

In summary, for the case of no channel fading, with a relatively small increase of 1.8 dB for *r*=1/2 and 2.33 dB for *r*=3/4 in E_b/N_0, errors-and-erasures decoding provides immunity to pulse-noise interference that is not present when soft decision decoding with linear combining is used. When errors-and-erasures decoding and soft decision decoding with linear combining are compared for the same E_b/N_0, errors-and-erasures decoding has a significant advantage over soft decision decoding with linear combining when approximately $E_b/N_I < 10 \log \rho^{-1}$ dB. From Figures 27 and 30, it is apparent that the performance with errors-and-erasures decoding is very dependent on E_b/N_0, which must be larger than that required to provide the desired P_b in the absence of pulse-noise interference in order to provide meaningful immunity to the effects of pulse-noise interference.

When channel fading is a factor and for code rate *r*=1/2, it is clear that errors-and-erasures decoding can only improve performance over that obtained with soft decision decoding with linear combining when pulse-noise interference is present by increasing E_b/N_0. As might be expected, the required increase in E_b/N_0 is much larger for more severe fading conditions. These results make it clear that the range of E_b/N_I and magnitude of performance improvement obtained with errors-and-erasures decoding relative to soft decision decoding with linear combining both increase with increasing E_b/N_0. This cost is relatively minor for $m \geq 2$ but becomes quite large for $m \leq 1$. In conclusion, when channel fading is a factor, for sufficiently large E_b/N_0, errors-and-erasures decoding will outperform soft decision decoding with linear combining regardless of E_b/N_I when pulse-noise interference is present, but on an equal E_b/N_0 basis, the reverse is true.

Another finding is that when channel fading is a factor, for code rate *r*=3/4, errors-and-erasures decoding cannot outperform soft decision decoding with linear

combining regardless of the increase in E_b/N_0 ; although, it is likely that if the number of memory elements (K) is increased, then performance comparable to the r=1/2 code will be obtained with the r=3/4 code.

Hence, the BPSK errors-and-erasures receiver performance is affected mainly by the code rate used and the channel fading affects the receiver less when code rate r=1/2 is used.

In this chapter, we examined the performance of a system utilizing a BPSK/QPSK waveform transmitted over a channel with no fading as well as over a Nakagami fading channel, both with PNI in addition to AWGN, for HDD, EED, and SDD with linear combining for code rates of 1/2 and 3/4. At the end of the chapter, we compared the performances of all these decoding procedures. Having examined the performance of BPSK/QPSK, we will do the same in Chapter V for 16QAM and 64QAM for the code rates as specified by the *IEEE 802.11g* WLAN standard, except we will not consider SDD.

THIS PAGE INTENTIONALLY LEFT BLANK

V. *M*QAM SIGNALS

A. HARD DECISION DECODING (HDD)

1. Performance in AWGN with PNI (No Fading)

The model of a *M*QAM receiver which utilizes HDD is shown in Figure 37.

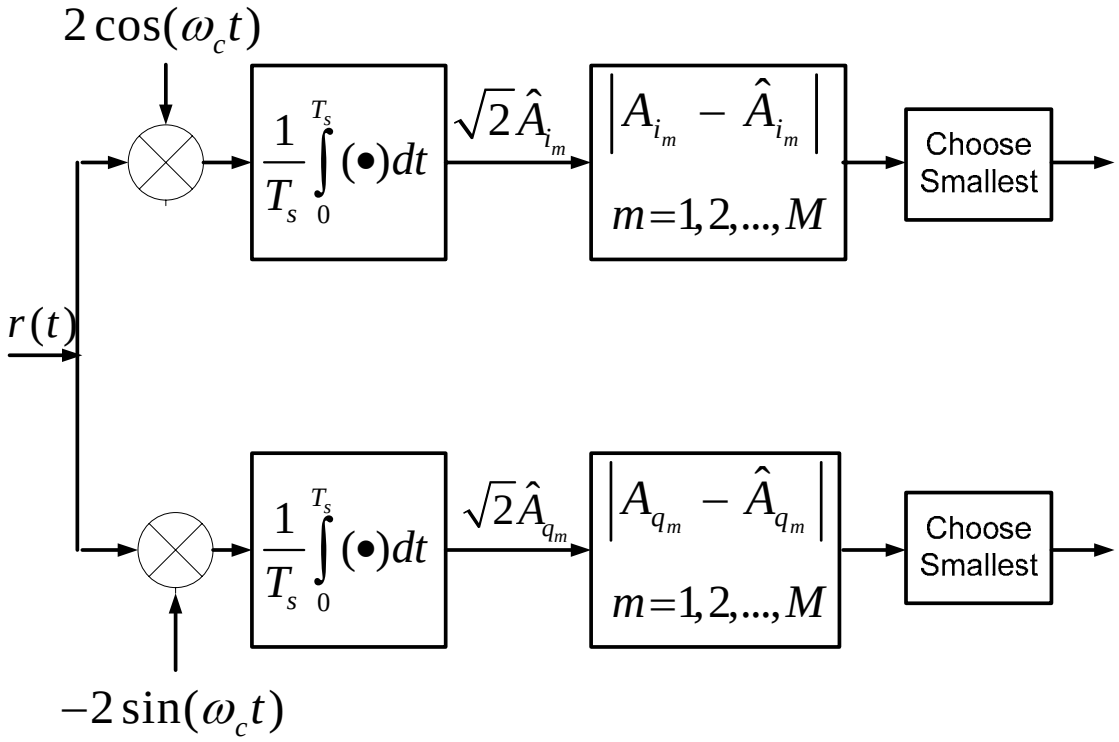

Figure 37. *M*QAM receiver with hard decision decoding.

In order to calculate the performance of a coded *M*QAM signal in AWGN with PNI, we must find the channel transition probability. When an *M*QAM system utilizes FEC, this probability is obtained from (2.5) and (2.15) as

$$p \approx \frac{4}{q}\left(1-\frac{1}{\sqrt{M}}\right)Q\left(\sqrt{\frac{3rq\gamma_b}{M-1}}\right) \tag{5.1}$$

Now, we can find the probability of channel bit error with PNI by combining (5.1) and (2.8) to get

$$p \approx \rho \left[\frac{4}{q}\left(1-\frac{1}{\sqrt{M}}\right) Q\left(\sqrt{\frac{3rq\gamma_b}{(M-1)(1+\gamma_b/\gamma_I\rho)}}\right)\right] + (1-\rho)\left[\frac{4}{q}\left(1-\frac{1}{\sqrt{M}}\right) Q\left(\sqrt{\frac{3rq\gamma_b}{M-1}}\right)\right] \quad (5.2)$$

Equation (5.2) is used to compute (2.17), which in turn is used in (2.16) with the values of B_d and d_{free} that correspond to the code rate shown in Table 2 to obtain an upper bound on the probability of information bit error.

a. 16QAM r=1/2

For bit rate 24 Mbps, 16QAM is used with a code rate of 1/2. Figure 38 is a plot of the performance obtained with HDD for various values of the factor ρ when $E_b/N_0 = 15\text{dB}$. It can be seen that varying ρ degrades the receiver performance by as much as 8 dB. When E_b/N_I is small, barrage noise interference (ρ = 1) is more effective than PNI, but as we increase E_b/N_I, the reverse is true.

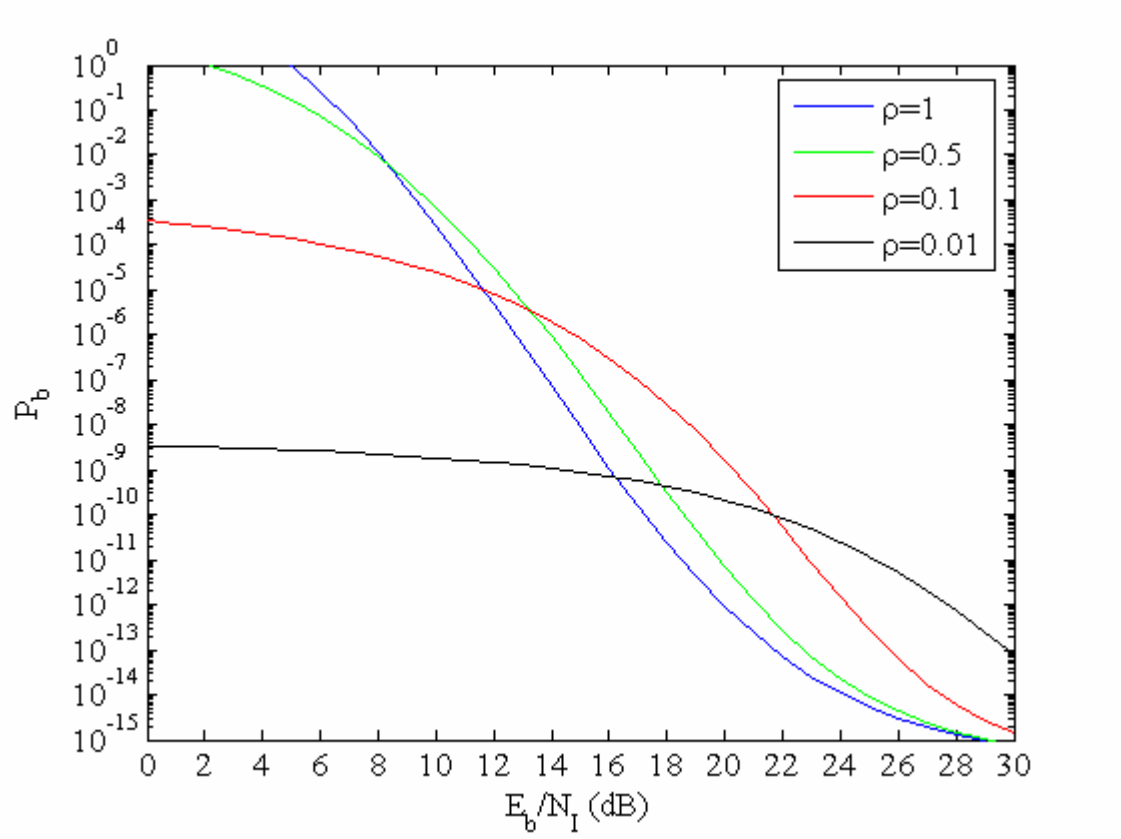

Figure 38. Performance of 16QAM in AWGN and PNI with *r*=1/2 convolutional source coding and HDD for a channel with no fading ($E_b/N_0 = 15\text{dB}$).

b. 16QAM r=3/4

For bit rate 36 Mbps, 16QAM is used with a code rate of 3/4. In Figure 39, in a manner analogous to Figure 38, the performance obtained with HDD for various values of the factor ρ when $E_b/N_0 = 15\text{dB}$ is plotted. In this case the results for the various values of ρ are analogous to the results shown in Figure 38; although, the effect of the PNI on the receiver is more severe, especially for very small ρ.

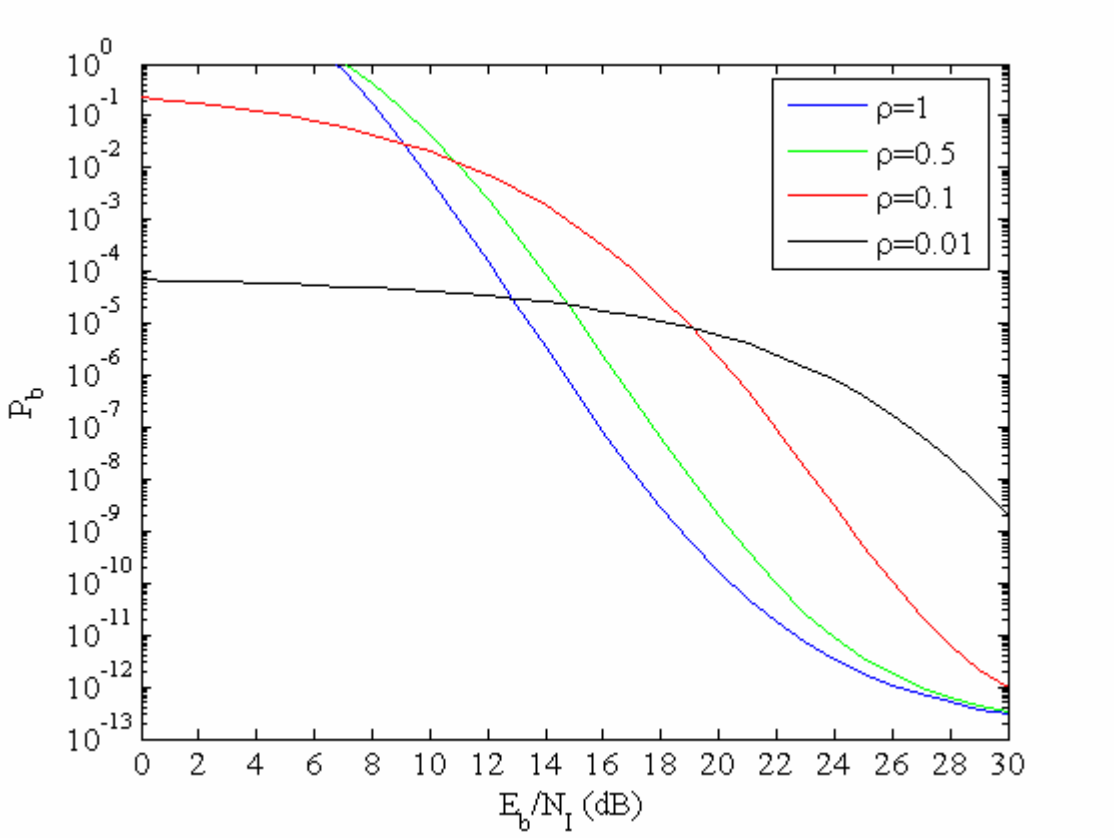

Figure 39. Performance of 16QAM in AWGN and PNI with *r*=3/4 convolutional source coding and HDD for a channel with no fading ($E_b/N_0 = 15\text{dB}$).

c. 64QAM r=2/3

For bit rate 48 Mbps, 64QAM is used with a code rate of 2/3. Figure 40 is a plot of the performance obtained with HDD for various values of the factor ρ when $E_b/N_0 = 15\text{dB}$. It can be seen that varying ρ hardly degrades receiver performance, and ρ=1 is approximately the worst case.

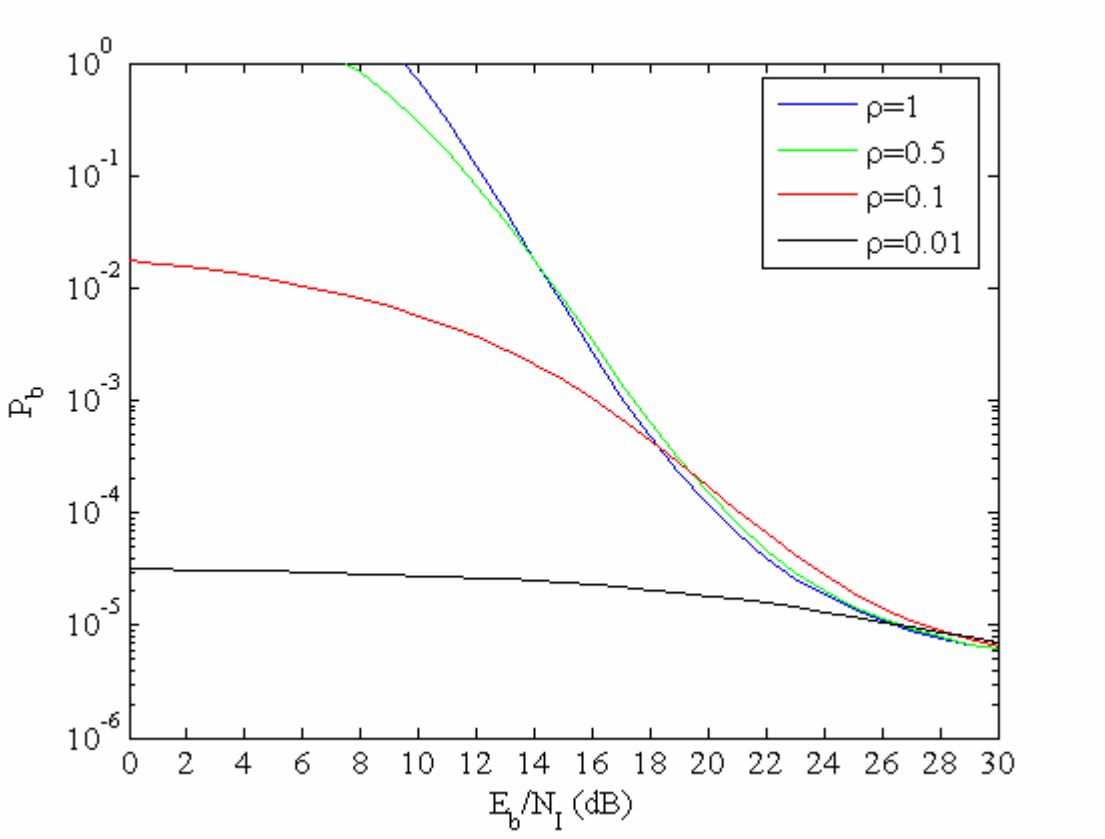

Figure 40. Performance of 64QAM in AWGN and PNI with *r*=2/3 convolutional source coding and HDD for a channel with no fading ($E_b/N_0 = 15\,\text{dB}$).

d. 64QAM r=3/4

For bit rate 54 Mbps, 64QAM is used with a code rate of 3/4. Figure 41 is a plot of the performance obtained with HDD for various values of the factor ρ when $E_b/N_0 = 15\,\text{dB}$. In this case the results are analogous to the results shown in Figure 40. The results for 64QAM are a good example of the effect of AWGN when PNI is present. The results for 64QAM show less sensitivity to PNI than the results for 16QAM, but if E_b/N_0 were increased so that the 64QAM system had the same asymptotic limit as the 16QAM system, then the 64QAM system would show the same sensitivity to ρ as the 16QAM system.

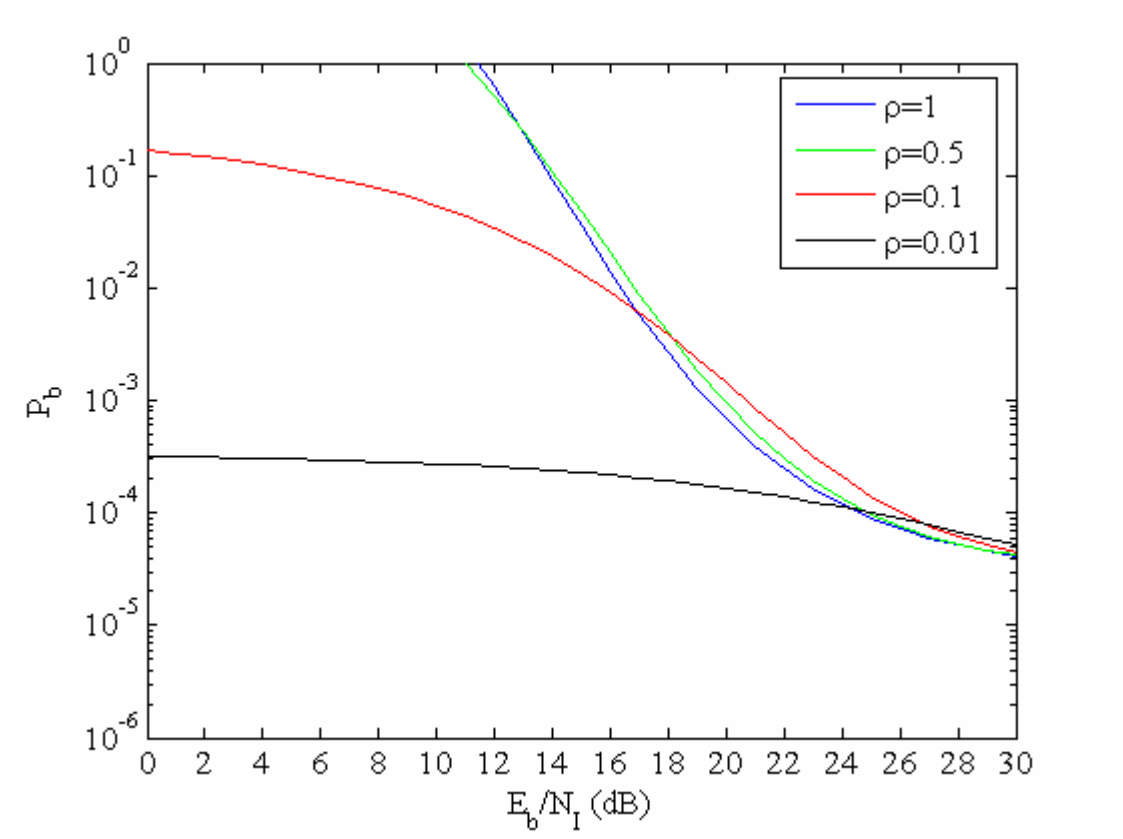

Figure 41. Performance of 64QAM in AWGN and PNI with r=3/4 convolutional source coding and HDD for a channel with no fading ($E_b/N_0 = 15\,\text{dB}$).

2. Performance in AWGN with PNI and Fading

When the channel is modeled as a Nakagami fading channel, then (5.2) is a conditional probability. The unconditional probability of channel bit error is now found by substituting (5.2) into (2.12) to obtain

$$p = \frac{4}{q}\left(1-\frac{1}{\sqrt{M}}\right)\int_0^\infty \left\{\rho\, Q\left(\sqrt{\frac{3rq\gamma_b}{(M-1)(1+\overline{\gamma}_b/\overline{\gamma}_I\rho)}}\right)+(1-\rho)Q\left(\sqrt{\frac{3rq\gamma_b}{M-1}}\right)\right\}\frac{1}{\Gamma(m)}\left(\frac{m}{\overline{\gamma}_b}\right)^m \gamma_b^{m-1} e^{-m\gamma_b/\overline{\gamma}_b} d\gamma_b \quad (5.3)$$

We can obtain a numerical solution for this equation or we can find an analytic solution using the identity

$$\int_0^{\infty} Q\left(\sqrt{2r\zeta\gamma_b}\right) f_{\Gamma_b}(\gamma_b)\, d\gamma_b = \frac{\Gamma(m+\frac{1}{2})(r\zeta\,\overline{\gamma}_b/m)^{1/2}}{2\sqrt{\pi}\Gamma(m+1)(1+r\zeta\,\overline{\gamma}_b/m)^{m+1/2}} \times {}_2F_1\left(1, m+\frac{1}{2}; m+1; \frac{1}{1+r\zeta\,\overline{\gamma}_b/m}\right) \tag{5.4}$$

where ${}_2F_1\left(1, b+\frac{1}{2}; b+1; z\right)$ is Gauss' hypergeometric function.

Equation (5.4) is used to compute (2.17), which in turn is used in (2.16) with the values of B_d and d_{free} corresponding to the code rate shown in Table 2 to obtain an upper bound on the probability of information bit error.

a. 16QAM r=1/2

In Figure 42, the performance is plotted for different fading conditions. In order to validate the results obtained using the analytical solution, the performance is obtained both analytically and numerically. For this figure, $E_b/N_0 = 15\,\text{dB}$ and $\rho = 0.5$.

It is clear from Figure 42 that both methods give virtually identical results for all fading conditions. Additionally, the performance observed for $m = 10$ is very close to the performance for a non-fading channel. As expected, the performance improves as m increases and approaches the non-fading limit $(m \to \infty)$.

In Figure 43, the effect of the factor ρ on receiver's performance is investigated. In this figure the performance is plotted for various values of ρ with $E_b/N_0 = 25\,\text{dB}$ and $m = 1$.

As can be seen, varying ρ affects the receiver performance significantly, particularly when $E_b/N_I < 18\,\text{dB}$. Moreover, it is seen that the barrage noise interference $(\rho = 1)$ is more effective than PNI. As ρ approaches zero, the performance converges to the AWGN limit. In conclusion, the bigger the value of ρ is, the poorer the performance.

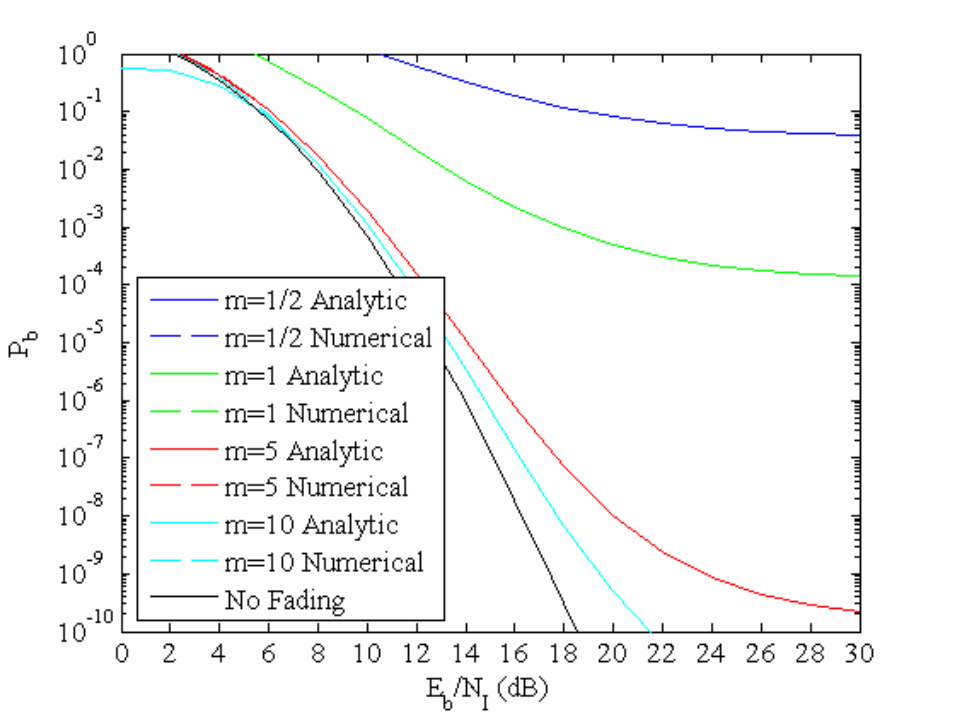

Figure 42. Performance of 16QAM in AWGN and PNI (ρ=0.5) with r=1/2 convolutional source coding and HDD for a Nakagami fading channel ($E_b/N_0 = 15\,\text{dB}$) computed both analytically and numerically.

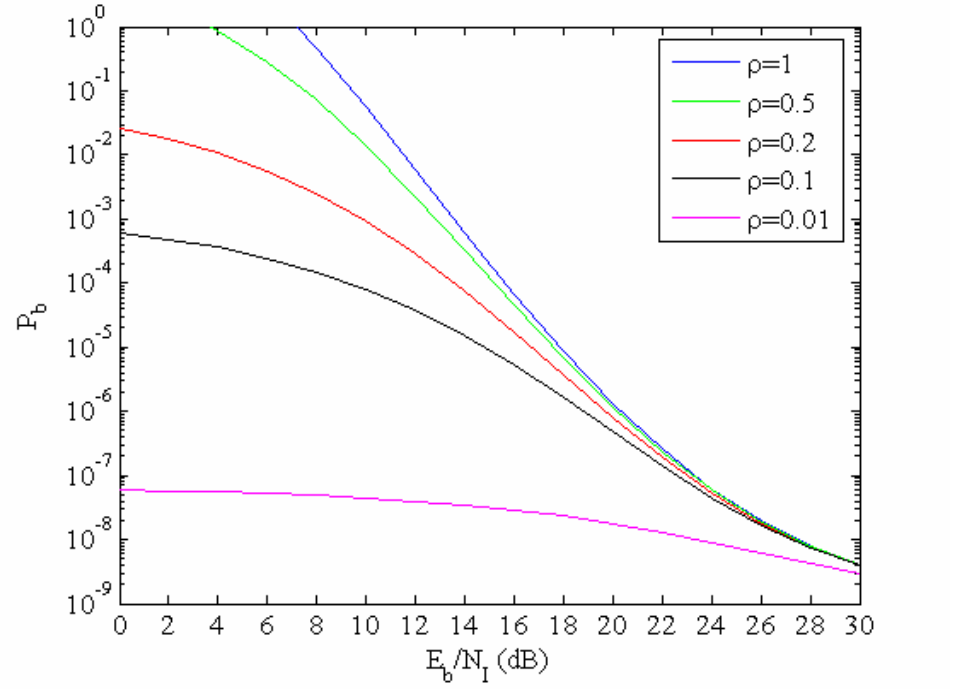

Figure 43. Performance of 16QAM in AWGN and PNI with r=1/2 convolutional source coding and HDD for a Nakagami fading channel (m=1) ($E_b/N_0 = 25\,\text{dB}$).

b. 16QAM r=3/4

Figures 44 and 45 are analogous to Figures 42 and 43, respectively, for 16QAM and a code rate of 3/4. Although we arrive at the same basic conclusions, it can be seen that for greater code rates (higher data rates), similar to BPSK/QPSK, the performance degradation is more severe as a result of channel fading.

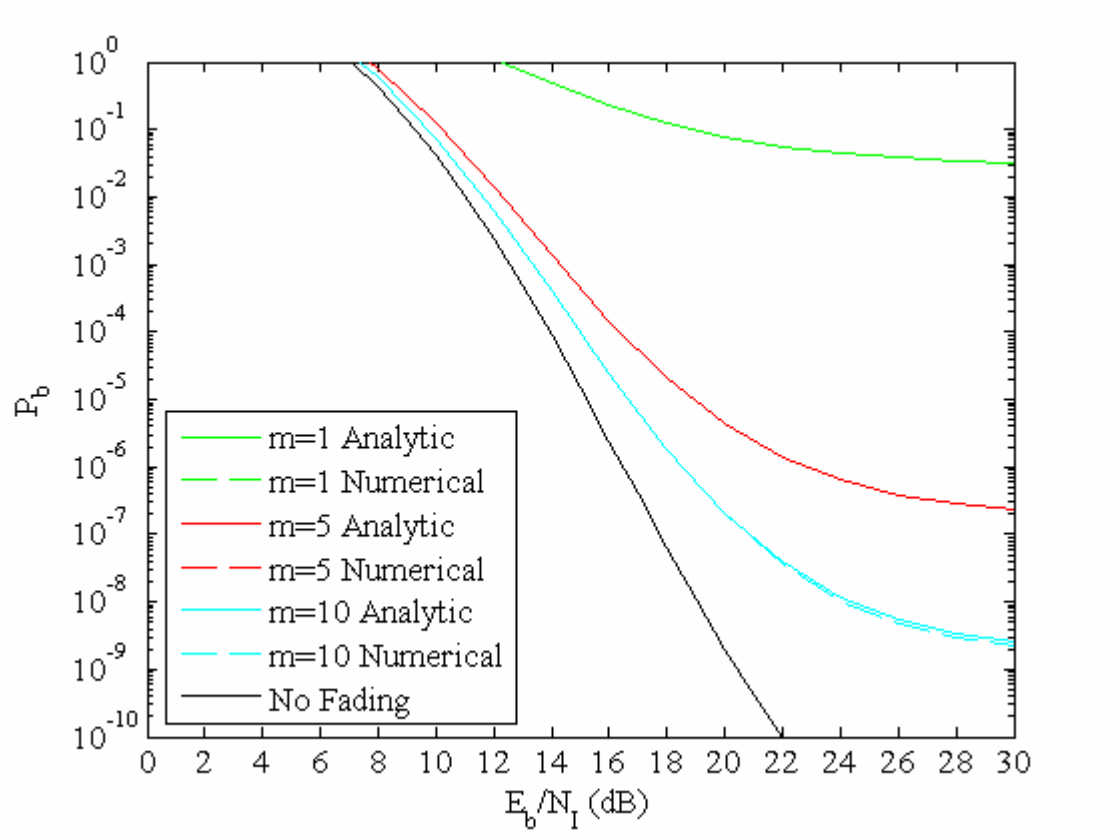

Figure 44. Performance of 16QAM in AWGN and PNI (ρ=0.5) with r=3/4 convolutional source coding and HDD for a Nakagami fading channel ($E_b/N_0 = 15\,\text{dB}$) computed both analytically and numerically.

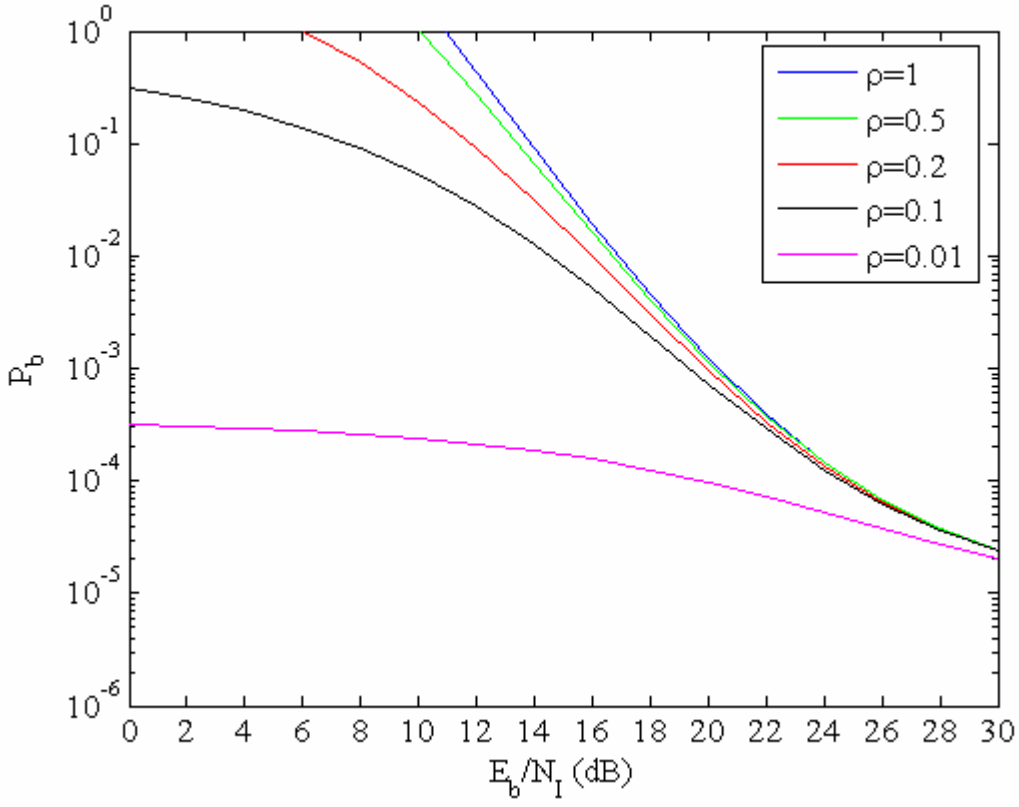

Figure 45. Performance of 16QAM in AWGN and PNI with r=3/4 convolutional source coding and HDD for a Nakagami fading channel (m=1) ($E_b/N_0 = 25\,\text{dB}$).

c. 64QAM r=2/3

As with previous analyses, in Figure 46 the performance is plotted for different fading conditions and in Figure 47 for various values of the parameter ρ. Again we arrive at the same basic conclusions as for the lower data rates. If we compare Figures 45 and 47, we can see that they are very close for the same values of E_b/N_I . This happens because, although we change the type of modulation from 16QAM to 64QAM and normally expect performance degradation, the code rate for 64QAM is smaller than for 16QAM. Concisely, when channel fading is a factor, performance is determined by the combination of modulation and code rate.

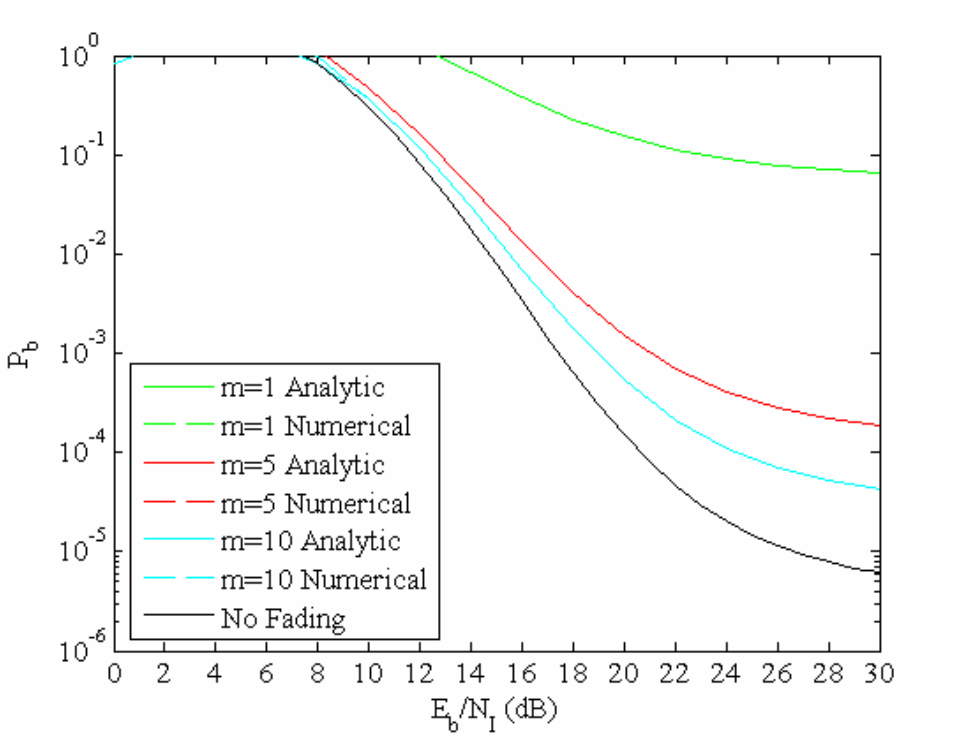

Figure 46. Performance of 64QAM in AWGN and PNI (ρ=0.5) with r=2/3 convolutional source coding and HDD for a Nakagami fading channel ($E_b/N_0 = 15\,\text{dB}$) computed both analytically and numerically.

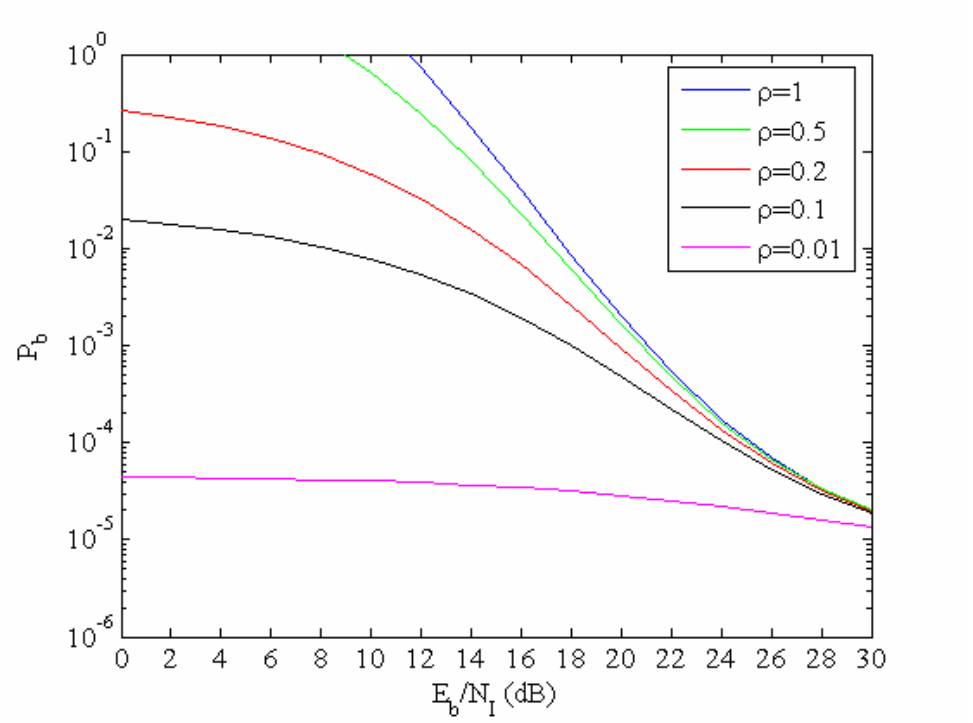

Figure 47. Performance of 64QAM in AWGN and PNI with r=2/3 convolutional source coding and HDD for a Nakagami fading channel (m=1) ($E_b/N_0 = 25\,\text{dB}$)

d. 64QAM r=3/4

Finally, for the highest data rate, 64QAM with a code rate of 3/4 is analyzed and the results shown in Figures 48 and 49. As might be expected, we reach the same basic conclusions as for the lower data rates.

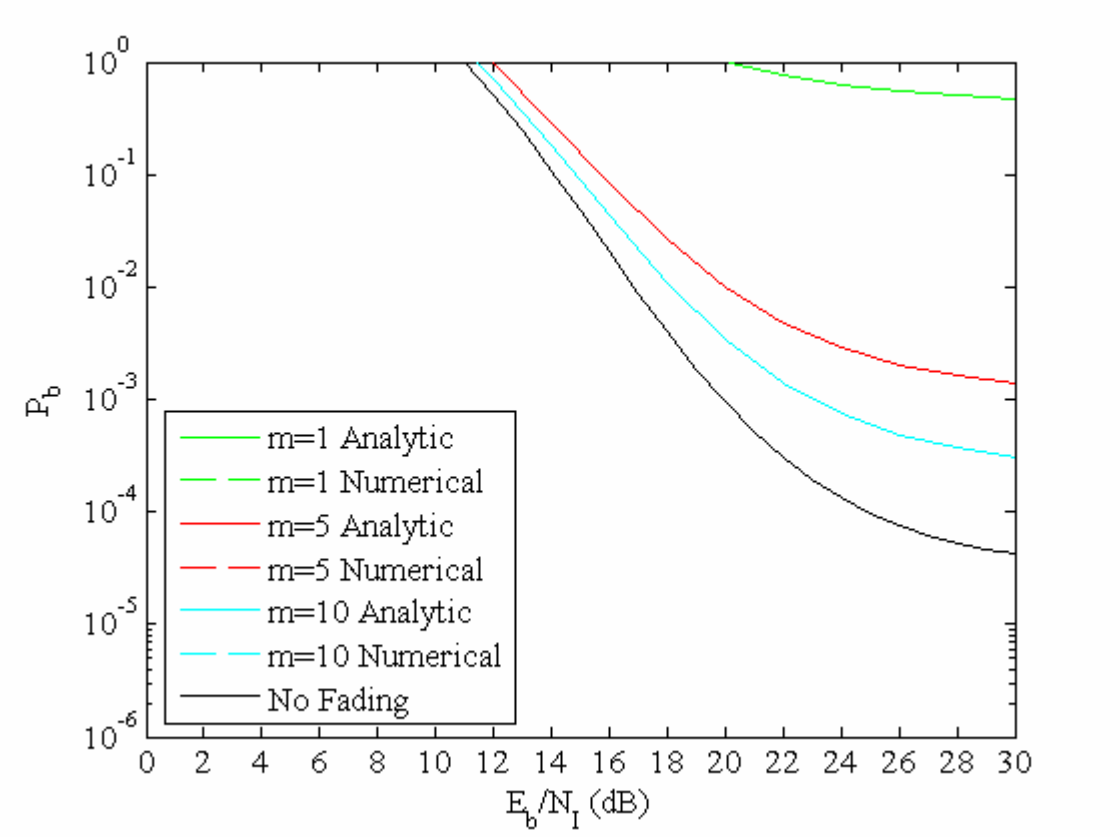

Figure 48. Performance of 64QAM in AWGN and PNI (ρ=0.5) with r=3/4 convolutional source coding and HDD for a Nakagami fading channel ($E_b/N_0 = 15\,\text{dB}$) computed both analytically and numerically.

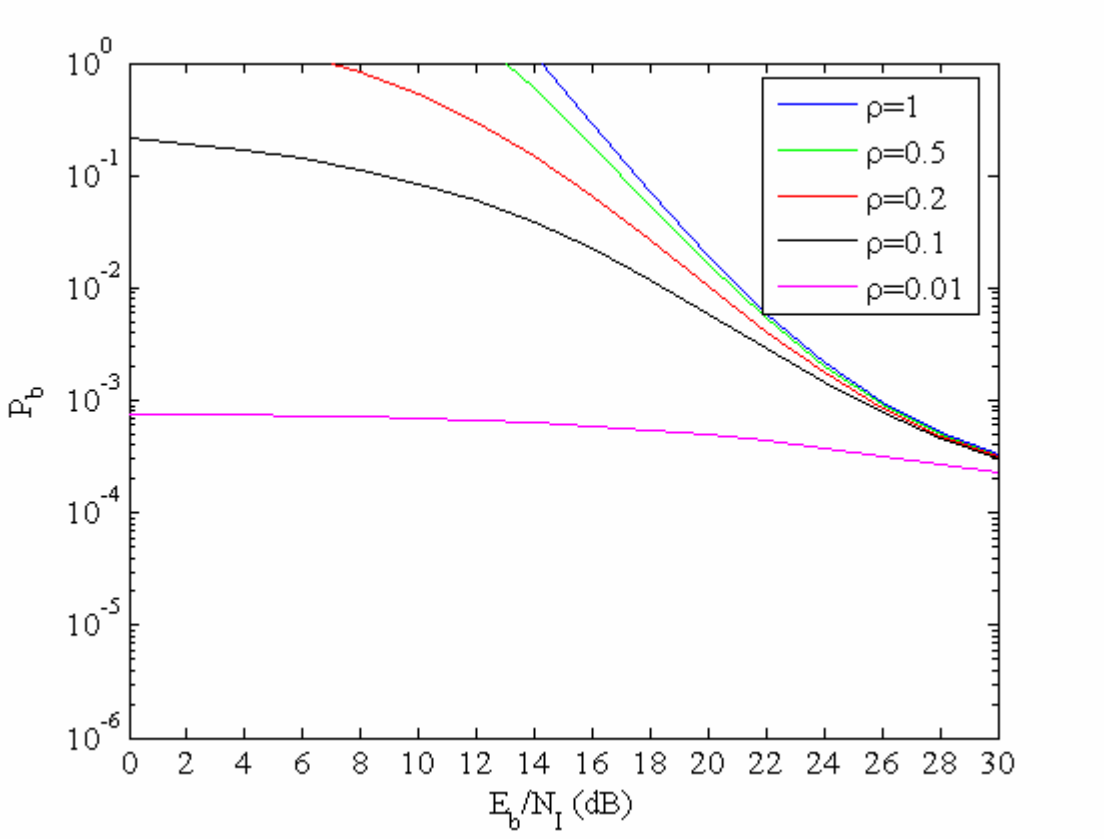

Figure 49. Performance of 64QAM in AWGN and PNI with r=3/4 convolutional source coding and HDD for a Nakagami fading channel (m=1) ($E_b/N_0 = 25\,\text{dB}$).

B. ERRORS-AND-ERASURES DECODING (EED)

Since the in-phase (I) and quadrature (Q) components of the received MQAM waveform are demodulated independently, MQAM with a rectangular constellation can be thought of as an M_iPAM signal on the in-phase component of the carrier and an M_qPAM signal on the quadrature component of the carrier where

$$M = 2^q = M_i M_q \tag{5.5}$$

The probability of channel symbol error for MQAM is

$$P_S = P_{S_i} \bigcup P_{Sq} = P_{S_i} + P_{S_q} - P_{S_i} \bigcap P_{Sq} \tag{5.6}$$

where P_{S_i} and P_{S_q} are, respectively, the probabilities of symbol error for M_iPAM and M_qPAM signals.

Since the *I* and *Q* components can be modeled as independent random processes, (5.6) becomes

$$P_S = P_{S_i} + P_{S_q} - P_{S_i} P_{Sq} \tag{5.7}$$

For square constellations, the preceding is only valid when *q* is even, like 16QAM and 64QAM. In this case $M_i = M_q$, $M = M_i^2$, $P_{S_i} = P_{Sq}$, and (5.7) simplifies to

$$P_S = 2P_{S_i} - P_{S_i}^2 \tag{5.8}$$

If an area $\pm V_T$ is established around the border of each symbol, in which we have symbol erasure instead of symbol error, as we can see in Figure 50 for 16QAM, , then the probability of channel symbol error for *M*QAM (a square constellation is assumed) is obtained in a manner analogous to (5.8) yet slightly different, since when we have a symbol error on one component and a symbol erasure on the other we count it as a symbol erasure, and is given by

$$P_S = 2P_{S_i} - P_{S_i}^2 - 2P_{S_i} P_{S_i,e} \tag{5.9}$$

where $P_{S_i,e}$ is the probability of symbol erasure for the M_iPAM signal.

Consequently, the probability of channel symbol erasure for *M*QAM is

$$P_{S,e} = 2P_{S_i,e} - P_{S_i,e}^2 \tag{5.10}$$

In the same way, the probability of correct channel symbol detection is

$$P_{S,C} = P_{S_i,C} \bigcap P_{S_q,C} = P_{S_i,C}^2 \tag{5.11}$$

or

$$P_{S,C} = 1 - P_S - P_{S,e} \tag{5.12}$$

where $P_{S_i,C}$ and $P_{S_q,C}$ are, respectively, the probabilities of correct symbol detection for M_iPAM and M_qPAM signals.

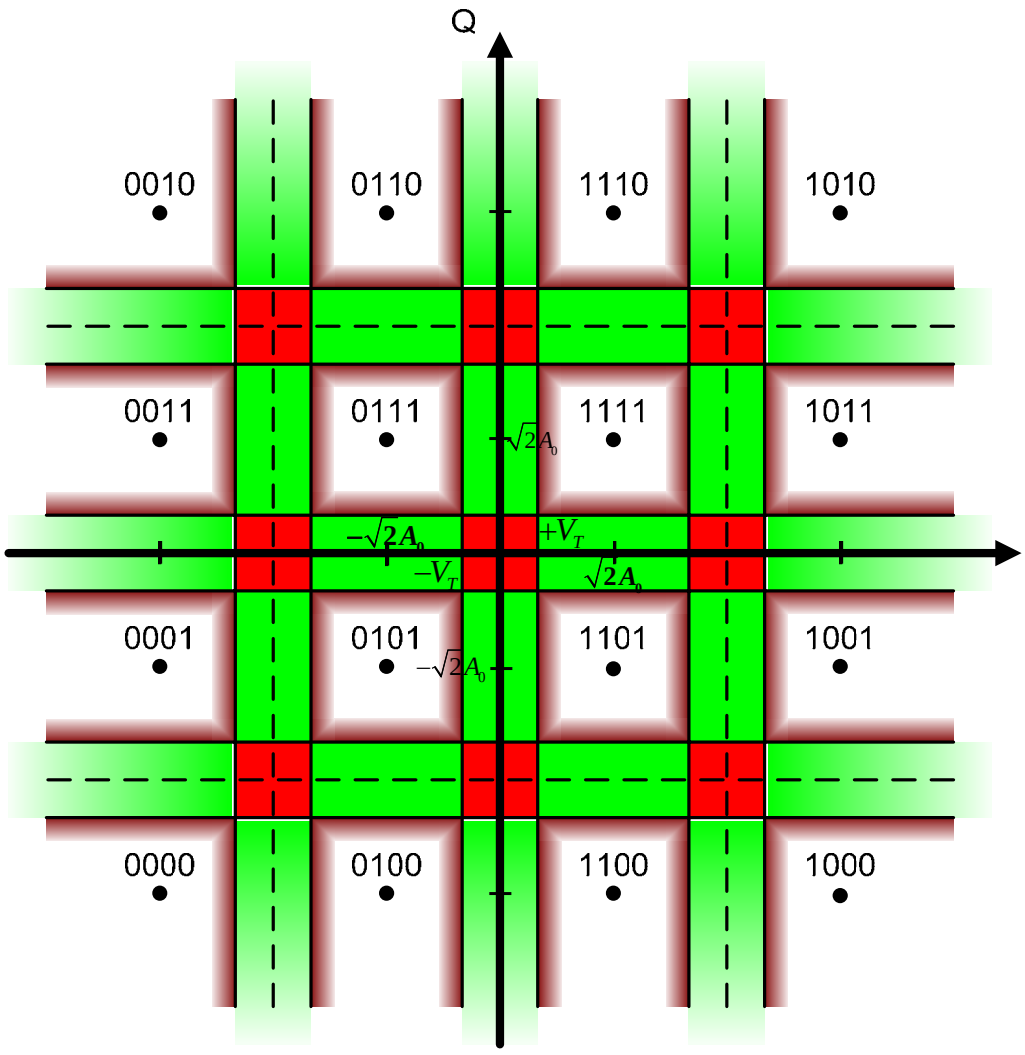

Figure 50. Constellation diagram for 16QAM.

Since for M_iPAM there are two exterior symbols and $M_i - 2$ interior symbols, then, assuming equally likely symbols, the probability of symbol error for M_iPAM is found from

$$P_{S_i} = \frac{1}{M_i}\left[\left(M_i - 2\right)P_{S_i,\text{int}} + 2P_{S_i,ext}\right] \tag{5.13}$$

where $P_{S_i,\text{int}}$ and $P_{S_i,ext}$ are, respectively, the probabilities of interior and exterior channel symbol error for M_iPAM.

The probability of symbol erasure for M_iPAM is found from

$$P_{S_i,e} = \frac{1}{M_i}\left[\left(M_i - 2\right)P_{S_i,e,\text{int}} + 2P_{S_i,e,ext}\right] \tag{5.14}$$

where $P_{S_i,e,\text{int}}$ and $P_{S_i,e,ext}$ are, respectively, the probabilities of interior and exterior channel symbol erasure for M_iPAM.

Similarly, the average probability of not making a symbol error can be found for M_iPAM as

$$P_{S_i,C} = \frac{1}{M_i}\left[\left(M_i - 2\right)P_{S_i,C,\text{int}} + 2P_{S_i,C,ext}\right] \tag{5.15}$$

or, from (5.13) and (5.14),

$$P_{S_i,C} = 1 - P_{S_i} - P_{S_i,e} \tag{5.16}$$

For the *M*QAM errors-and-erasures demodulator shown in Figure 51 and for AWGN or any other symmetric noise, the probability of channel symbol error for the equivalent M_iPAM signal on the in-phase and the quadrature component for interior and exterior symbols are, respectively, as illustrated in Figures 52 and 53,

$$P_{S_i,\text{int}} = \Pr\left\{\left|X_i - \overline{X_i}\right| \geq \sqrt{2}A_0 + V_T\right\} = 2Q\left(\frac{\sqrt{2}A_0 + V_T}{\sigma}\right) \tag{5.17}$$

$$P_{S_i,ext} = \Pr\left\{X_i \leq \overline{X_i} - \left(\sqrt{2}A_0 + V_T\right)\right\} = Q\left(\frac{\sqrt{2}A_0 + V_T}{\sigma}\right) \tag{5.18}$$

where $\sigma^2 = N_T / rT_b$, N_T is the total one-sided noise power spectral density, T_S is the symbol duration, *r* is the code rate, $\sqrt{2}A_0$ is the amplitude of both the in-phase and the quadrature component of the signal for the lowest energy symbol, and V_T, as mentioned before, is the threshold that delineates errors from erasures.

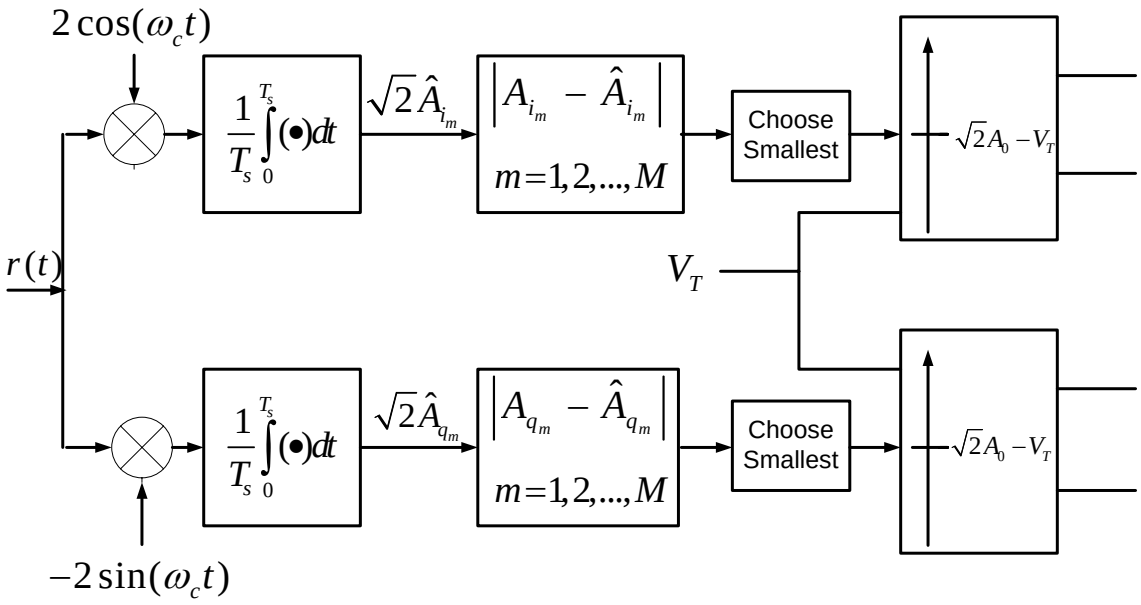

Figure 51. *M*QAM receiver with errors-and-erasures demodulation.

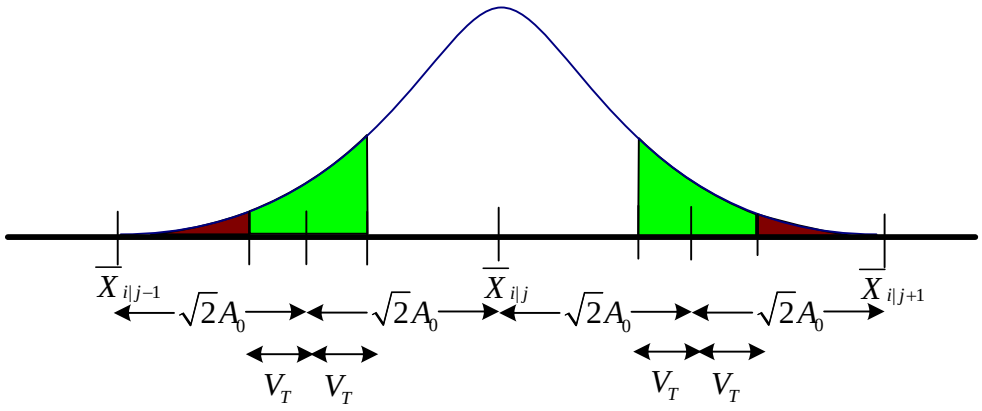

Figure 52. Gaussian probability density function for interior symbol of M_iPAM .

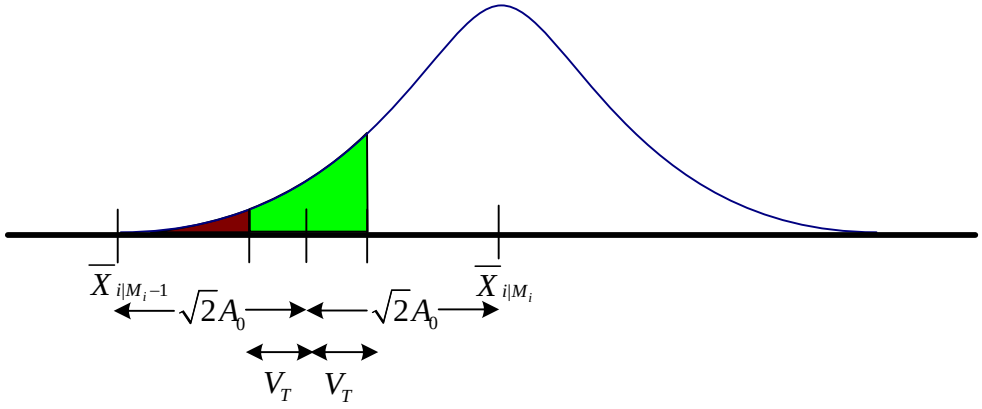

Figure 53. Gaussian probability density function for exterior symbol of M_iPAM .

Similarly, the probability of channel symbol erasure and the probability of not making a channel symbol error for the equivalent M_iPAM signal on the in-phase and the quadrature component for interior and exterior symbols are, respectively, as illustrated in Figures 52 and 53,

$$P_{S_i,e,\text{int}} = \Pr\left\{\sqrt{2}A_0 - V_T < \left|X_i - \overline{X_i}\right| < \sqrt{2}A_0 + V_T\right\} = \\ = 2\left[Q\left(\frac{\sqrt{2}A_0 - V_T}{\sigma}\right) - Q\left(\frac{\sqrt{2}A_0 + V_T}{\sigma}\right)\right] \tag{5.19}$$

$$P_{S_i,e,ext} = \Pr\left\{\overline{X_i} - \left(\sqrt{2}A_0 + V_T\right) < X_i < \overline{X_i} - \left(\sqrt{2}A_0 - V_T\right)\right\} = \\ = Q\left(\frac{\sqrt{2}A_0 - V_T}{\sigma}\right) - Q\left(\frac{\sqrt{2}A_0 + V_T}{\sigma}\right) \tag{5.20}$$

$$P_{S_i,C,\text{int}} = \Pr\left\{\left|X_i - \overline{X_i}\right| < \sqrt{2}A_0 - V_T\right\} = 1 - 2Q\left(\frac{\sqrt{2}A_0 - V_T}{\sigma}\right) \tag{5.21}$$

$$P_{S_i,C,ext} = \Pr\left\{X_i > \overline{X_i} - \left(\sqrt{2}A_0 - V_T\right)\right\} = 1 - Q\left(\frac{\sqrt{2}A_0 - V_T}{\sigma}\right) \tag{5.22}$$

Now, the average probability of symbol error and the average probability of symbol erasure for M_iPAM can be found, respectively, by substituting (5.17) and (5.18) into (5.13) as well as (5.19) and (5.20) into (5.14) to get

$$P_{S_i} = 2\left(1 - \frac{1}{M_i}\right)Q\left(\frac{\sqrt{2}A_0 + V_T}{\sigma}\right) \tag{5.23}$$

and

$$P_{S_i,e} = 2\left(1 - \frac{1}{M_i}\right)\left[Q\left(\frac{\sqrt{2}A_0 - V_T}{\sigma}\right) - Q\left(\frac{\sqrt{2}A_0 + V_T}{\sigma}\right)\right] \tag{5.24}$$

The average probability of correct symbol detection for M_iPAM can be found by substituting either (5.21) and (5.22) into (5.15) or (5.23) and (5.24) into (5.16) to get

$$P_{S_i,C} = 1 - 2\left(1 - \frac{1}{M_i}\right)Q\left(\frac{\sqrt{2}A_0 - V_T}{\sigma}\right) \tag{5.25}$$

Defining $V_T = \alpha\sqrt{2}A_0$ where $0 < \alpha \le 1$ and replacing σ, we get, respectively, from (5.23), (5.24), and (5.25)

$$P_{S_i} = 2\left(1-\frac{1}{M_i}\right)Q\left[\left(1+\alpha\right)\sqrt{\frac{2rA_0^2T_S}{N_0}}\right] \tag{5.26}$$

$$P_{S_i,e} = 2\left(1-\frac{1}{M_i}\right)\left\{Q\left[\left(1-\alpha\right)\sqrt{\frac{2rA_0^2T_S}{N_0}}\right]-Q\left[\left(1+\alpha\right)\sqrt{\frac{2rA_0^2T_S}{N_0}}\right]\right\} \tag{5.27}$$

$$P_{S_i,C} = 1-2\left(1-\frac{1}{M_i}\right)Q\left[\left(1-\alpha\right)\sqrt{\frac{2rA_0^2T_S}{N_0}}\right] \tag{5.28}$$

Recognizing that the energy of the lowest amplitude symbols is $E_0 = 2A_0^2T_S$, we can express the average energy per information symbol for a square constellation as $E_S = (1/3)(M-1)E_0$. Substituting (5.26) and (5.27) into (5.9) and (5.10), we obtain, respectively, the average probability of channel symbol error and the average probability of channel symbol erasure for *M*QAM as

$$\begin{aligned} P_S = {} & 4\left(1-\frac{1}{\sqrt{M}}\right)Q\left[\left(1+\alpha\right)\sqrt{\frac{3rE_S}{(M-1)N_0}}\right] \\ & \times\left\{1-\left(1-\frac{1}{\sqrt{M}}\right)\left[2Q\left[\left(1-\alpha\right)\sqrt{\frac{3rE_S}{(M-1)N_0}}\right]-Q\left[\left(1+\alpha\right)\sqrt{\frac{3rE_S}{(M-1)N_0}}\right]\right]\right\} \end{aligned} \tag{5.29}$$

$$\begin{aligned} P_{S,e} = {} & 4\left(1-\frac{1}{\sqrt{M}}\right)\left\{Q\left[\left(1-\alpha\right)\sqrt{\frac{3rE_S}{(M-1)N_0}}\right]-Q\left[\left(1+\alpha\right)\sqrt{\frac{3rE_S}{(M-1)N_0}}\right]\right\} \\ & \times\left\{1-\left(1-\frac{1}{\sqrt{M}}\right)\left\{Q\left[\left(1-\alpha\right)\sqrt{\frac{3rE_S}{(M-1)N_0}}\right]-Q\left[\left(1+\alpha\right)\sqrt{\frac{3rE_S}{(M-1)N_0}}\right]\right\}\right\} \end{aligned} \tag{5.30}$$

When $E_S/N_0 >> 1$, then (5.29) and (5.30) simplify to

$$P_S \approx 4\left(1-\frac{1}{\sqrt{M}}\right)Q\left[(1+\alpha)\sqrt{\frac{3rE_S}{(M-1)N_0}}\right] \tag{5.31}$$

$$P_{S,e} \approx 4\left(1-\frac{1}{\sqrt{M}}\right)\left\{Q\left[(1-\alpha)\sqrt{\frac{3rE_S}{(M-1)N_0}}\right]-Q\left[(1+\alpha)\sqrt{\frac{3rE_S}{(M-1)N_0}}\right]\right\} \tag{5.32}$$

It can be shown graphically that this approximation is very good (almost exact) except for very small E_S/N_0 (very large P_S).

Similarly, the probability of correct channel symbol detection for *M*QAM can be found by substituting either (5.28) into (5.11) or (5.29) and (5.30) into (5.12) to get

$$P_{S,C} = \left\{1-2\left(1-\frac{1}{\sqrt{M}}\right)Q\left[(1-\alpha)\sqrt{\frac{3rE_S}{(M-1)N_0}}\right]\right\}^2 \tag{5.33}$$

If we use the approximations, substituting (5.31) and (5.32) into (5.12), we obtain

$$P_{S,C} \approx 1-4\left(1-\frac{1}{\sqrt{M}}\right)Q\left[(1-\alpha)\sqrt{\frac{3rE_S}{(M-1)N_0}}\right] \tag{5.34}$$

Therefore, we see that (5.34) is an approximation of (5.33) for $E_S/N_0 >> 1$.

When a Gray code is utilized for *M*QAM, two *q*-bit adjacent symbols differ in only one bit. Hence, the bit error probability for *M*QAM is

$$p \approx \frac{P_S}{q} \tag{5.35}$$

or, from (5.31),

$$p \approx \frac{4}{q}\left(1-\frac{1}{\sqrt{M}}\right)Q\left[(1+\alpha)\sqrt{\frac{3rE_S}{(M-1)N_0}}\right] \tag{5.36}$$

When there is a symbol erasure on either the in-phase or the quadrature component but not both, then the channel bit erasure probability for *M*QAM for this region is

$$p_{e|XOR} \approx \frac{2P_{S_i,e} - 2P_{S_i,e}^2}{q} \tag{5.37}$$

since the two q-bit adjacent symbols differ in only one bit and, consequently, only one bit will be erased from the total q bits in the symbol.

When there is a symbol erasure on both I and Q components, then the channel bit erasure probability for MQAM is

$$p_{e|AND} \approx \frac{2\ P_{S_i,e}^2}{q} \tag{5.38}$$

since the four q-bit adjacent symbols differ in two bits and, as a consequence, only two bits will be erased from the total q bits in the symbol.

Therefore, the total channel bit erasure probability for MQAM is the sum of (5.37) and (5.38):

$$p_e \approx \frac{2\,P_{S_i,e}}{q} \tag{5.39}$$

If we substitute $P_{S_i,e}$ from (5.27) into (5.39), we obtain

$$p_e \approx \frac{4}{q}\left(1-\frac{1}{\sqrt{M}}\right)\left\{Q\left[(1-\alpha)\sqrt{\frac{3rE_S}{(M-1)N_0}}\right]-Q\left[(1+\alpha)\sqrt{\frac{3rE_S}{(M-1)N_0}}\right]\right\} \tag{5.40}$$

which, if we use the approximation for $P_{S,e}$ (5.32), is

$$p_e \approx \frac{P_{S,e}}{q} \tag{5.41}$$

Expressed another way, with the approximation we take into account the extra bit erasures for the regions where we have a symbol erasure on both the I and Q components.

In summary, the probabilities of channel symbol error and channel symbol erasure for MQAM are

$$p \approx \frac{4}{q}\left(1-\frac{1}{\sqrt{M}}\right)Q\left[(1+\alpha)\sqrt{\frac{3qrE_b}{(M-1)N_0}}\right] \tag{5.42}$$

$$p_e \approx \frac{4}{q}\left(1-\frac{1}{\sqrt{M}}\right)\left\{Q\left[(1-\alpha)\sqrt{\frac{3qrE_b}{(M-1)N_0}}\right]-Q\left[(1+\alpha)\sqrt{\frac{3qrE_b}{(M-1)N_0}}\right]\right\} \quad (5.43)$$

or

$$p_e \approx \frac{4}{q}\left(1-\frac{1}{\sqrt{M}}\right)Q\left[(1-\alpha)\sqrt{\frac{3qrE_b}{(M-1)N_0}}\right]-p \quad (5.44)$$

where q is the number of bits per symbol and $E_b = E_S/q$ is the average energy per information bit.

1. Performance in AWGN with PNI (No Fading)

The probability of channel bit error and channel bit erasure with PNI is found by combining (5.42) and (5.44) with (2.8), respectively, to get

$$p(\gamma_b) = \frac{4}{q}\left(1-\frac{1}{\sqrt{M}}\right)\left\{\rho\, Q\left[(1+\alpha)\sqrt{\frac{3qr\gamma_b}{(M-1)(1+N_I/\rho N_0)}}\right] + (1-\rho)\, Q\left[(1+\alpha)\sqrt{\frac{3qr\gamma_b}{M-1}}\right]\right\} \quad (5.45)$$

$$p_e(\gamma_b) = \frac{4}{q}\left(1-\frac{1}{\sqrt{M}}\right)\left\{\rho Q\left[(1-\alpha)\sqrt{\frac{3qr\gamma_b}{(M-1)(1+N_I/\rho N_0)}}\right] + (1-\rho)Q\left[(1-\alpha)\sqrt{\frac{3qr\gamma_b}{M-1}}\right]\right\} - p(\gamma_b) \quad (5.46)$$

where $\gamma_b = a_c^2 T_b / N_0 = E_b / N_0$ is the average energy per bit-to-AWGN power spectral density ratio.

These equations are used to compute (3.8), (3.9), and, finally, (3.10), which in turn is used in (2.16) with the values of B_d and d_{free} that correspond to the code rate shown in Table 2 to obtain an upper bound on the probability of information bit error.

a. 16QAM r=1/2

Figure 54 is a plot of the performance obtained with errors-and-erasures decoding for various values of the parameter α when $\rho = 0.5$ and $E_b/N_0 = 15\,\text{dB}$. As can be seen, like the case of BPSK/QPSK with a code rate of 1/2, performance is

relatively insensitive to α for $P_b > 10^{-5}$ and is relatively insensitive for $0.5 \geq \alpha \geq 0.3$ when $P_b > 10^{-10}$; although, $\alpha = 0.5$ yields the best results overall.

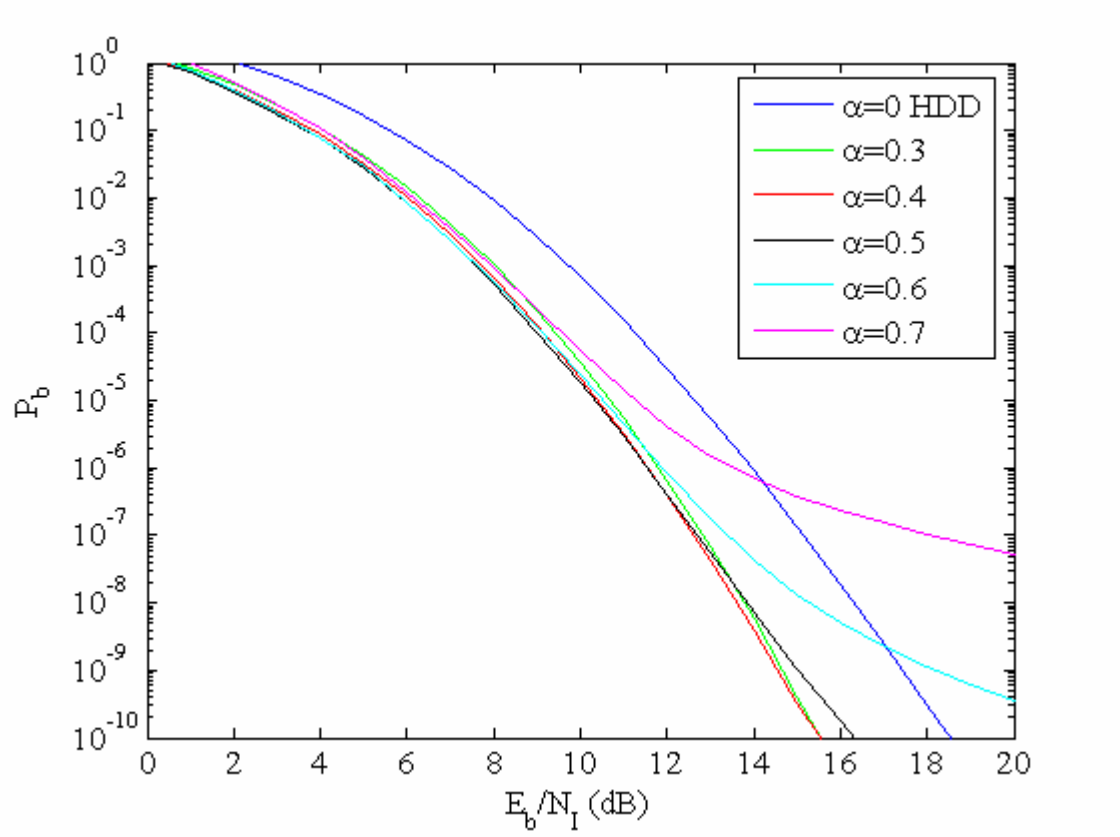

Figure 54. Performance of 16QAM in AWGN and PNI (ρ=0.5) with r=1/2 convolutional source coding and EED for a channel with no fading ($E_b/N_0 = 15\,\text{dB}$).

Figure 55 is a plot of the performance obtained with errors-and-erasures decoding for various values of the parameter ρ when $\alpha = 0.5$ and $E_b/N_0 = 11\,\text{dB}$. This value of E_b/N_0 was chosen since this yields $P_b = 10^{-8}$ for $E_b/N_I = 30\,\text{dB}$. As can be seen, while pulse-noise interference does somewhat degrade performance for certain values of E_b/N_I and ρ, to a large extent the effect of pulse-noise interference has been eliminated. As with HDD, as ρ approaches zero, the performance converges to the AWGN limit, and, generally, the bigger the value of ρ is, the poorer the performance.

There is a small range of E_b/N_I where $\rho<1$ results in performance poorer than for $\rho=1$, but generally, the degradation is less than 2 dB.

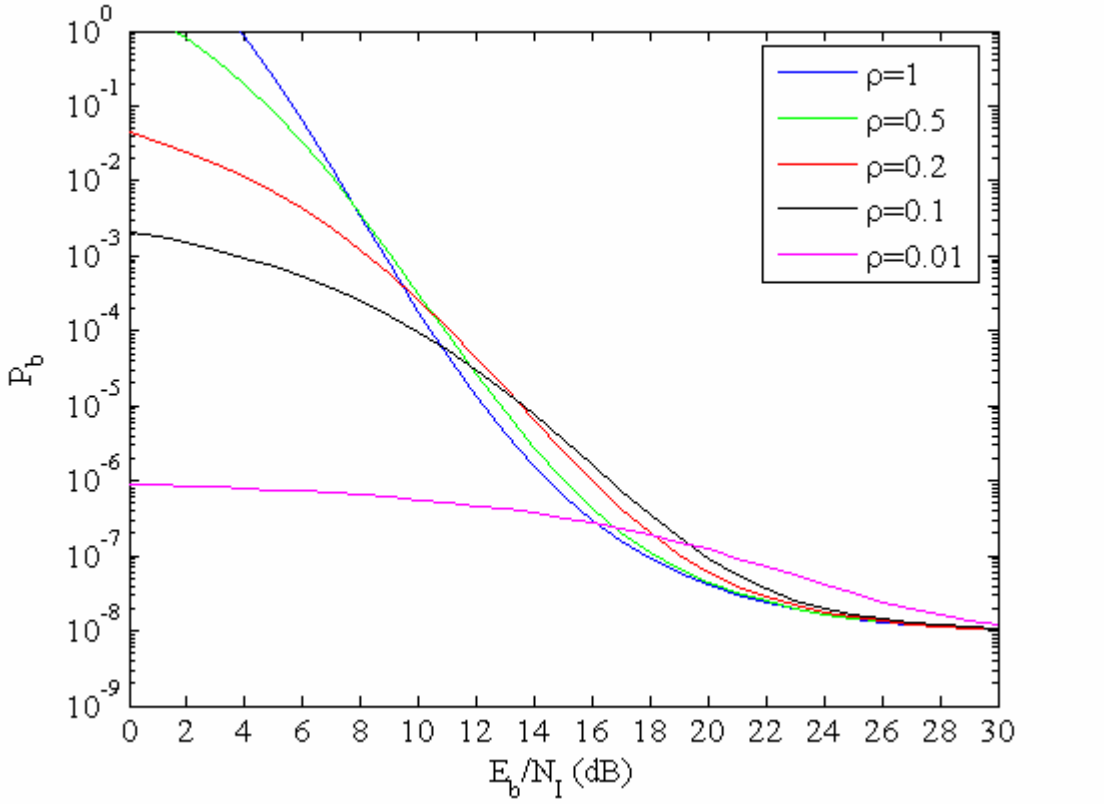

Figure 55. Performance of 16QAM in AWGN and PNI with *r*=1/2 convolutional source coding and EED (α=0.5) for a channel with no fading ($E_b/N_0=11\text{dB}$).

b. 16QAM r=3/4

Figure 56 is a plot of the performance obtained with errors-and-erasures decoding for various values of the parameter α when $\rho=0.5$ and $E_b/N_0=15\text{dB}$. In this case, $\alpha=0.4$ gives better results than $\alpha=0.5$, which gave the best results for *r*=1/2.

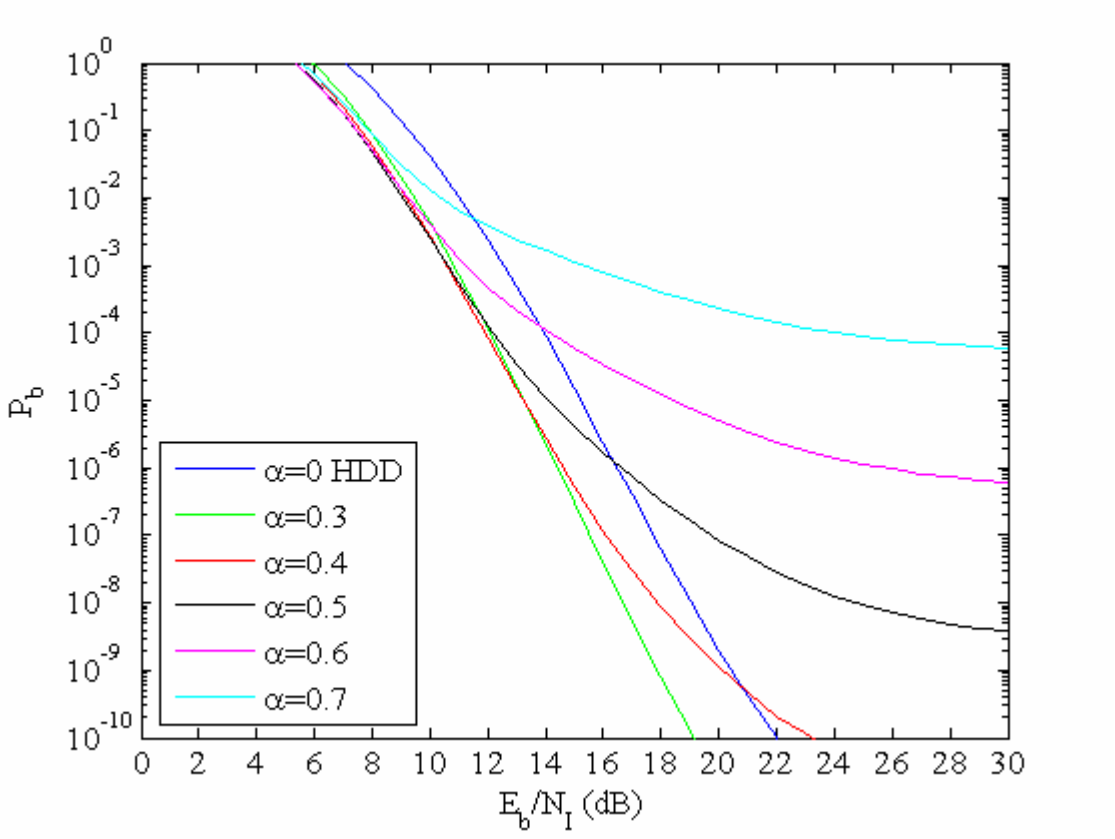

Figure 56. Performance of 16QAM in AWGN and PNI (ρ=0.5) with r=3/4 convolutional source coding and EED for a channel with no fading ($E_b/N_0 = 15\,\text{dB}$).

Figure 57 is a plot of the performance obtained with errors-and-erasures decoding for various values of the parameter ρ when $\alpha = 0.4$ and $E_b/N_0 = 13.05\,\text{dB}$. This value of E_b/N_0 was chosen since this yields $P_b = 10^{-8}$ for $E_b/N_I = 30\,\text{dB}$. In this case, we arrive at similar conclusions as with the previous case for r=1/2, but there is clearly a much greater sensitivity to PNI for the higher code rate, especially when ρ is very small.

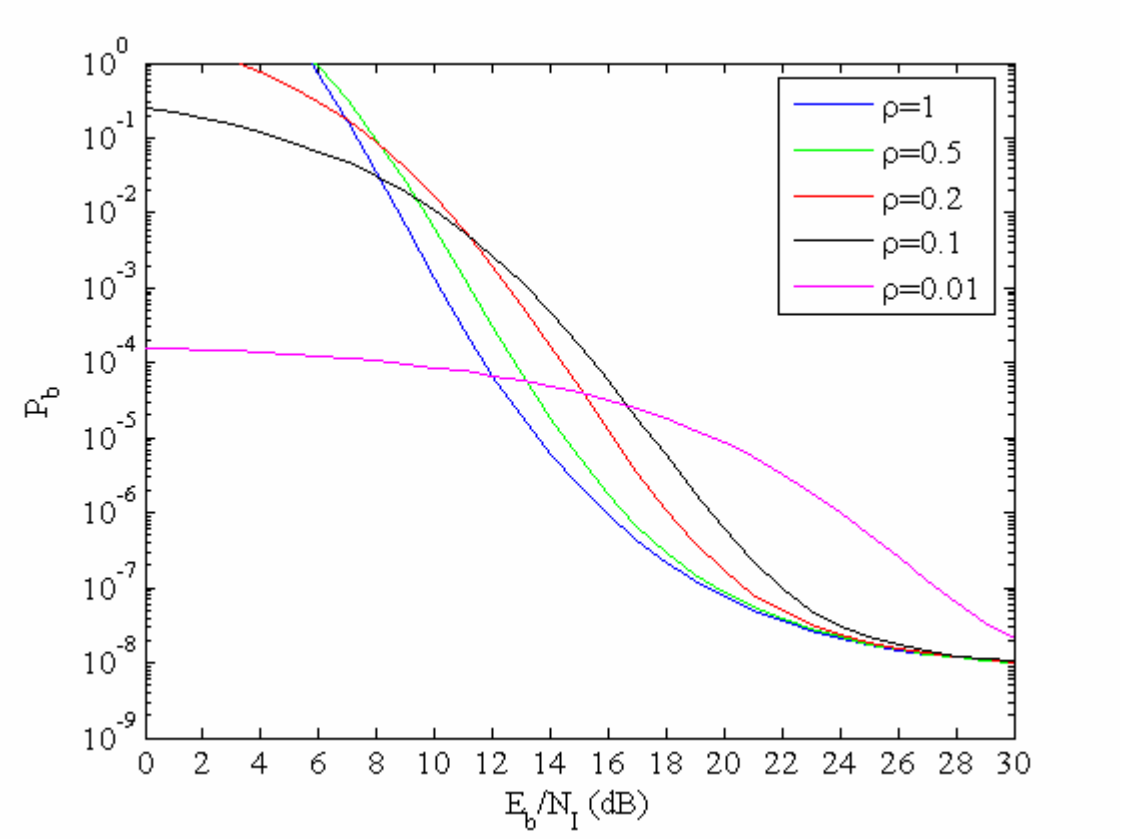

Figure 57. Performance of 16QAM in AWGN and PNI with r=3/4 convolutional source coding and EED (α=0.4) for a channel with no fading ($E_b/N_0 = 13.05\,\text{dB}$).

c. 64QAM r=2/3

Figure 58 is a plot of the performance obtained with errors-and-erasures decoding for various values of the parameter α when $\rho = 0.5$ and $E_b/N_0 = 15\,\text{dB}$. In this case, similar to 16QAM with code rate 3/4, $\alpha = 0.4$ gives better results than $\alpha = 0.5$.

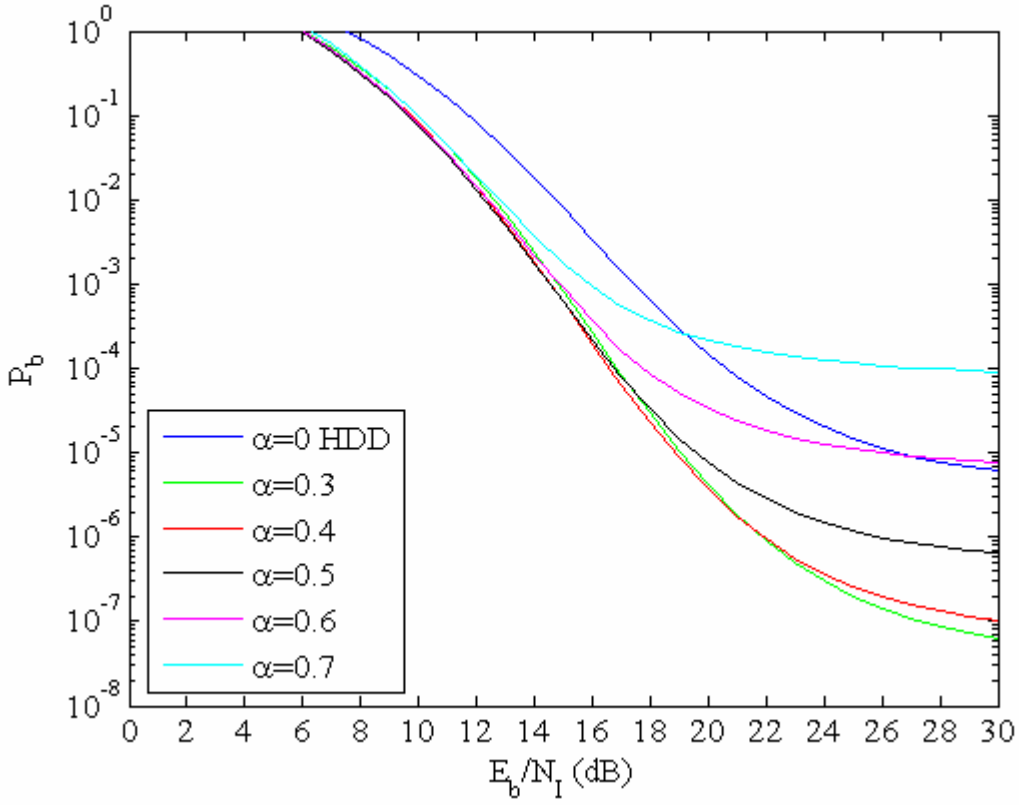

Figure 58. Performance of 64QAM in AWGN and PNI (ρ=0.5) with r=2/3 convolutional source coding and EED for a channel with no fading ($E_b/N_0 = 15\,\text{dB}$).

Figure 59 is a plot of the performance obtained with errors-and-erasures decoding for various values of the parameter ρ when $\alpha = 0.4$ and $E_b/N_0 = 15.7\,\text{dB}$. This value of E_b/N_0 was chosen since this yields $P_b = 10^{-8}$ for $E_b/N_I = 30\,\text{dB}$. As can be seen, PNI degrades performance much less than 16QAM with r=3/4 but more than 16QAM with r=1/2. Clearly, the ability of the system to reject PNI is closely related to the code rate when code rate is increased but the number of memory elements in the encoder are not.

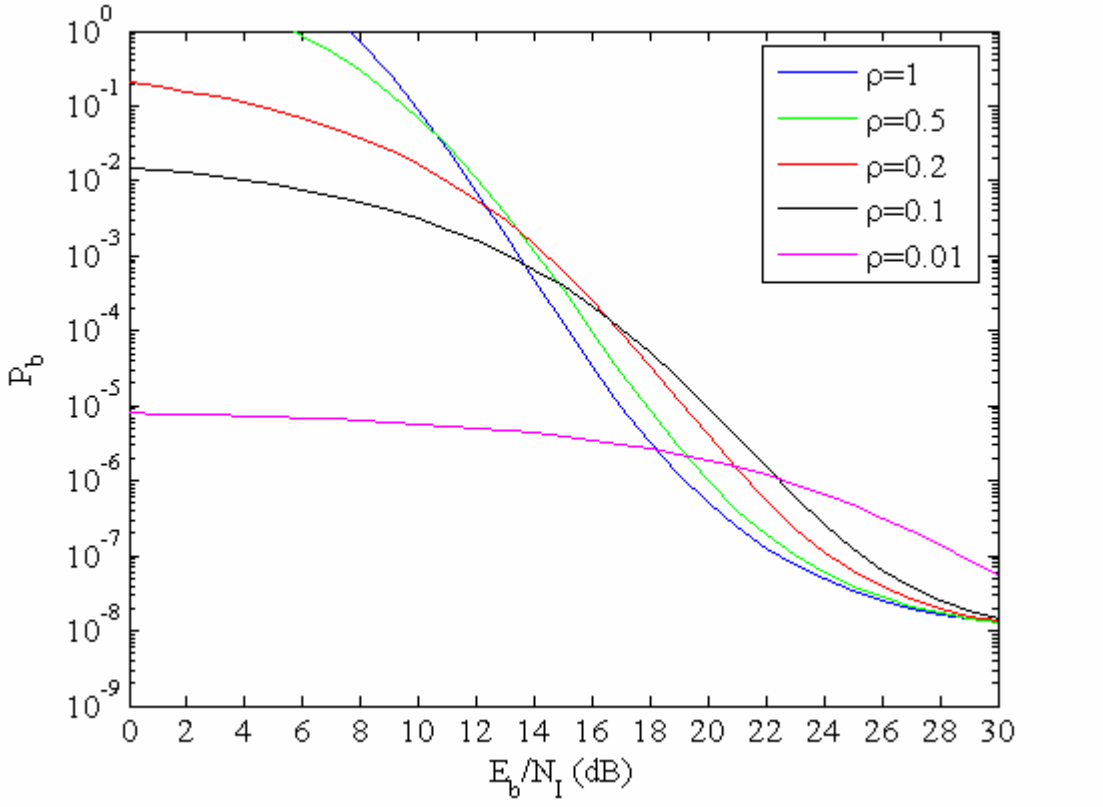

Figure 59. Performance of 64QAM in AWGN and PNI with *r*=2/3 convolutional source coding and EED (α=0.4) for a channel with no fading ($E_b/N_0 = 15.7\,\text{dB}$).

d. 64QAM r=3/4

Finally, for 64QAM with a code rate of 3/4, the performance obtained with errors-and-erasures decoding for various values of the parameter α when $\rho = 0.5$ and $E_b/N_0 = 15\,\text{dB}$ can be seen in Figure 60. Again, $\alpha = 0.4$ yields the best overall performance.

Figure 61 is a plot of the performance obtained with errors-and-erasures decoding for various values of the parameter ρ when $\alpha = 0.4$ and $E_b/N_0 = 17.22\,\text{dB}$. This value of E_b/N_0 was chosen since this yields $P_b = 10^{-8}$ for $E_b/N_I = 30\,\text{dB}$. As can be seen, similar to 16QAM with *r*=3/4, PNI is much more of a factor than for *r*=1/2 and *r*=2/3.

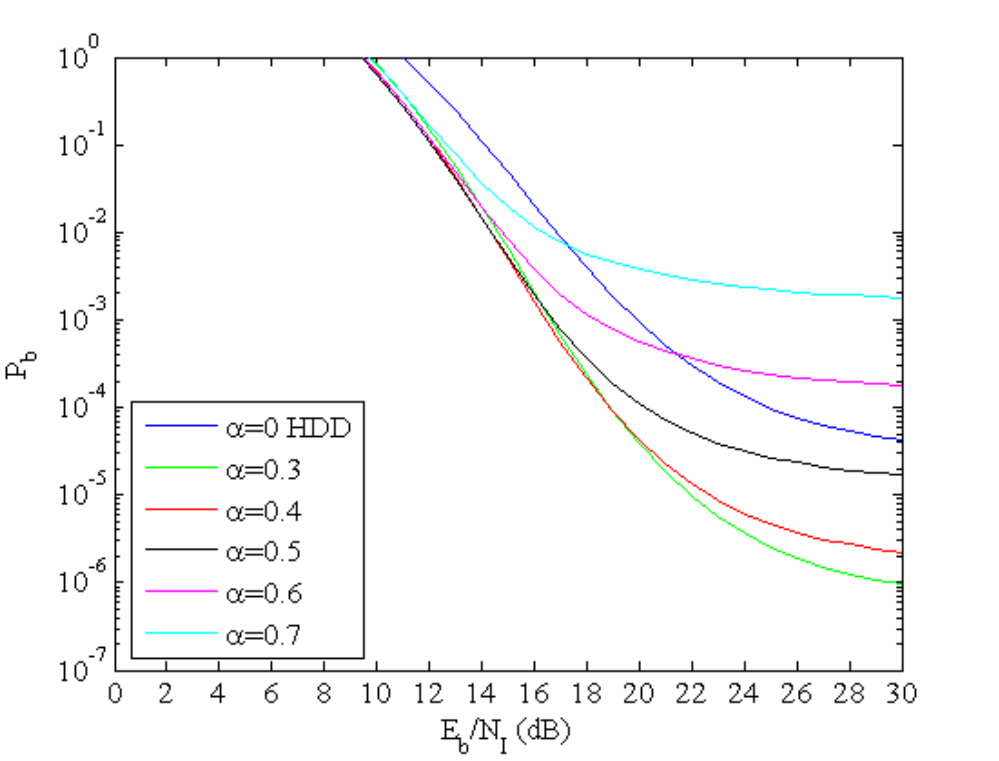

Figure 60. Performance of 64QAM in AWGN and PNI (ρ=0.5) with r=3/4 convolutional source coding and EED for a channel with no fading ($E_b/N_0 = 15\,\text{dB}$).

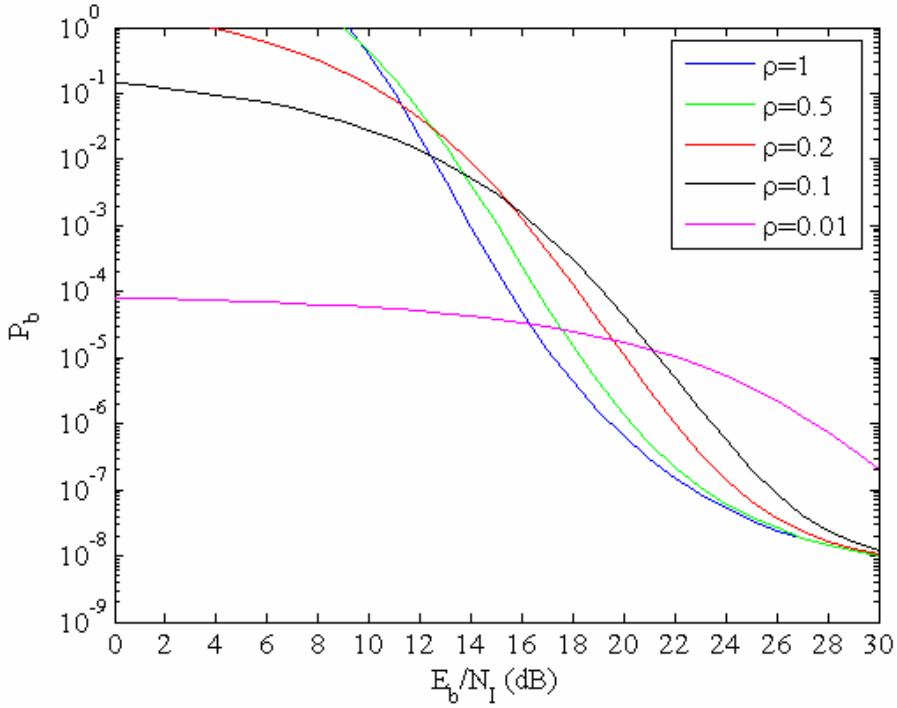

Figure 61. Performance of 64QAM in AWGN and PNI with r=3/4 convolutional source coding and EED (α=0.4) for a channel with no fading ($E_b/N_0 = 17.22\,\text{dB}$).

2. Performance in AWGN with PNI and Fading

When the channel is modeled as a Nakagami fading channel, then (5.45) and (5.46) are conditional probabilities. The unconditional probabilities of channel bit error and channel bit erasure are found by substituting (5.45) and (5.46) into (2.12), respectively. The integrations required to obtain these unconditional probabilities can be evaluated numerically or analytically using the identity (5.4).

a. 16QAM r=1/2

In Figure 62, the performance is plotted for different fading conditions. In order to validate the results obtained using the analytical solution, the performance is obtained both analytically and numerically. For this figure $E_b/N_0 = 15\,\text{dB}$, $\rho = 0.5$, and $\alpha = 0.4$. It is clear that both methods give virtually identical results for all fading conditions. As can be seen, the receiver performance worsens as the fading conditions worsen and improves as m increases, approaching for m=10 the non-fading condition $(m \to \infty)$.

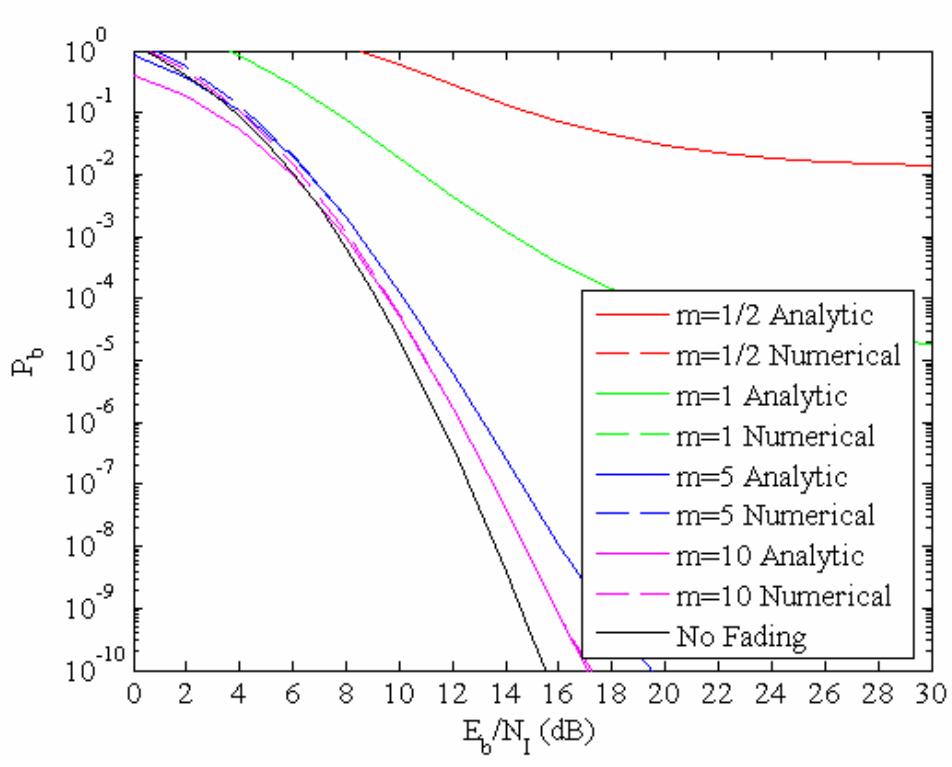

Figure 62. Performance of 16QAM in AWGN and PNI (ρ=0.5) with r=1/2 convolutional source coding and EED (α=0.4) for a Nakagami fading channel ($E_b/N_0 = 15\,\text{dB}$) computed both analytically and numerically.

Figure 63 is a plot of the performance obtained with errors-and-erasures decoding for various values of the parameter α when $\rho = 0.5$, $m = 1$, and $E_b/N_0 = 15\,\text{dB}$. As can be seen, $\alpha = 0.4$ yields the best overall performance.

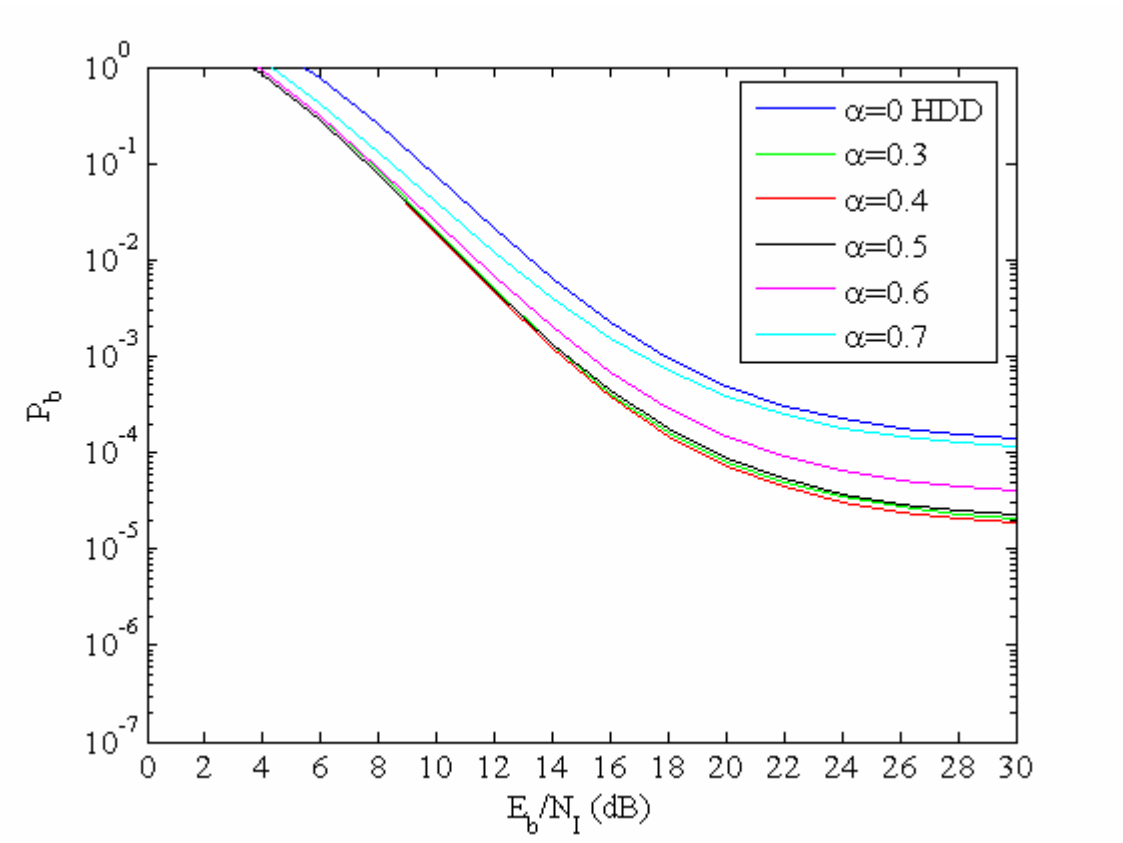

Figure 63. Performance of 16QAM in AWGN and PNI (ρ=0.5) with r=1/2 convolutional source coding and EED for a Nakagami fading channel (m=1) ($E_b/N_0 = 15\,\text{dB}$).

In Figure 64, the effect that the factor ρ has on the receiver's performance is shown. In this figure, the performance is plotted for various values of the parameter ρ when $E_b/N_0 = 25\,\text{dB}$, $m = 1$, and $\alpha = 0.4$. As can be seen, varying ρ affects the receiver performance significantly, particularly when $E_b/N_I < 16\,\text{dB}$. Like HDD, it is clear that barrage noise interference ($\rho = 1$) is more effective than PNI. As ρ approaches zero, the performance converges to the AWGN limit.

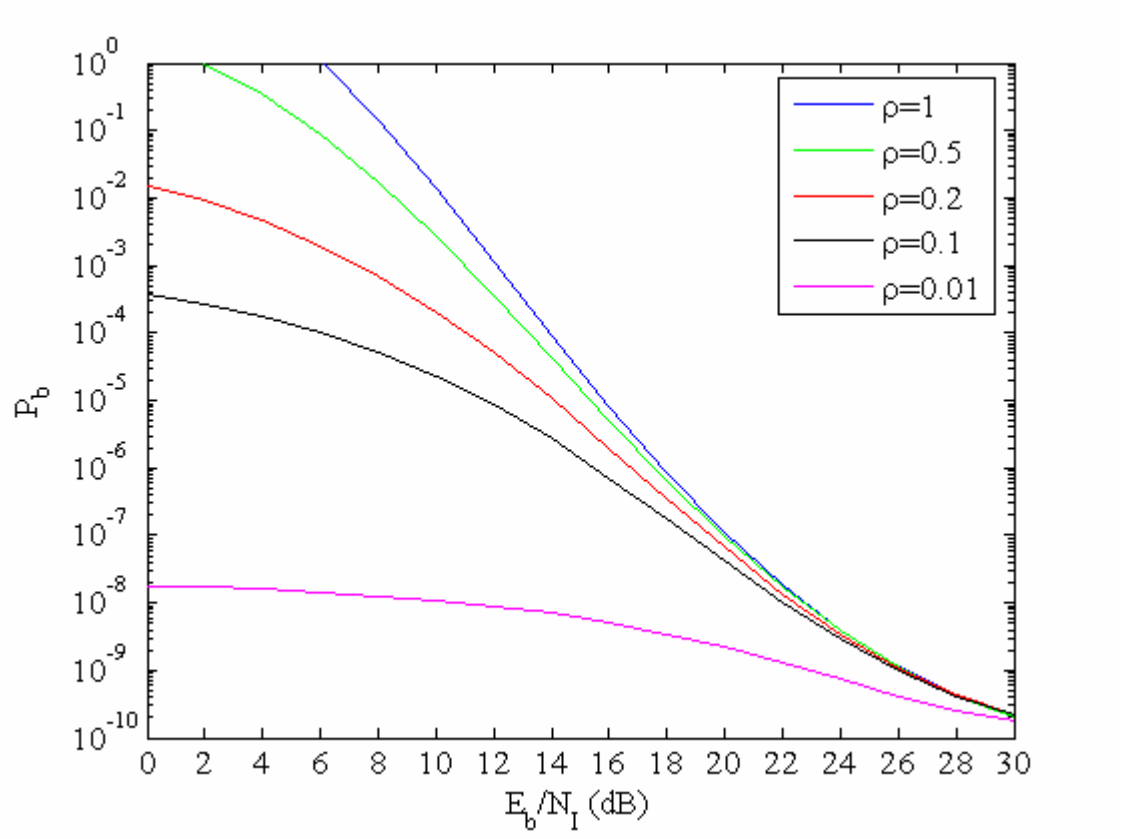

Figure 64. Performance of 16QAM in AWGN and PNI with r=1/2 convolutional source coding and EED (α=0.4) for a Nakagami fading channel (m=1)($E_b/N_0 = 25\,\text{dB}$).

b. 16QAM r=3/4

Figures 65, 66, and 67 are analogous to Figures 62, 63, and 64, respectively, for a code rate of 3/4 instead of 1/2. It is obvious that in this case the effect of the channel fading is more severe, and the effect of PNI is very similar for both code rates.

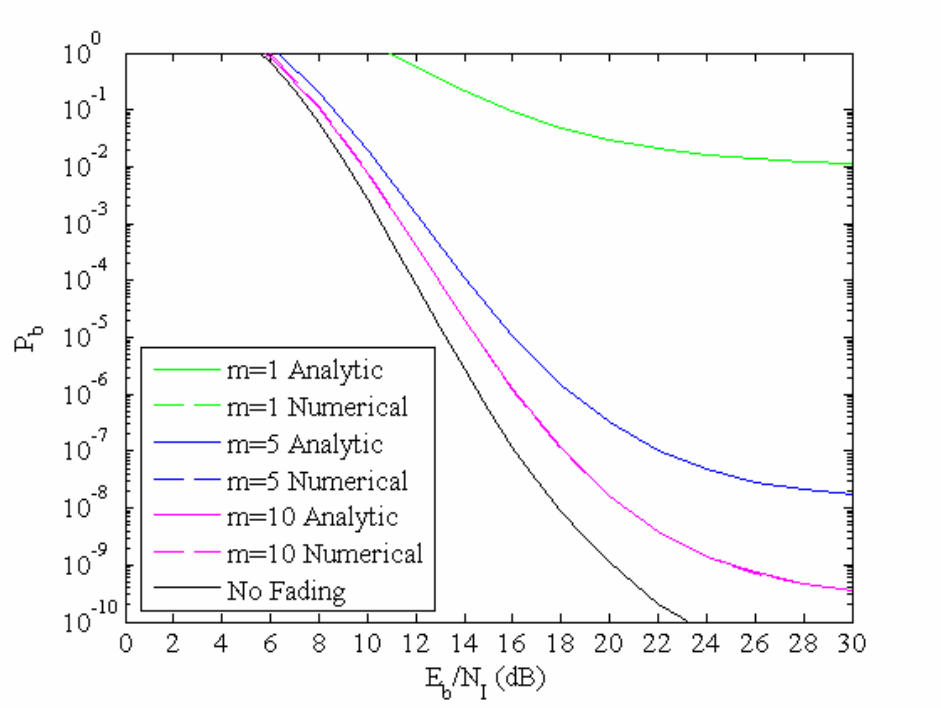

Figure 65. Performance of 16QAM in AWGN and PNI (ρ=0.5) with r=3/4 convolutional source coding and EED (α=0.4) for a Nakagami fading channel ($E_b/N_0 = 15\,\text{dB}$) computed both analytically and numerically.

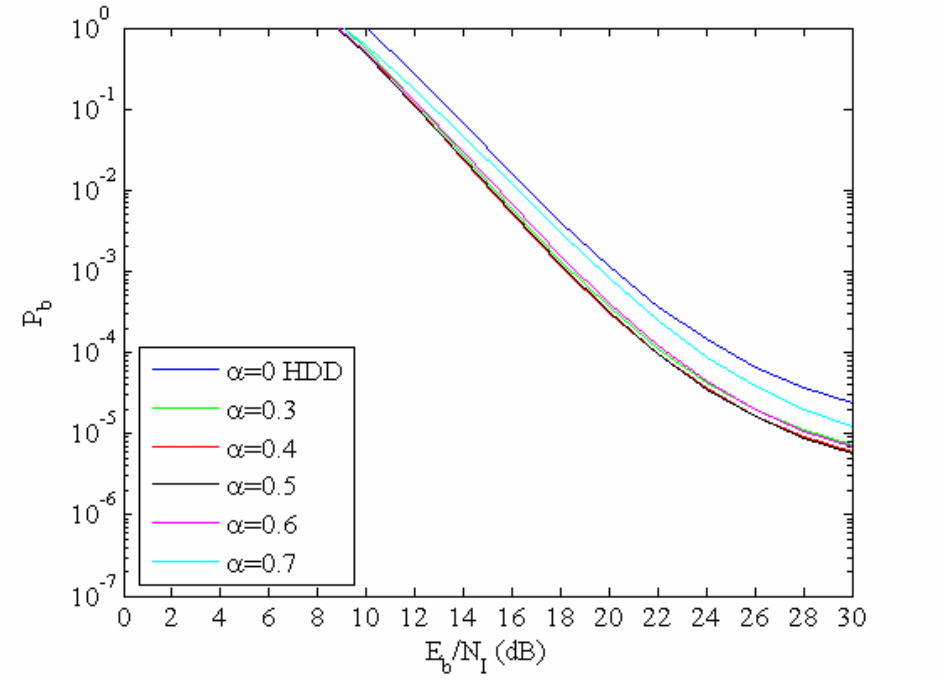

Figure 66. Performance of 16QAM in AWGN and PNI (ρ=0.5) with r=3/4 convolutional source coding and EED for a Nakagami fading channel (m=1) ($E_b/N_0 = 25\,\text{dB}$).

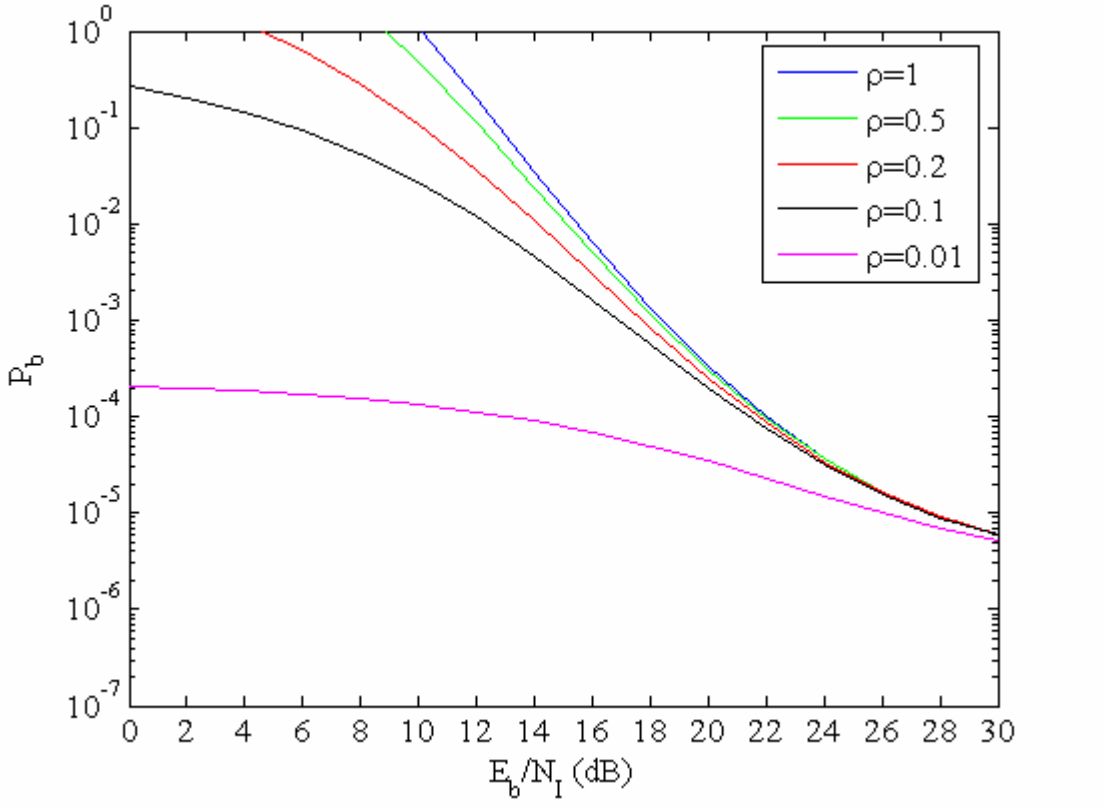

Figure 67. Performance of 16QAM in AWGN and PNI with r=3/4 convolutional source coding and EED (α=0.4) for a Nakagami fading channel (m=1) ($E_b/N_0 = 25\text{dB}$).

c. 64QAM r=2/3

As with previous analyses, in Figure 68 the performance is plotted for different fading conditions, and in Figures 69 and 70 for various values of the parameter ρ and a, respectively. If we compare Figures 67 and 70, we can see that they are very close to each other. This happens because, although we change the type of modulation from 16QAM to 64QAM, that normally leads to performance degradation, the code rate for 64QAM is smaller than for 16QAM, and performance does not change much. Similar to HDD, when channel fading is a factor, performance is determined by the combination of modulation and code rate.

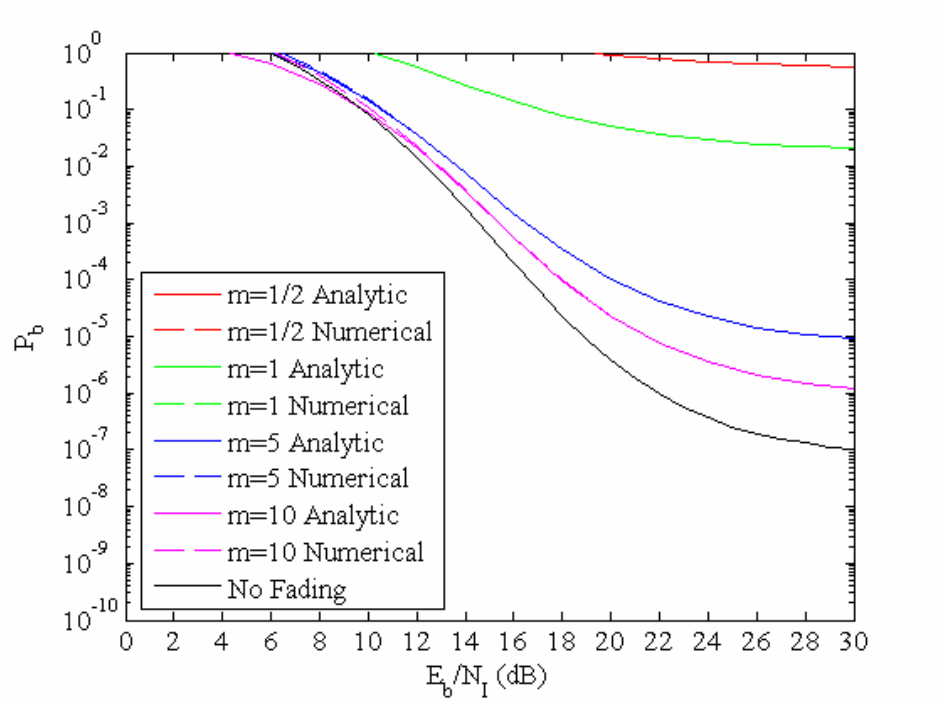

Figure 68. Performance of 64QAM in AWGN and PNI (ρ=0.5) with r=2/3 convolutional source coding and EED (α=0.4) for a Nakagami fading channel ($E_b/N_0 = 15\,\text{dB}$) computed both analytically and numerically.

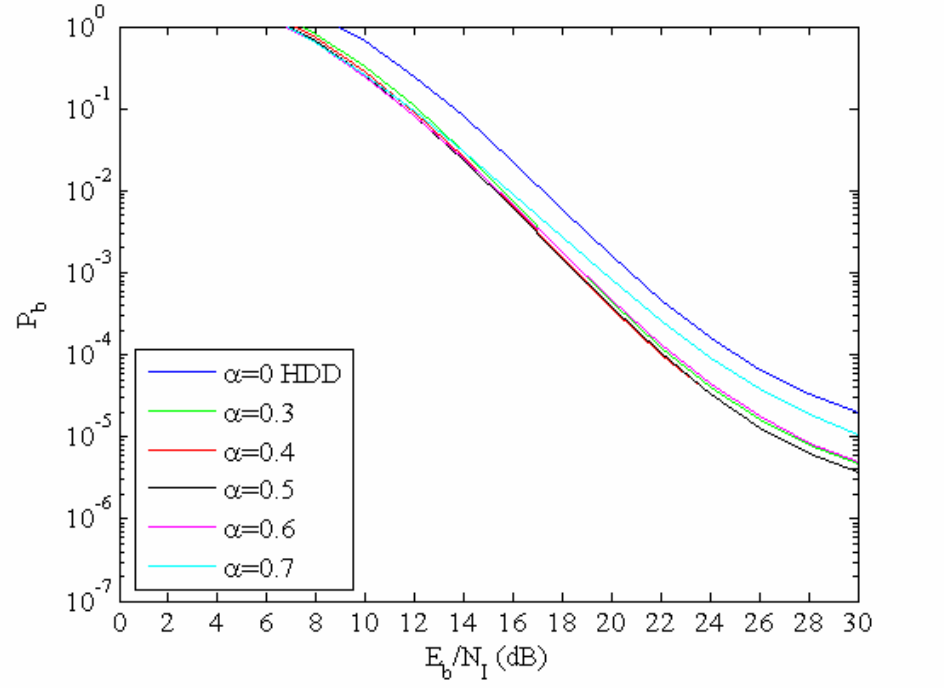

Figure 69. Performance of 64QAM in AWGN and PNI (ρ=0.5) with r=2/3 convolutional source coding and EED for a Nakagami fading channel (m=1) ($E_b/N_0 = 25\,\text{dB}$).

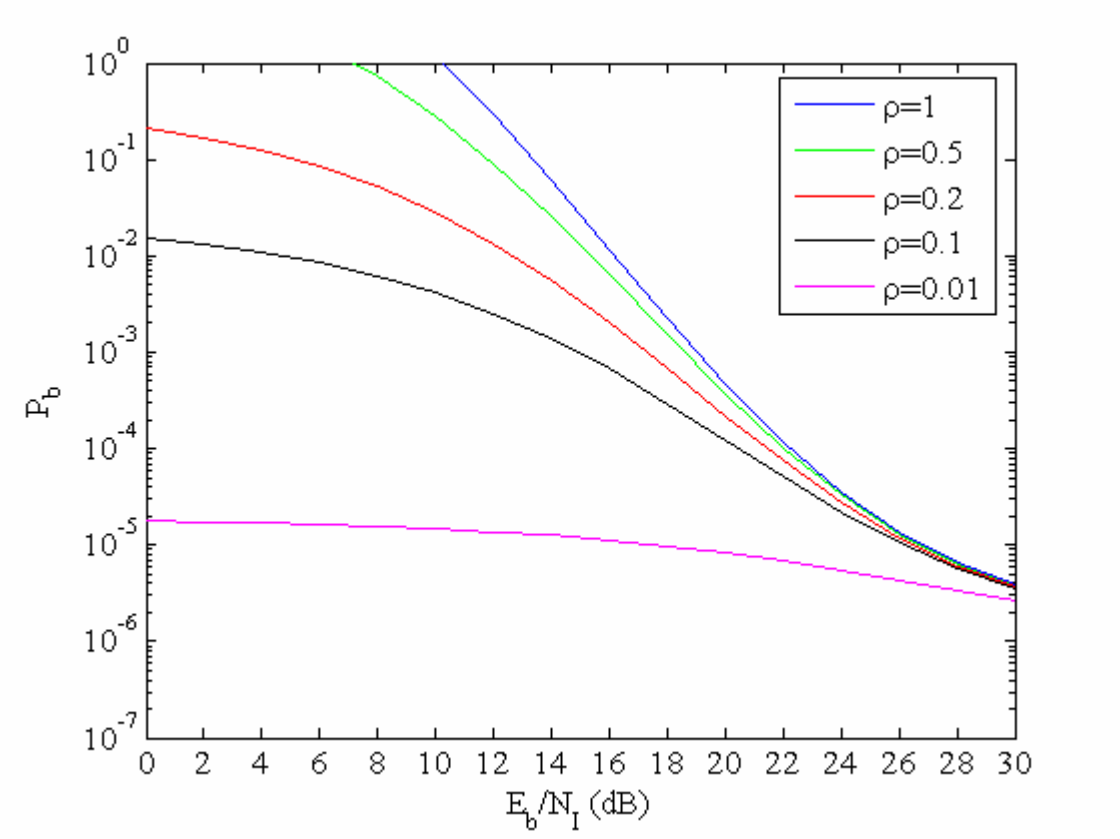

Figure 70. Performance of 64QAM in AWGN and PNI with r=2/3 convolutional source coding and EED (α=0.4) for a Nakagami fading channel (m=1) ($E_b/N_0 = 25\text{dB}$).

d. 64QAM r=3/4

Finally, for the higher data rate, 64QAM with a code rate of 3/4 is analyzed in Figures 71, 72, and 73. As might be expected, we reach the same conclusions with the lower data rates. Comparing Figures 67 and 73, we see the expected degradation in performance that occurs in going from 16QAM to 64QAM.

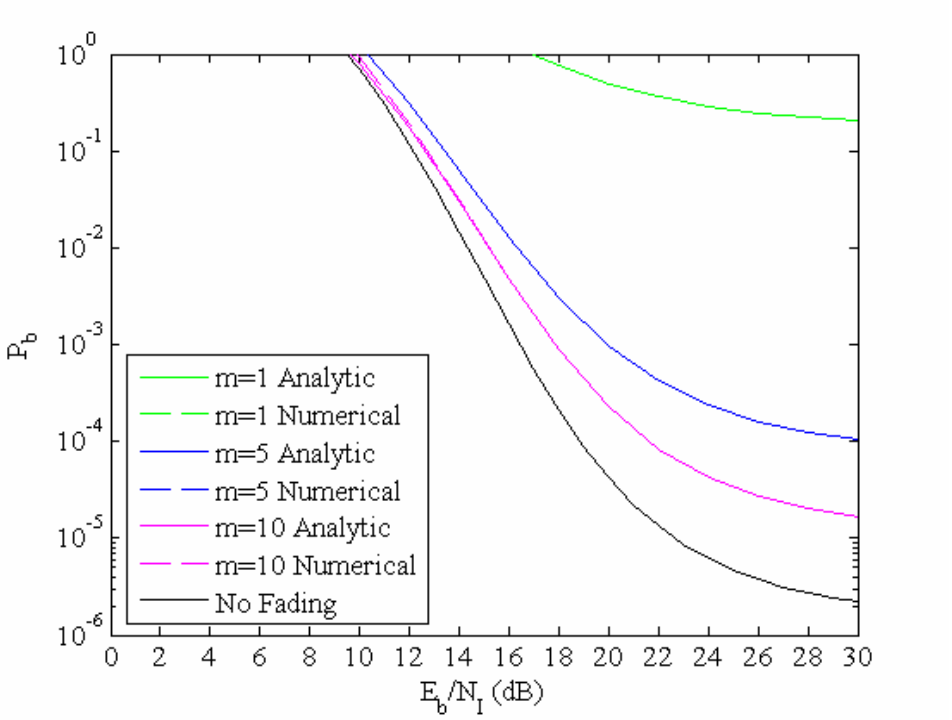

Figure 71. Performance of 64QAM in AWGN and PNI (ρ=0.5) with r=3/4 convolutional source coding and EED (α=0.4) for a Nakagami fading channel ($E_b/N_0 = 15\,\text{dB}$) computed both analytically and numerically.

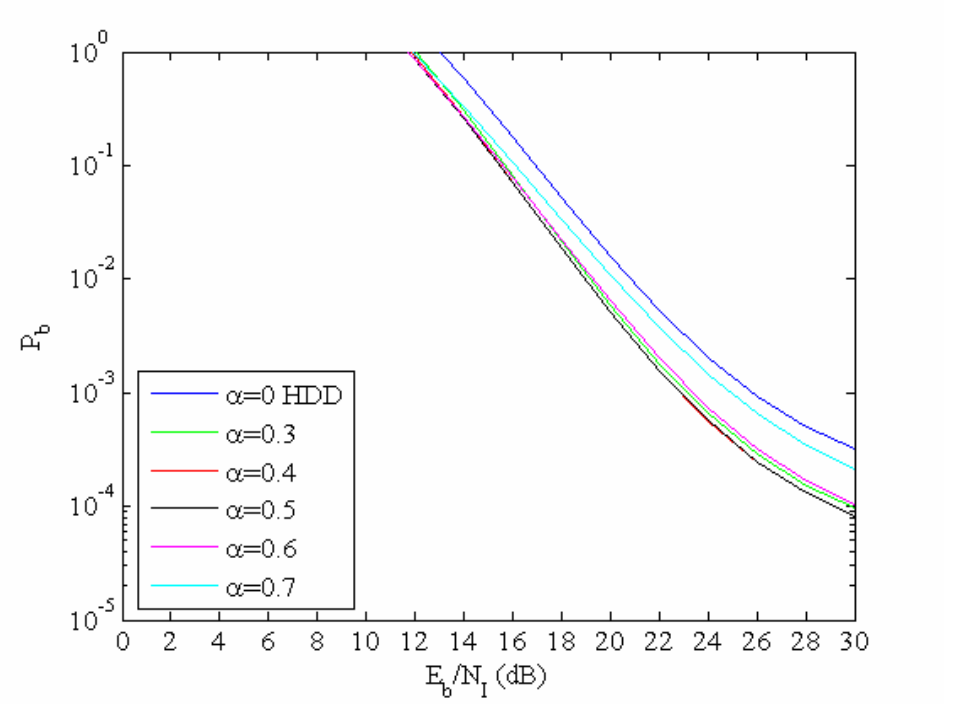

Figure 72. Performance of 64QAM in AWGN and PNI (ρ=0.5) with r=3/4 convolutional source coding and EED for a Nakagami fading channel (m=1) ($E_b/N_0 = 25\,\text{dB}$).

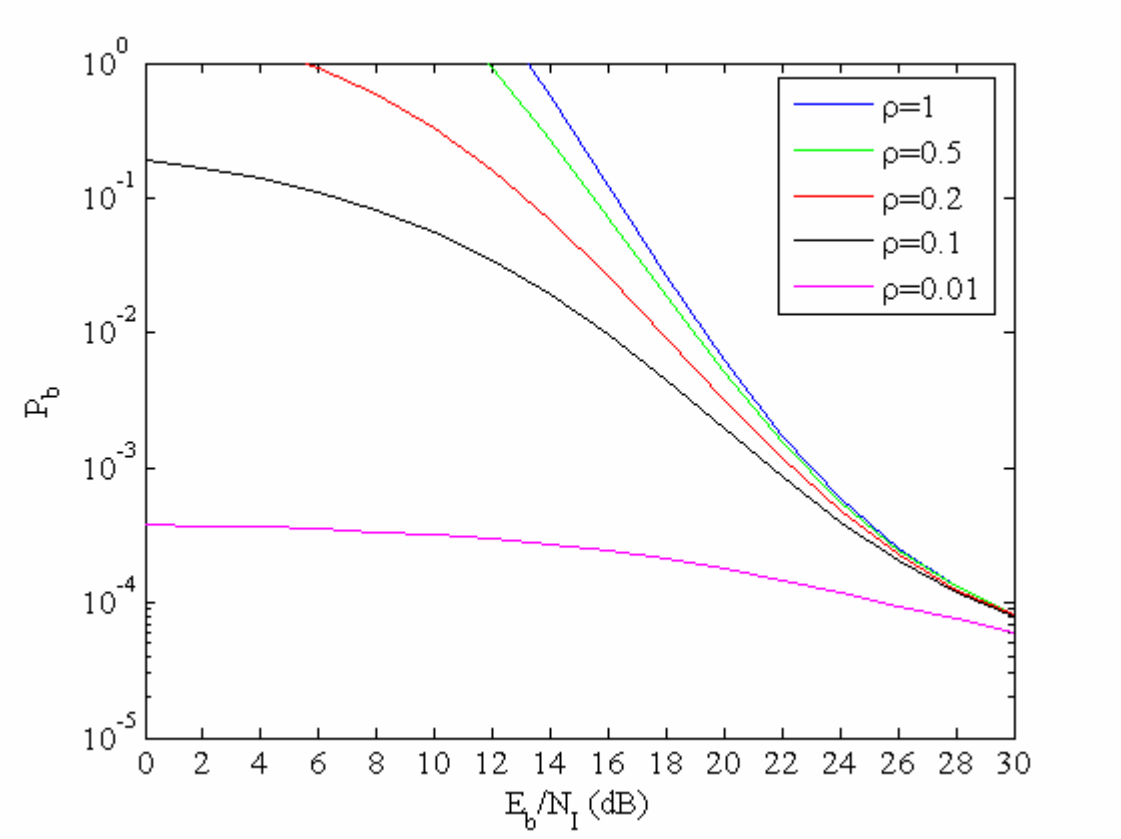

Figure 73. Performance of 64QAM in AWGN and PNI with r=3/4 convolutional source coding and EED (α=0.4) for a Nakagami fading channel (m=1) ($E_b/N_0 = 25\,\text{dB}$).

C. COMPARISONS OF THE PERFORMANCE WITH HDD AND EED.

1. Comparisons in AWGN with PNI (No Fading)

Figures 74, 75, and 76 are a comparison of the performance of 16QAM and 64QAM obtained with EED to that obtained with HDD for $E_b/N_0 = 25\,\text{dB}$ with ρ = 1, ρ = 0.1, and ρ = 0.01, respectively. In all cases, generally, the performance obtained for EED is superior relative to that obtained for errors-only HDD.

In Figure 74, where ρ = 1, which corresponds to continuous noise interference, the performance of 64QAM (code rates of 2/3 and 3/4) and 16QAM (r=1/2) with HDD is clearly inferior relative to EED, while for 16QAM (r=3/4), EED has a significant advantage over HDD for $E_b/N_I < 17\,\text{dB}$. Additionally, 64QAM with a code rate of 3/4 and EED outperforms 64QAM with a code rate of 2/3 and HDD.

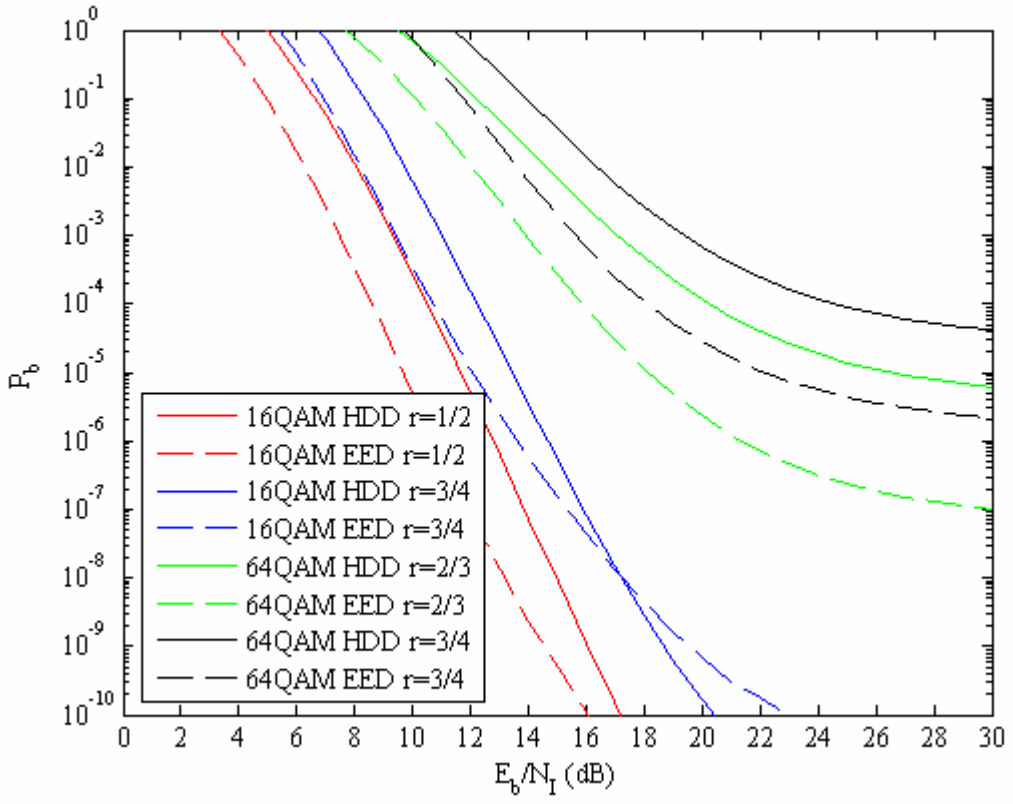

Figure 74. Performance of 16QAM and 64QAM for EED and HDD for a channel with no fading, $E_b/N_0 = 15\,\text{dB}$, and ρ = 1.

In Figure 75, ρ = 0.1. In this case, when E_b/N_I is small and the probability of bit error is large, the advantage of EED over HDD is small, but for larger E_b/N_I, EED has a distinct advantage over HDD. It can also be seen that for 16QAM, the range of E_b/N_I over which EED clearly outperforms HDD is larger. This is an artifact of the E_b/N_0 used. If E_b/N_0 is increased for 64QAM, then the range of E_b/N_I over which EED clearly outperforms HDD increases. In this case, it can be seen that for $E_b/N_I < 11\,\text{dB}$, 64QAM with a code rate of 2/3 outperforms 16QAM with a code rate of 3/4 regardless of the decoding procedure, and for $E_b/N_I < 16\,\text{dB}$, 64QAM (r=2/3) with EED outperforms 16QAM (r=3/4) with HDD. Furthermore, for $E_b/N_I > 21\,\text{dB}$, the performance obtained for 64QAM (r=3/4) with EED is superior to that obtained for 64QAM (r=2/3) with HDD.

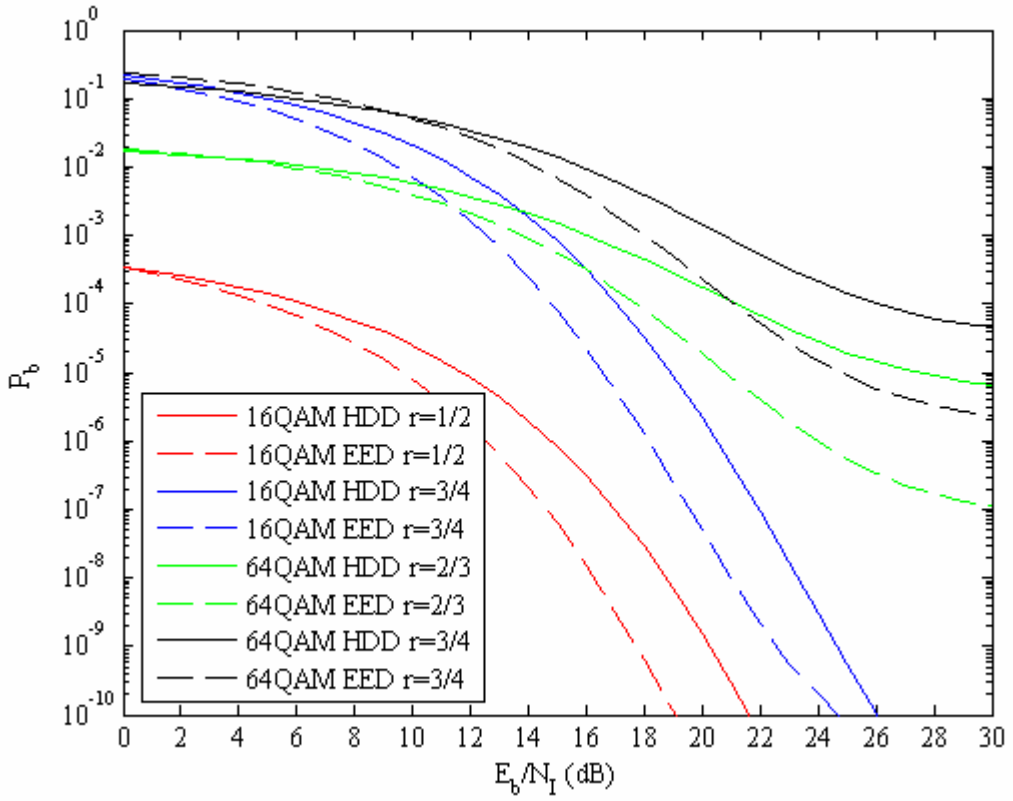

Figure 75. Performance of 16QAM and 64QAM for EED and HDD for a channel with no fading, $E_b/N_0 = 15\,\text{dB}$, and ρ = 0.1.

In Figure 76, ρ = 0.01. In this case the performances obtained for 16QAM (r=3/4) with EED and HDD for $E_b/N_I < 12\,\text{dB}$ are virtually indistinguishable from one another, and for $E_b/N_I > 20\,\text{dB}$, EED outperforms HDD. For 64QAM the performance obtained for HDD is clearly inferior relative to that obtained for EED for all E_b/N_I for both code rates; although, for $E_b/N_I < 14\,\text{dB}$, 64QAM with a code rate of 2/3 and HDD outperform 16QAM with a code rate of 3/4 regardless of the decoding procedure, and for $E_b/N_I < 20\,\text{dB}$ 64QAM (r=2/3) with EED outperforms 16QAM (r=3/4) with HDD and EED. Furthermore, for $E_b/N_I > 28\,\text{dB}$, the performance obtained for 64QAM (r=3/4) with EED is superior to that obtained for 64QAM (r=2/3) with HDD. A significant observation is that for $E_b/N_I < 22\,\text{dB}$ and for 16QAM with a code rate of 1/2, HDD outperforms EED, but if E_b/N_0 is decreased, the reverse is true.

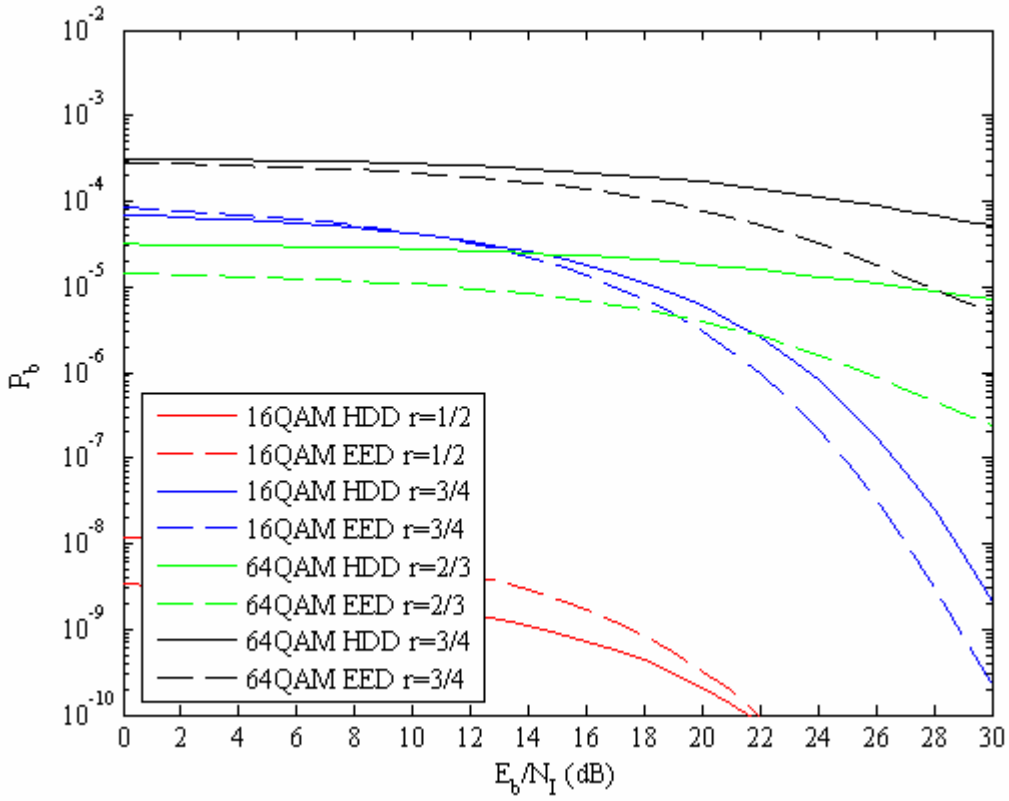

Figure 76. Performance of 16QAM and 64QAM for EED and HDD for a channel with no fading, $E_b/N_0 = 15\,\text{dB}$, and ρ = 0.01.

2. Comparisons in AWGN with PNI and Fading

The effect of channel fading can be seen in Figures 77, 78, and 79, where *m*=0.5, *m*=1.0, and *m*=2.0, respectively. In each case, ρ=0.5 and E_b/N_0 is chosen so that $P_b = 10^{-8}$ for $E_b / N_I >> 1$, for 16QAM with EED and a code rate of 3/4. In each case, we see that EED outperforms HDD for all E_b / N_I.

An interesting observation is that, while the performance obtained for 64QAM with code rate 2/3 for *m*=2 is inferior to that obtained for 16QAM with code rate 3/4, as we move to more severe fading conditions, for *m*=1 the two performances are approximately equal, and for *m*=0.5, 64QAM with a code rate of 2/3 outperforms 16QAM with a code rate of 3/4. Hence, when channel fading is a factor, higher data rates may be more robust than some of the lower ones.

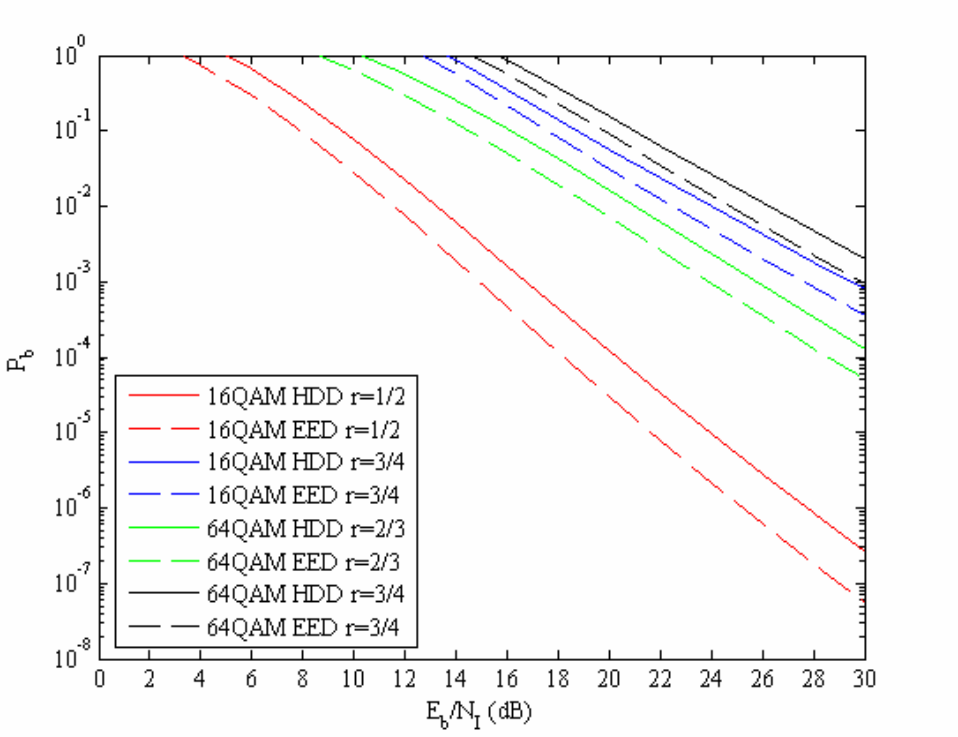

Figure 77. Performance of 16QAM and 64QAM for EED and HDD for a Nakagami fading channel with m=0.5, $E_b/N_0 = 60\,\text{dB}$, and ρ = 0.5.

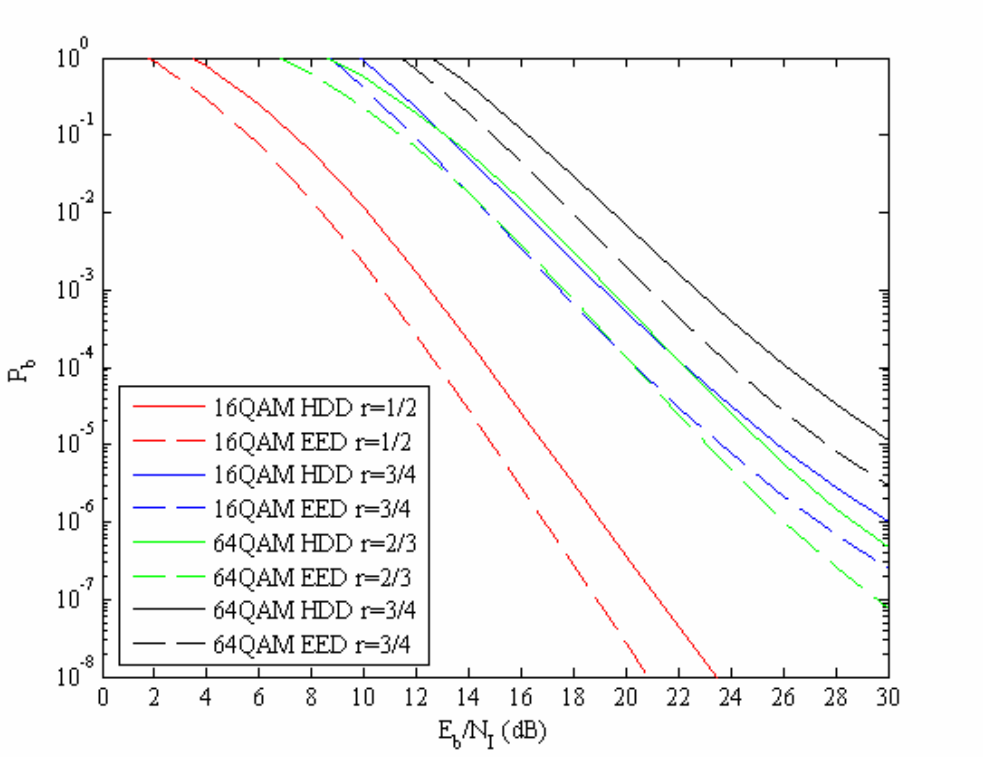

Figure 78. Performance of 16QAM and 64QAM for EED and HDD for a Nakagami fading channel with m=1, $E_b/N_0 = 32.7\,\text{dB}$, and ρ = 0.5.

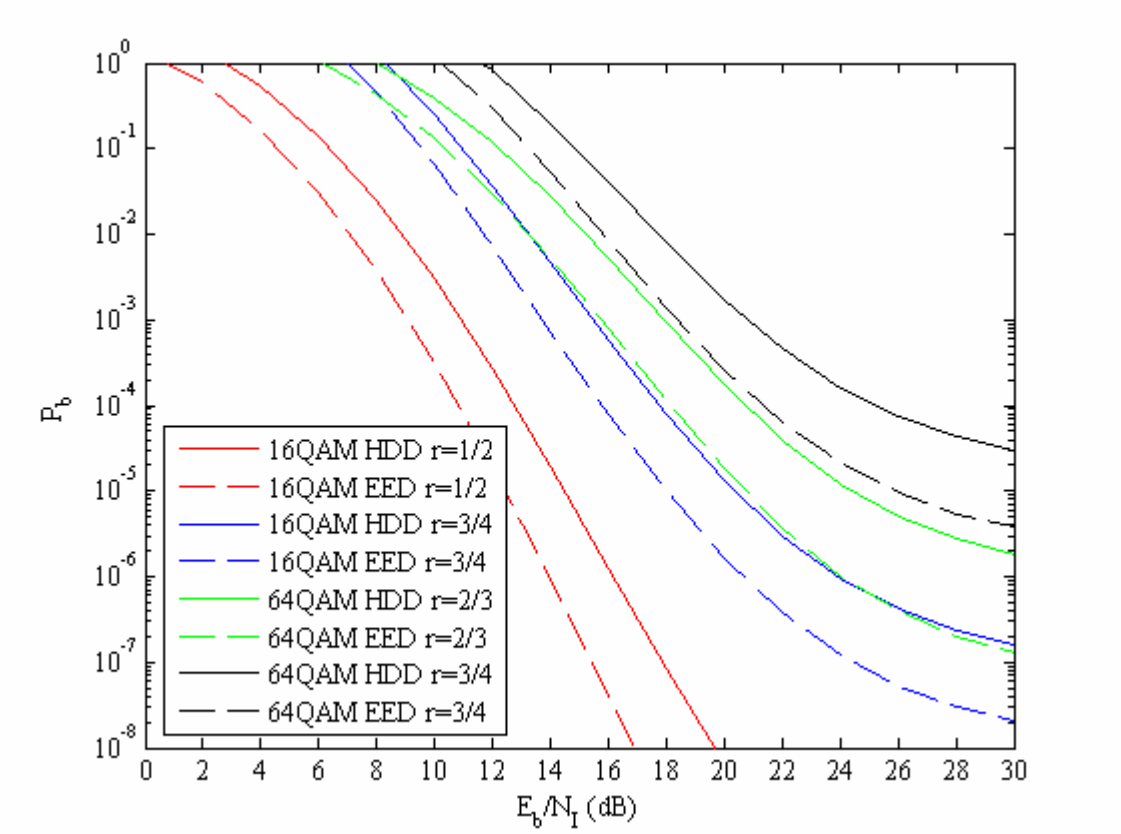

Figure 79. Performance of 16QAM and 64QAM for EED and HDD for a Nakagami fading channel with m=2, $E_b/N_0 = 20.6\,\text{dB}$, and ρ = 0.5.

D. CONCLUSIONS

For *M*QAM modulation with binary convolutional coding, EED can effectively minimize the effect of PNI on P_b for channels with no fading. When compared to HDD, EED provides clearly better performance for $E_b/N_I > 10\,\text{dB}$. For fading channels, *M*QAM modulation with binary convolutional coding and EED outperforms HDD regardless of E_b/N_I when PNI is present. In some cases 64QAM with a code rate of 2/3 provides better performance than 16QAM with a code rate of 3/4. Hence, when channel fading is a factor, performance is determined by the combination of modulation and code rate. In short, *M*QAM modulation with binary convolutional coding and EED effectively minimizes the effect of pulse-noise interference and outperforms HDD whether the channel experiences fading or not.

This concludes the performance analysis of *M*QAM modulated signals with errors-and-erasures decoding. In the next and final chapter, the important findings of this thesis research are summarized with some comments and closing statements.

THIS PAGE INTENTIONALLY LEFT BLANK

VI. CONCLUSIONS

The goal of this thesis was to investigate the performance of *IEEE 802.11g* wireless local area network (WLAN) standard receivers when the signal is transmitted over a frequency-selective, slowly fading Nakagami channel in a pulse-noise interference environment when errors-and-erasures Viterbi decoding is used. The different combinations of modulation (both binary and non-binary) and convolutional code rates specified by the WLAN standard were examined. The performance obtained with errors-and-erasures decoding (EED) was compared with the performance obtained with errors-only hard decision Viterbi decoding (HDD) as well as that obtained with soft decision Viterbi decoding (SDD) for binary modulation, while for non-binary modulation, EED performance was compared with HDD performance.

A. FINDINGS

It was shown that when PNI is present, EED yields all of the benefits of errors-only HDD with respect to minimizing the effects of PNI while simultaneously improving performance over what can be obtained with errors-only HDD. It was found that EED can significantly improve performance under some conditions when pulse-noise interference is present.

1. Conclusions for BPSK/QPSK Signals

For channels with no fading, errors-and-erasures decoding can effectively minimize the effect of pulse-noise interference on P_b. When compared to soft decision decoding with linear combining for the same E_b/N_0, errors-and-erasures decoding provides better performance for $E_b/N_I < 10 \log \rho^{-1}$ dB; but when errors-and-erasures decoding is given a small advantage in E_b/N_0 (1.8 dB for *r*=1/2 and 2.33 dB for *r*=3/4), then errors-and-erasures decoding provides as good or better performance for all E_b/N_I. The performance with errors-and-erasures decoding is very dependent on E_b/N_0, which must be larger than that required to provide the desired P_b in the absence of pulse-noise interference in order to provide meaningful immunity to the effects of pulse-noise interference.

For fading channels, errors-and-erasures decoding, with a code rate of 1/2 will outperform soft decision decoding with linear combining regardless of E_b/N_I when pulse-noise interference is present if E_b/N_0 is sufficiently large, but on an equal E_b/N_0 basis, the reverse is true. For channels with extremely severe fading (m = 0.5), E_b/N_0 must be greater than 10 dB more than for soft decision decoding with linear combining in order for performance with errors-and-erasures decoding to be superior.

It is also found that, when channel fading is a factor, for code rate r=3/4 errors-and-erasures decoding cannot outperform soft decision decoding with linear combining regardless of the increase in E_b/N_0; although, it is likely that that if the number of memory elements (K) is increased, then performance comparable to the r=1/2 code will be obtained with the r=3/4 code.

In short, errors-and-erasures decoding can effectively minimize the effect of pulse-noise interference and outperform soft decision decoding with linear combining given an advantage in E_b/N_0, where the required advantage is relatively small for channels with no fading, increases as m decreases for Nakagami fading channels, and exceeds 10 dB when channel fading is severe (m<1).

2. Conclusions for *M*QAM Signals

For *M*QAM modulation with binary convolutional coding, EED can effectively minimize the effect of PNI on P_b for channels with no fading. When compared to HDD, EED provides clearly better performance for $E_b/N_I > 10\,\text{dB}$.

For fading channels, *M*QAM modulation with binary convolutional coding and EED outperforms HDD regardless of E_b/N_I when PNI is present. In some cases, especially when the fading conditions are severe, 64QAM with a code rate of 2/3 provides better performance than 16QAM with a code rate of 3/4. Hence, when channel fading is a factor, the higher data rate may provide a more robust link than some of the lower data rates.

In short, *M*QAM modulation with binary convolutional coding and EED effectively minimizes the effect of pulse-noise interference and outperforms HDD whether the channel experiences fading or not.

B. FUTURE WORK

Now that this study is complete, there are several areas in which follow-on research would be beneficial. First of all, the comparison of EED with SDD with linear combining should be examined for *M*QAM signals.

Furthermore, the performance with errors-and-erasures can be examined for other types of interference, such as pulsed-single tone interference.

The findings of this thesis may be used for the development of a smart receiver (soft radio) which could understand the conditions of the environment in order to change decoding procedures for best performance and higher data rates.

Finally, in addition to the analysis performed in this thesis, the examination of the performance with errors-and-erasures decoding via simulation could be performed.

C. CLOSING COMMENTS

The examination of the performance of *IEEE 802.11g* receivers with errors-and-erasures decoding in the presence of PNI in addition to AWGN may be beneficial to those who are utilizing the standard for military applications, where the presence of a pulse-noise interferer is possible. The implementation of an EED decoder is relatively straightforward as compared to SDD designed to minimize the performance degradation due to PNI and is not significantly more difficult than errors-only HDD.

THIS PAGE INTENTIONALLY LEFT BLANK

LIST OF REFERENCES

[1] Proakis, J. G., *Digital Communications, 4th ed.*, McGraw-Hill, New York, NY, 2001.

[2] Lee, J. S., Miller, L. E., and Kim, Y. K., "Probability of error analysis of a BFSK frequency-hopping system with diversity under partial-band jamming interference-Part II: Performance of square-law nonlinear combining soft decision receivers," IEEE Trans. Commun., vol. COM-32, pp. 1243–1250, December 1984.

[3] Lee, J. S., Miller, L. E., and French, R. H., "The analyses of uncoded performances for certain ECCM receiver design strategies for multihops/symbol FH/MFSK waveforms," IEEE J. Selected Areas Commun., vol. SAC-3, pp. 611–620, September. 1985.

[4] Lee, J. S., French, R. H., and Miller, L. E., "Error-correcting codes and nonlinear diversity combining against worst case partial-band noise jamming of FH/MFSK systems," IEEE Trans. Commun., vol. COM-36, pp. 471–478, April 1988.

[5] Wang, Q., Gulliver, T. A., Bhargava, V. K., and Felstead, E. B., "Performance of error-erasure-correction decoding of Reed-Solomon codes for frequency-hop communications in multitone interference," IEE Proc., vol. 136, pt. I, pp. 298–304, August 1989.

[6] Macdonald, T. G. and Pursley, M. B., "Staggered interleaving and iterative errors-and-erasures decoding for frequency-hop packet radio," IEEE Trans. Wireless Commun., vol. 2, pp. 92–98, January 2003.

[7] Sklar, B., *Digital Communications: Fundamental and Applications*, 2nd edition, Prentice Hall, Upper Saddle River, NJ, 2001

[8] Lin, S. and Costello Jr., D. J., *Error Control Coding: Fundamentals and Applications*, Prentice Hall, Englewood Cliffs, NJ, 1983.

[9] Kosa, Irfan, *Performance of IEEE 802.11a Wireless LAN Standard over Frequency-Selective, Slowly Fading Nakagami Channels in a Pulsed Jamming Environment*, Master's thesis, Naval Postgraduate School, Monterey, CA, 2002.

[10] Kalogrias, Christos, *Performance analysis of the IEEE 802.11a WLAN standard optimum and sub-optimum receiver in frequency selective, slowly fading Nakagami channels with AWGN and pulsed-noise interference*, Master's thesis, Naval Postgraduate School, Monterey, CA, 2004.

[11] Taxeidis, Konstantinos, *Performance Analysis of IEEE 802.11g Waveform Transmitted Over A Fading Channel with Pulse-Noise Interference*, Master's thesis, Naval Postgraduate School, Monterey, CA, 2006.

[12] Institute of Electrical and Electronics Engineers Standard, 802.11a, *Wireless LAN Medium Access Control (MAC) and Physical Layer (PHY) Specifications: High-Speed Physical Layer Extension in the 5 GHz Ban*d, IEEE, New York, 16 September 1999.

[13] Odenwalder, J. P., *Optimum decoding of convolutional codes,* Ph.D. dissertation, University of California, Los Angeles, 1970.

[14] Clark, Jr., G. C. and Cain, J. B., *Error-Correction Coding for Digital Communications,* Plenum Press, New York, NY, 1981.

INITIAL DISTRIBUTION LIST

1. Defense Technical Information Center
   Ft. Belvoir, Virginia

2. Dudley Knox Library
   Naval Postgraduate School
   Monterey, California

3. Chairman
   Department of Electrical and Computer Engineering
   Naval Postgraduate School
   Monterey, California

4. Chairman
   Department of Physics
   Naval Postgraduate School
   Monterey, California

5. Professor R. Clark Robertson
   Department of Electrical and Computer Engineering
   Naval Postgraduate School
   Monterey, California

6. Professor Richard Harkins
   Department of Physics
   Naval Postgraduate School
   Monterey, California

7. Embassy of Greece, Naval Attaché
   Washington DC

8. LT Georgios Zouros
   Hellenic Navy General Staff
   Athens, Greece